SOL-GEL LANTHANUM PHOSPHATE, COMPOSITES AND COATINGS FOR FUNCTIONAL APPLICATIONS

THESIS SUBMITTED TO
COCHIN UNIVERSITY OF SCIENCE AND TECHNOLOGY
IN PARTIAL FULFILMENT OF THE REQUIREMENTS
FOR THE DEGREE OF

DOCTOR OF PHILOSOPHY
IN CHEMISTRY

UNDER THE FACULTY OF SCIENCE

BY
SANKAR SASIDHARAN
Under the guidance of
Dr. KG.K. WARRIER
&
Co-guidance of
Dr. S. ANANTHAKUMAR

MATERIALS SCIENCE AND TECHNOLOGY DIVISION
NATIONAL INSTITUTE FOR INTERDISCIPLINARY SCIENCE AND TECHNOLOGY

COUNCIL OF SCIENTIFIC AND INDUSTRIAL RESEARCH
THIRUVANANTHAPURAM, KERALA, INDIA - 695019

JANUARY 2015

DECLARATION

I hereby declare that the work embodied in the thesis entitled "**SOL-GEL LANTHANUM PHOSPHATE, COMPOSITES AND COATINGS FOR FUNCTIONAL APPLICATIONS**" is the result of investigations carried out by me at Materials Science and Technology Division, National Institute for Interdisciplinary Science and Technology (CSIR-NIIST), Thiruvananthapuram, under the supervision of Dr. K. G. K. Warrier and the co-supervision of Dr. S. Ananthakumar and the same has not been submitted elsewhere for any other degree.

Sankar Sasidharan

Thiruvananthapuram

January 2015

राष्ट्रीय अंतरविष्यी विजान तथा प्रौघोगिकी संस्थान
NATIONAL INSTITUTE FOR INTERDISCIPLINARY SCIENCE AND TECHNOLOGY

वैजानिक एंव प्रौघोगिकी अनुसंधान प्रयोग्शाला
इन्डस्ट्रियल इस्टेट डाक घ्रर, तिरुवनन्तपुरम, भरत-695019

Council of Scientific and Industrial Research
Industrial Estate P.O., Pappanamcode, Thiruvananthapuram, India - 695019

January 2015

This is to certify that the work embodied in the thesis entitled **"SOL-GEL LANTHANUM PHOSPHATE, COMPOSITES AND COATINGS FOR FUNCTIONAL APPLICATIONS"** has been carried out by Mr. Sankar Sasidharan under my supervision and the co-supervision of Dr. S. Ananthakumar at Materials Science and Technology Division, National Institute for Interdisciplinary Science and Technology, (CSIR-NIIST), Thiruvananthapuram, in partial fulfillment of the requirements for the award of the Degree of Doctor of Philosophy in Chemistry, under the Faculty of Science, Cochin University of Science and Technology, Cochin and the same has not been submitted elsewhere for any other degree. All the relevant corrections and modifications suggested by the audience at the pre-synopsis viva voce and recommended by the doctoral committee are incorporated in the thesis.

S. Ananthakumar
Thesis Co- Supervisor

(K .G. K. Warrier)
Thesis Supervisor

ACKNOWLEDGMENTS

I have enormous pleasure to express my deep sense of gratitude to Dr. K. G. K. Warrier, my research supervisor, for his adroit guidance, intellectual support, constant encouragement, constructive criticism and above all, the freedom he gave me during the entire course of my doctoral work. I am indebted to him for all the efforts he has put in for the successful completion of this thesis.

My heartfelt acknowledgments to Dr. U. S. Hareesh and Dr. N. N. Balagopal for their constructive criticism, valuable suggestions, technical advice and support during the study and I would also like to express my sincere thanks to Dr. S. Ananthakumar, my thesis Co-supervisor for his constant support and inspiration during the tenure of this work. A special word of acknowledgement is to Dr. Saju Pillai and Dr Satyajith Shukla for the timely questions and suggestions.

I wish to thank Dr. Suresh Das and Dr. B. C. Pai, present and former Directors of the CSIR-National Institute for Interdisciplinary Science and Technology for providing me the necessary facilities for carrying out the work. I express my sincere thanks to Dr. M.L.P Reddy and Dr M.T Sebastian, present and past Heads of MSTD for their support during this study.

I am immensely thankful to Mr. A. Peer Mohamed for helping me with the instruments. I would also like to thank Mr. P. Mukundan for material characterization during the early stages of my work. I also acknowledge Mr. P. Perumal for some of the technical advices during my early stay in NIIST.

Dr. Krishnakumar B, Mrs. Anupama V.N and Mr. Prajeesh GPV (ENVT, CSIR-NIIST) are gratefully acknowledged for the studies on perchlorate.

I thankfully acknowledge the contributions of XRD, SEM and TEM groups of CSIR-NIIST, especially Dr. U. Shyamaprasad, Mr. P. Guruswamy, Mr. M. R. Chandran, Mr. Chandrakanth, Mrs. Lucy Paul, Mr. M. Kiran and Mr. Robert Philip.

Dr. Prabha D. Nair (SCTIMST, Trivandrum), Dr P.V.A Padmanabhan and Mr. Pragatheeswaran (BARC, Mumbai), Dr. Sreemoolanadhan (VSSC, Trivandrum), Dr Anil

Kumar (Noritake, Japan) are being gratefully acknowledged for helping with instrumentation facility during various stages of the work.

I always cherish the sincere support and help of my senior colleagues Dr. P. Shajesh, Dr. M. Jayasankar, Dr. Rajesh Komban, Dr. P. R. Aravind ,Dr. S. Anas, Mrs. Athira N. Raj, Dr Smitha V.S, Mrs. K. A. Manjumol , Dr. Jaimy K. B. Dr P. S. Suchitra, Mr. S. Vinod, Mr. A. Mirash, Mr. Divish, Mr. Senguttuvan, Mr. P. Hareesh for loving companionship and ardent support throughout the period of this work.

Words fall short in expressing my gratitude to I wish to thank my present colleagues Mrs. T. S. Sree Remya, Mrs. Asha Krishnan, Ms. P. Suyana, Ms. N. B. Sumina, Mrs. Mega Joy, Ms. Minju Thomas, Ms. S. Swetha, Mr. Ms. Vidya Kattoor, Ms. Shijina Nambiar, Ms. P. V. Subha, Mrs. N. Harsha, Mr. M. Midhun, Mr. Manu Jose, Mr. Arun, Mr. Firoz, Mr. Akhil K. Nair, Mrs. K. B. Babitha, Mr. K. V. Mahesh, Mr. S. Vaisakh, Mr. S. Sujith, Ms. V. Linsha, Mrs. Soumya, Ms. Jean Mariya, Mr. Balanand and Ms. Minju Ashok . In different ways, their support was crucial for the completion of the thesis. Their humor and friendship have made my stay at NIIST really enjoyable. The support and companionship with senior as well as present colleagues of other divisions (CSTD, AGNP, MSTD and PEET) are also kindly acknowledged which made my stay memorable and comfortable at CSIR- NIIST.

I would like to express my heartfelt thanks to all those whose numerous efforts and help made this thesis a reality.

I gratefully acknowledge the Council of Scientific and Industrial Research, New Delhi, for the Research Fellowship and Financial assistance from IRE Ltd.

Sankar Sasidharan

CONTENTS

		Page
Declaration		**i**
Certificate		**ii**
Acknowledgements		**iii**
Contents		**v**
Preface		**ix**
List of abbreviations		**xii**
Chapter 1	**Introduction to Rare Earth Phosphates - Lanthanum Phosphate , Sol- Gel Synthesis – Properties, Applications and Proposed Work**	
1.1	Rare Earth Phosphates	**1**
1.1.1	Classification and Structure of $RePO_4$	**2**
1.2	Properties and Applications	**5**
1.3	**Synthesis of Lanthanum Phosphate - Review**	**10**
1.4	**Lanthanum Phosphate based composites**	**19**
1.4.1	$LaPO_4$-Y_2O_3 Composite	**20**
1.4.2	$LaPO_4$ - ZrO_2 Composite	**21**
1.5	Lanthanum phosphate for biological/environmental applications	**22**
1.6	Lanthanum phosphate and composites as non-reactive surfaces against molten metals	**23**
1.7	Machinability of Lanthanum Phosphate	**24**

1.8	Sol-Gel Technique for Material Synthesis	**24**
1.8.1	The Sol-Gel Process	**26**
1.8.2	Advantages of Sol- Gel Technique	**28**
1.9	Summary of literature-Gaps in current information and proposed research work	**28**
	References	**31**
Chapter 2	**Nanosize Lanthanum Phosphate and Composites through Sol Gel Approach – *Synthesis, Characterization* and *Applications***	
	Part 1- Experimental	
2.1.	Synthesis of Stoichiometric $LaPO_4$ Particles	**36**
2.1.1.	Experimental	**36**
2.1.2.	Characterization	**37**
2.2	**$LaPO_4$-Y_2O_3 Composite**	**39**
2.2.1	Experimental	**40**
2.2.2	Characterization	**40**
2.3	**$LaPO_4$-ZrO_2 Composite**	**42**
2.3.1	Experimental	**42**
2.4.	**Coatings**	**44**
2.4.1	$LaPO_4$ Nanocoatings	**44**
2.4.2	Plasma Spray coating	**45**
2.5	Sintered $LaPO_4$ and $LaPO_4$- Y_2O_3 for machinability and reactive metal melting studies	**46**

	Part 2- Results and Discussion	
2.6	Stoichiometric Lanthanum Phosphate	**47**
2.6.1	Mechanical properties	**56**
2.7	$LaPO_4$- Y_2O_3 Nano Composite	**59**
2.8	$LaPO_4$– ZrO_2 composite	**68**
2.8.1	Thermal conductivity	**75**
2.9	Plasma Spray coating	**77**
	Conclusions	**80**
	References	**82**
Chapter 3	Non-Wetting as well as Non-reactive properties of Lanthanum Phosphate and Composites	
3.1.	**Hydrophobic property of Lanthanum Phosphate**	**84**
3.1.1	Introduction	**84**
3.1.2	Experimental	**87**
3.1.3	Results and Discussion	**88**
3.1.4.	$LaPO_4$ Coatings on Glass substrates	**92**
3.1.5	Summary	**96**
3.2	**$LaPO_4$ Non-Reactivity with molten metals**	**97**
3.2.1	Introduction	**97**
3.2.2	Lanthanum phosphate Monoliths/Crucibles	**98**
3.2.3	Lanthanum phosphate reactivity with metals	**99**
3.2.3.1	Reactivity with Zinc metal	**99**
3.2.3.2	Reactivity with Aluminium Metal	**100**

3.2.3.3	Reactivity and contact angle measurement with Ag metal	**103**
3.2.4	Wetting experiments of $LaPO_4$ for molten metal reactivity	**104**
3.3	Surface Energy of $LaPO_4$	**105**
3.4	Reactivity with Uranium Metal for $LaPO_4/Y_2O_3$ Composite	**108**
	Conclusions	**110**
	References	**111**
Chapter 4	**Colloidal Processing of Lanthanum Phosphate**	**112**
4.1	**Introduction**	**113**
4.2	Experimental	**116**
4.2.1	$LaPO_4$ Monolith Synthesis	**116**
4.2.2	Perchlorate adsorption studies	**117**
4.2.3	Biofilm Growth on $LaPO_4$ substrate	**117**
4.3	Results and Discussion	**118**
4.3.1	Adsorption of perchlorate ions using porous $LaPO_4$ monoliths	**123**
4.3.2	Porous Lanthanum Phosphate as Substrates for Biofilm growth	**128**
	Conclusions	**131**
	References	**132**
Chapter 5	**Summary of Investigations**	**134**
	List of Publications	**142**

PREFACE

Lanthanum phosphate is one among the lanthanide family of "Rare Earths" following the periodic table of elements. Known under the generic name, Monazite, the rare earth phosphates have melting points above 1900 °C, high thermal phase stability, low thermal conductivity and thermal expansion coefficient similar to some of the high temperature oxides like alumina and zirconia.

Chapter 1 deals with introduction to $REPO_4$ (rare earth phosphates) including occurrence and structural features with special reference to $LaPO_4$. A detailed literature survey is reported and analysis done on the diverse properties and applications of $LaPO_4$. The reported synthesis techniques and properties are covered in detail. The definite advantage of sol gel processing over other wet chemical techniques is suggested. Other than thermal stability, lanthanum phosphate has a low hardness value and can be machined easily, unlike other ceramic materials. Considerable literature is available on the various luminescent compositions with $LaPO_4$ as host. In this respect, although less investigated, the lanthanum phosphate is learnt to have excellent possibilities for use in various applications. A few of the properties which need further investigation are $LaPO_4$ based composites, hydrophobic properties, non-reactivity with molten metals and bio functionality.

Chapter 2 describes the sol-gel based synthesis procedure adopted for the preparation of stoichiometric $LaPO_4$ by first precipitating from lanthanum chloride, converting to precursor gels and further processing to nano size powder. The morphological and structural features as well as thermal phase stability are presented. $LaPO_4$ has 100-120 nm size in the as precipitated

condition and 60-80 nm as sol particles with rod like morphology (average aspect ratio 4), and good thermal stability. The powder could be pressed to discs and sintered to > 99% density by heating at 1300 $^{\circ}$C due to the fine size obtained. Nano composites of $LaPO_4$ with Y_2O_3 and ZrO_2 were also prepared with varying compositions in the range 5-20 wt% oxides. The data on grain growth control of $LaPO_4$ in presence of zirconia addition and the low thermal conductivity of the composite are also presented.

In **chapter 3** two major properties which are less investigated earlier were studied in detail. The inherent property of water non-wettability (hydrophobicity) and non-reactivity with molten metal are investigated further. $LaPO_4$ has low wetting features with water possessing contact angles >95^{o} and this is explained based on the electronic structure of the rare earths in general. $LaPO_4$ coatings were made on glass and these coatings exhibited contact angles >120^{o}. The high contact angle is attributed to the synergistic effect of inherent hydrophobicity of rare earth phosphates as well as the surface roughness created by the rod shaped particles. The study covers a detailed structure property correlation of lanthanum phosphate coatings and morphological features with surface wettability followed by contact angle measurements.

Non-wetting and non-reactivity with molten metal is a property which is being looked for by the metal processing industry. In this chapter, detailed high temperature melting and reactivity experiments were done on $LaPO_4$ with common metals such as Zinc, Aluminium and Silver and the resultant samples were analyzed. $LaPO_4$ crucibles were also moulded by casting process for melting metals which are found non-reactive. None of the metals investigated had reaction with $LaPO_4$ and high temperature contact angle measurement done on silver showed a value as high as 125^{o}.

Chapter 4 gives the results of investigation on processing of $LaPO_4$ to porous substrates by thermal gelation process involving methyl cellulose as the organic intermediate (0.25 wt%) where 50% porous $LaPO_4$ was obtained on gel cast sample sintered at 1300 ^oC. These porous substrates showed multifunctional property of high volume adsorption of perchlorate ions from aqueous medium and also growing of biofilms containing perchlorate reducing microbes. The growth of biofilms is explained on the basis of hydrophobic nature of the surface which promotes the biofilm growth. Both the above aspects are being reported for the first time.

Chapter 5 concludes the thesis by giving a brief summary of the major findings of the study and Structure-property correlation has been drawn between the structural and morphological characteristics of $LaPO_4$ and observed properties of non-wettability, non-reactivity and biofilm formation.

Thus, the thesis gives a detailed study on the synthesis of $LaPO_4$ and its composites using a modified sol gel process. The versatility on the applicability of $LaPO_4$ in multifunctional and high temperature applications is well established.

List of Abbreviations

AFM	Atomic Force Microscopy
BET	Brunauer-Emmet-Teller
ClO_4^-	Perchlorate
DLS	Dynamic Light Scattering
DTA	Differential Thermal Analysis
EDX	Energy Dispersive X-ray Spectroscopy
FT-IR	Fourier Transform Infrared
JCPDS	Joint Committee on Powder Diffraction Standards
$LaPO_4$	Lanthanum Phosphate
$LnPO_4$	Lanthanide Phosphate
PPE	Photopyroelctric
PRB	Perchlorate Reducing Bacteria
$RePO_4$	Rare earth Phosphate
SEM	Scanning Electron Microscopy
TBC	Thermal Barrier Coating
TEM	Transmission Electron Microscopy
TGA	Thermo Gravimetric Analysis
TMA	Thermo Mechanical Analysis
WCA	Water Contact Angle
XRD	X-Ray Diffraction
Y_2O_3	Yttria
ZrO_2	Zirconia

Chapter 1

Introduction to Rare Earth Phosphates - Lanthanum Phosphate, Sol- Gel Synthesis – Properties, Applications and Proposed Work

1.1 Rare Earth Phosphates

As defined by IUPAC, a rare earth element (REE) or rare earth metal is one of a set of seventeen chemical elements in the periodic table, specifically the fifteen **lanthanides** plus **scandium** and **yttrium**. The rare earths are not in fact very rare since cerium is the 25th most abundant element in the earth's crust at 60 ppm, more common than lead, but since rare earth elements are usually spread and not as rare earth minerals in usable deposits, and this shortage gave these elements the name, "rare earths". They make possible the high tech world we live in today – everything from the miniaturization of electronics, to the enabling of green energy and medical technologies, to supporting a myriad of essential telecommunications and defence systems. They are the elements that have become irreplaceable to our world of technology owing to their unique magnetic, phosphorescent, and catalytic properties.

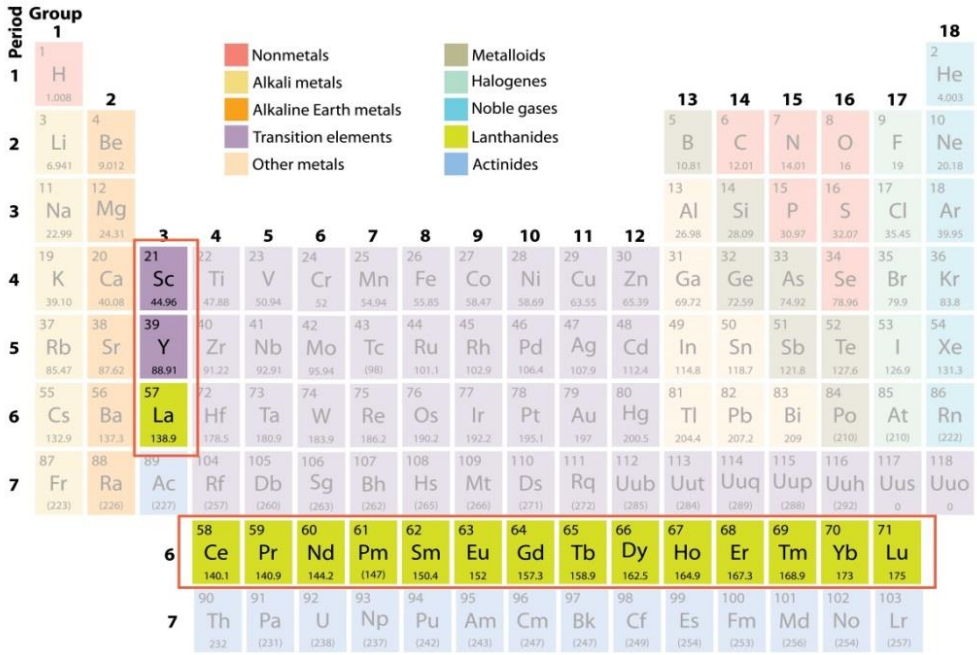

The interest in lanthanide orthophosphate has grown recently, in both research and applications due to the promising properties. The rare earths (RE; here considered as lanthanides +Y) phosphates, $RE(PO_4)$, exist in nature as the phases monazite and Xenotime; monazite preferentially incorporates the larger, light rare earth elements (LREEs, here La-Gd) whereas Xenotime tends to incorporate the smaller, heavy rare earth elements (HREEs, here Tb-Lu, +V).

Monazite is an anhydrous monoclinic rare earth orthophosphate **($RePO_4$)** mineral, where Re is mostly cerium with significant amount of lanthanum, neodymium and praseodymium. A few deposits of monazite serve as primary source of thorium (Th, 8-10 %) as well as secondary source of uranium (U) containing uranium oxide (U_3O_8, 0.38%). Due to the high demand of uranium and thorium in our country for strategic use, the processing of monazite is very important which results in plenty of rare earth as by product.

1.1.1Classification and Structure of $RePO_4$

Anatomically lanthanide phosphate or rare earth phosphate ($RePO_4$) is mainly classified under five types[1], such as **a) Monazite**, monoclinic type $LnPO_4$ (Ln=La_Gd), **b) Xenotime**, tetragonal type $LnPO_4$ (Ln=Tb-Lu), **c) Rabhdophane**, hexagonal type $LnPO_4.0.5\ H_2O$ (Ln=La-Dy) d) **Weinschenkite** type $LaPO_4.\ 2\ H_2O$ (Ln=Gd-Yb) and **e) Orthorhombic** type $DyPO_4\ 1.5\ H_2O$. The orthophosphates from Ho to Lu as well as Y exist only in the tetragonal zircon (Xenotime) structure, while the orthophosphates from La to Dy exist in the hexagonal and monoclinic structures. On the other hand, the orthophosphates of Gd, Dy and Tb exist in four different phases excepting the ortho-rhombic type. Although the exact reason is not yet clear, it is believed that this could be associated with the change of lanthanide ion radius.[2]

Structure of hexagonal $RePO_4$ (R = La, Ce & Nd) was first proposed in 1950 by Mooney.[3] According to his concept, $RePO_4$ is considered as columns of alternate Re^{3+} and PO_4^{3-} ions extending along the 'c' axis with each column linked to four neighbouring columns. The phosphate ions are formed by a phosphorous atom surrounded by oxygen tetrahedral. In this arrangement the Re^{3+} ion is coordinated to eight oxygen atoms, which forms a pair of four oxygen each. One of the pairs contains oxygen atoms from corners of four different phosphates (tetrahedral structure), which is shorter distance (2.34 Å) and the oxygen atoms that form edges between phosphate tetrahedral make up the other set, which is longer distance of 2.66 Å. The Re-Re separation is ~ 4.13 Å and O-P distance fixed at 1.56 Å**.** The whole structure contains open channels running along the hexagonal axis and the schematic representation of structure is shown in *Figure 1*. The available space can be described as cylindrical, oxygen lined tunnels of diameter 5.3 Å.

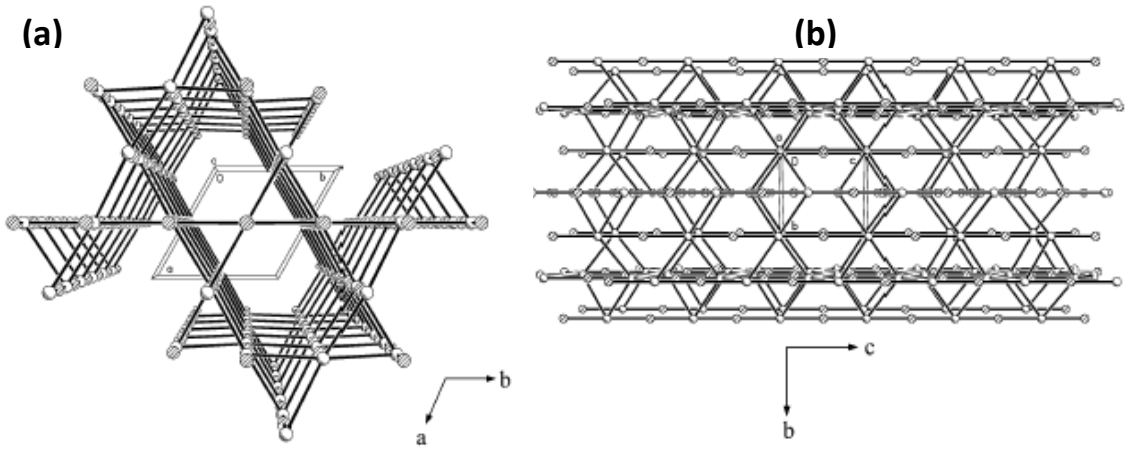

Figure 1) (**a**) Packing view of $RePO_4$ along the *c* axis. (**b**) Packing view of $RePO_4$ along *t*he axis. (*Acta Crystallogr.* **1950**, 3, 337 and *J. Am. Chem. Soc.* **2003**, 125, 16025)

Many attempts are reported on the possible structure of $RePO_4$ or general monazite. *Beall Et al.* suggested the structure of cerium phosphate ($CePO_4$) as nine co-ordinated in 1981.[4] Mullica et al. in 1984 studied the crystal structure of $LaPO_4$ from three-dimensional single-crystal X-ray diffraction data.[5] The respective residual indices R_1 and R_2 have been refined to

0.020 and 0.021, based on 625 unique reflections. Crystallization occurs in the monoclinic space group $P2_1/n$ (No. 14) with a = 6.825(4), b = 7.057(2), c = 6.482(2) Å, and β = 103.21(4) °. Z = 4. The lanthanum metal atom is nine-coordinated to oxygen atoms forming a polyhedron best described as a pentagonal interpenetrating tetrahedron. The lanthanide metal atoms are coordinated with nine oxygens and are linked together by very slightly distorted tetrahedral phosphate groups. The nine oxygen atoms ligating the lanthanide atoms form a polyhedron that is best described as a pentagonal interpenetrating tetrahedron.[6] According to *Du et al.*. the phosphates of rare earths are coordinated with nine oxygen atoms which are lined together by tetrahedral phosphate groups (*figure 2*).[7]

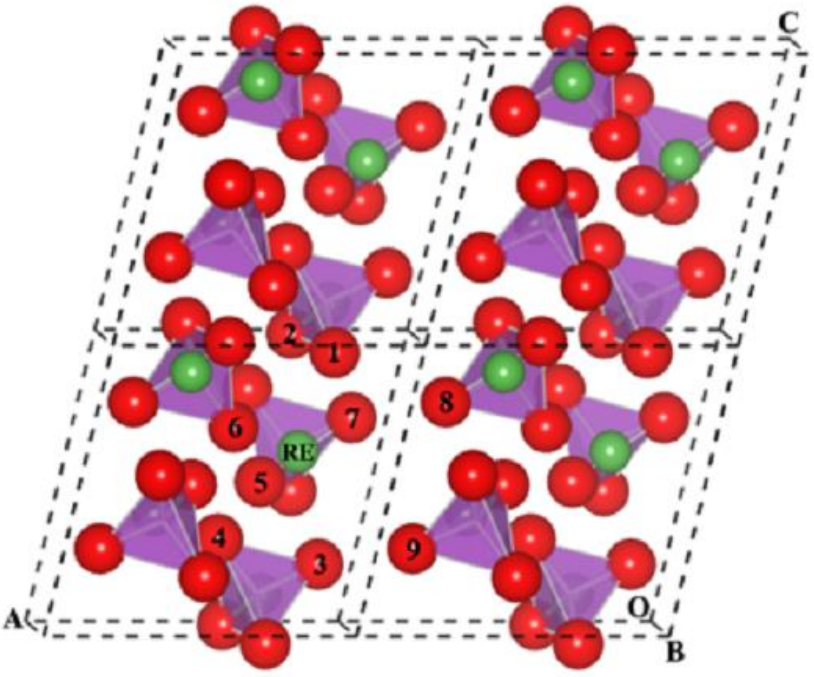

Figure 2) Crystal structure of natural monazite (**Adopted from** *J. Am. Ceram. Soc*., 92 [11] 2687–2692 (**2009**), the distorted tetrahedral represents PO_4 units; RE is nine fold coordinated by O atoms (indexed by nos. 1–9)

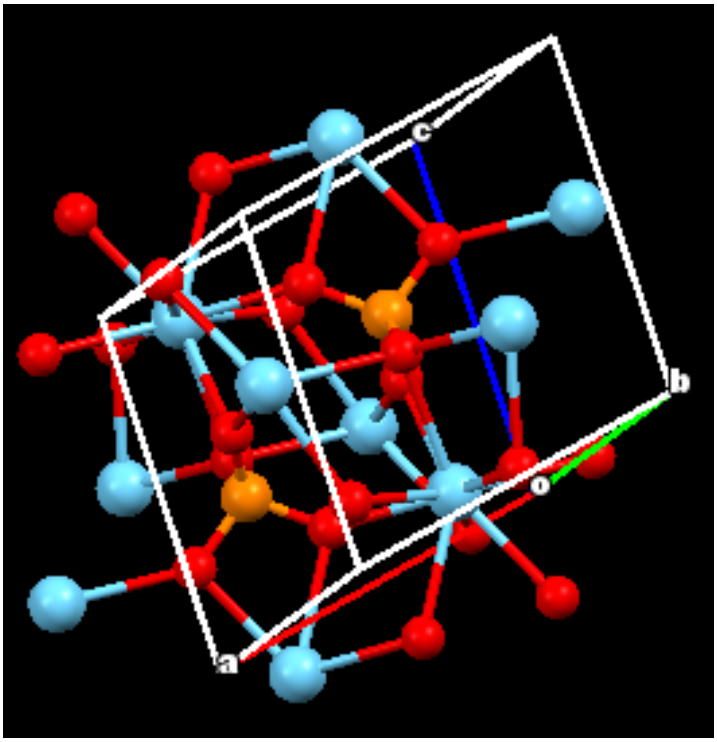

Figure 3) Structure of $LaPO_4$ with its unit cell (La-Light blue, P-yellow, O-red)

1.2 Properties and Applications

Monazite ($RePO_4$) is nontoxic, almost completely insoluble in water, dilute acids and bases. It is highly refractory with high melting point and thermally stable with no decomposition up to the melting point, and not easily reduced

In 1987 *Hikichi et al.* found that the melting point of synthetic monazite is in the range of 1900-2000.[8] According to their study, natural monazite from Japan (2057 °C), synthetic monazite $RePO_4$ (R=La, 2072 °C; R=Ce, 2045 °C; R=Pr, 1938 °C; R=Nd, 1975 °C; R=Sm, 1916 °C), and synthetic Xenotime $RePO_4$ (R=Y, 1995 °C; R=Er, 1896 °C). When compared to aluminum and calcium phosphate, which are already known for their application as refractory material, [9] rare earth phosphates have excellent thermal phase stability.[10]

One important property of rare earth phosphates is that they are characterized with low conductivity, while majority high temperature materials are found to be good thermal conductors. The reason for the low thermal conductivity is that they have high mean atomic mass and their structures are similar to network silicates with various arrangements of corner and edge-sharing PO_4 tetrahedra rather than SiO_4 tetrahedra.

Thermal conductivity of $LaPO_4$ is 3.61 W/mK at 25 °C and 1.30 W/mK at 1000 °C while that of $NdPO_4$ is 3.59 W/mK and 1.59 W/mK respectively. $CePO_4$ has a thermal conductivity of 1.81 W/mK at 500 °C.[11, 12] The combined effects of the increase of both the anharmonicities in the lattice vibrations and the bond strength with the gradual altering from $LaPO_4$ to $GdPO_4$ is considered to be responsible for the trends in the behaviour with respect to thermal conductivity.

Thermal expansion co-efficient of $LaPO_4$ is found to be similar to alumina .The linear thermal expansion coefficient of $LaPO_4$ is in the range of 7.5 x 10^{-6}/ °C at 20°C to 10 x 10^{-6}/ °C at 1000 °C.[13] The linear thermal expansion coefficient of the $CePO_4$ ceramics is 9 x 10^{-6}/°C to 11 X 10-6/°C (200- 1300°C).[14] Alumina has a coefficient of thermal expansion value of 10 x10^{-6}/ °C.[14] The hardness of $LaPO_4$ is reported to be 5 Gpa characterizing it as a relatively soft ceramics. Considering the toughness and young's modulus of $LaPO_4$, it is on the lower side on comparing with alumina, zirconia, and mullite .[16- 19]

	Melting Point (°C)	**Thermal conductivity (W/mK) at 25 °C**	**Thermal expansion coefficient**	**Hardness (GPa)**
$LaPO_4$	2072	3.61	9.6 x10^{-6}	5
Alumina	2040	43	10x10^{-6}	16
Zirconia	2715	3	11x10^{-6}	15
SiC	2730	60	4 x10^{-6}	27

Table 1) *Comparison of different thermal and mechanical properties*

Lanthanum Phosphate is known for its ability to function as a solid state proton conductor.[20] *Kitamura et al.*. [21] had studied the electrical conduction in $LaPO_4$ with the monazite structure ($P2_1/n$) by using conductivity measurements at 500–925 °C. From the conductivities obtained for undoped and 1 mol% Sr-doped $LaPO_4$ under wet (H_2O and D_2O) and dry atmospheres, it was observed that $LaPO_4$ began to conduct protons under wet atmosphere by substituting Sr for La. The protonic conduction was dominant in the materials though electron holes contributed slightly to the total conductivity as temperature is increased.

Dielectric constant (*K*) is found to be low for $LaPO_4$ ceramics. *Narasimha et al.*. [22] measured the dielectric value in the frequency region 10^2 to 10^7 Hz and in the temperature range −193 to 280° C. At room temperature (≈ 30°C), *K* decreases with frequency up to 10^5 Hz, beyond which it attains a constant value; tanδ behaves in a similar way. The values of *K* and tanδ at 30°C and 10^6 Hz for this material are 14 and 2.7×10^{-3}, respectively. As a function of temperature *K* exhibits two stages of increase, (i) a slow stage up to −30° C and (ii) a fast one beyond −30° C which is considerably frequency dependent, *K* having larger values at lower frequencies.

Extending the applicability of $LaPO_4$ due to excellent properties, studies are reported recently for catalytic applications, nuclear waste immobilization as well as biological applications. $LaPO_4$ has been identified to be a very good Lewis – acid catalyst and used in vapour phase reactions. The catalytic activity of different rare earth phosphates varied depending on the type of rare earth elements (La---> Y), type of phosphates (Monazite, Xenotime. etc.) and type of phosphorous (H_3PO_4 and $(NH_4)_2HPO_4$) precursors. *Yusaku Takita et al.*. studied the use of lanthanum phosphate in oxidative dehydrogenation of iso-butane to iso-butene, $LaPO_4$ has also been used for ethanol dehydration and also in hetero-Diels–Alder reaction. [23]

Investigations on the area of photoluminescence of $LaPO_4$ have also emerged in near time and are found to act as excellent host for lanthanides for the development of luminescent materials for various applications.[24,25] *Peter Schuetz* worked on the formation of nanostructured, ultrathin films of fluorescent nanoparticles (NPs) within the identical size range as quantum dots, but with a different kind of fluorescence, using rare-earth-doped lanthanum phosphate particles ($LaPO_4$).[26] Recently core shell strategies have been introduced to increase the quantum yield of the nanoparticle which was on the lower side using conventional synthesis procedures adopted in the beginning. *Yang et al.* used a $LaPO_4$ shell on the $LaPO_4$:Ce^{3+}, Tb^{3+} nanowires showed increased intensity for the particles where the shell thickness plays an important role on the improved intensity.[27] *Buissette et al.* showed the increased stability against oxidation effects by using a complexing agent and making a shell of $LaPO_4.xH_2O$ over the phosphates of La, Ce and Tb.[28]

With the high chemical stability and low toxicity of $LaPO_4$, applications related to bio functionalization and bio probe applications are being investigated.[29] Recently *Felix Meiser et al.*[30] reported the first demonstration of the bio functionalization of nanometre-sized colloidal $LaPO_4$ Nano Particles (NPs), where Green (Ce/Tb-doped) $LaPO_4$ NPs were conjugated to the model protein avidin, a tetrameric protein that can bind with high affinity to four biotin molecules. Further they claim with features such as dopant-tunable emission, photon up conversion properties, and the possibility to detect multiple labels using a single excitation wavelength with no spectral overlap, are proposed to offer considerable promise for the use of bio functionalized rare-earth-doped lanthanide phosphate NPs in various biotechnological applications.

More recently *Jonathan Woodward et al.* incorporated (actinium-225) ^{225}Ac into lanthanum phosphate NPs to determine whether the radioisotopes would be retained within the dense mineral lattice. The ^{225}Ac-doped NPs were conjugated to the monoclonal antibody mAb 201B, which targets mouse lung endothelium through the vasculature, to ascertain the targeting efficacy and in vivo retention of radioisotopes. Standard bio distribution techniques and micro SPECT/CT imaging of ^{225}Ac as well as the daughter radioisotopes showed that the NPs accumulated rapidly in mouse lung after intravenous injection. The study proved the potential applicability of nanoscale lanthanum phosphate for sequestering toxic daughter radionuclides .[31]

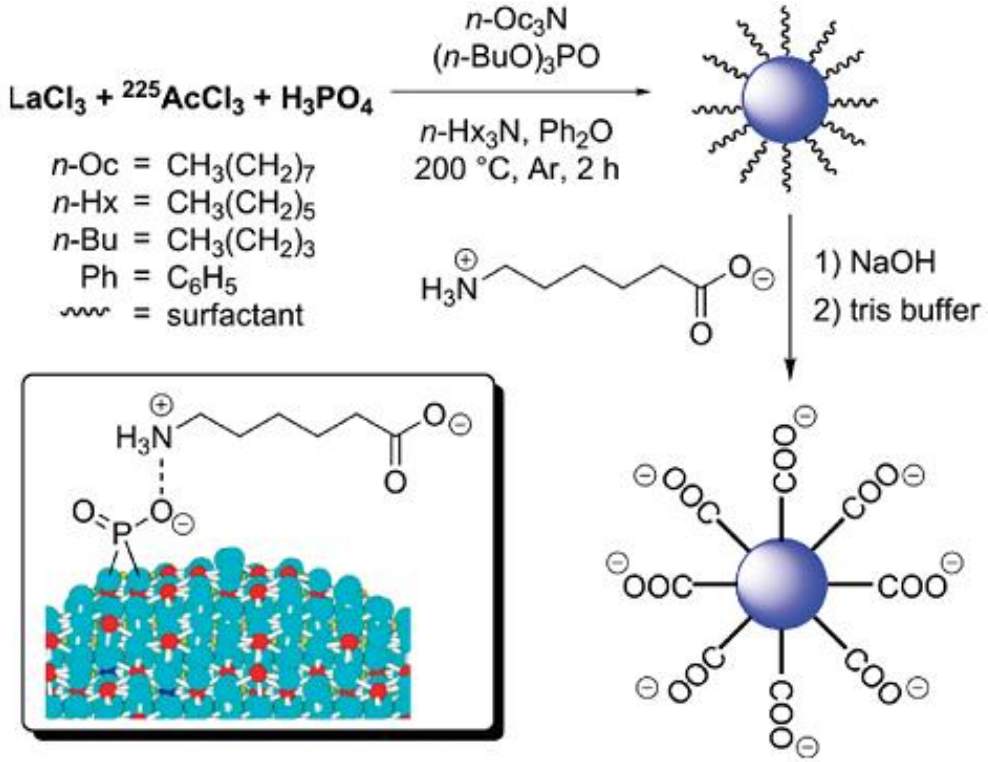

Figure 4) Schematic depiction of synthesis and surface modification of La (225 Ac) PO_4 (*Bioconjugate Chem*. 22, **2011**, 766)

Recent study showed the potential applicability of rare earth phosphates and $LaPO_4$ in particular as materials to act as hosts for radioactive waste immobilization with low leaching rates.[32] *Olivier Terra et al.* reported good properties of monazites for the immobilization of radioactive waste and especially for trivalent actinides. Indeed, the solid solutions of $La_{1-x}Gd_xPO_4$ exhibit good sintering properties and a high resistance to aqueous alteration (RL ¼ 10^{-6} to $10^{-4}gm^{-2}$ day^{-1}) even in acidic media, confirmed the very good retention properties of this kind of phosphate based matrix for the immobilization of radionuclides.[33]

However Lanthanum Phosphate ($LaPO_4$) representing most of the rare earth phosphates, has been increasingly investigated as a high temperature material due to the favourable physical and thermal properties. There is considerable advantage with the traditional high temperature phosphates like $AlPO_4$ which has a melting point of ~1700 °C.The nature of $LaPO_4$ interface with many oxides including alumina proves it to be an excellent material for ceramic matrix composites.

1.3 Synthesis of Lanthanum Phosphate ($LaPO_4$) – Review

Lanthanum phosphate synthesis gathered attention after *Hikichi et al.* established the phase stability in 1987.[8] Considerable reports are available on the synthesis of lanthanum phosphate on techniques like solid state synthesis, precipitation, hydrothermal, solid – liquid reaction, colloidal, micro wave, ultrasonication and sol-gel. The starting compound in nearly all the above techniques is rare earth nitrate, carbonate or acetate and the phosphate obtained are in submicron or nanometre range.

Ruigang et al. [34] synthesized lanthanum phosphate powders by direct solid–liquid reaction of lanthanum oxide and phosphoric acid at the La:P ratio of 1:1. Phase-pure and fine grain size $LaPO_4$ powders could be obtained by calcining the as-received powders at the temperature higher than 600 °C. Lanthanum oxide was dissolved in diluted phosphoric acid

at the La to P ratio of 1:1 and this direct reaction between lanthanum oxide and phosphoric acid was clean with no by-products other than water by the reaction:

$$La_2O_3 + 2H_3PO_4 \rightarrow 2LaPO_4 + 3H_2O$$

Crystallisation from boiling phosphoric acid solution was used by *Kijowska* [35] to synthesize Ln phosphates (Ln=La, Ce, Pr, Nd, Sm, Eu, Gd, Tb, Dy, Ho, Er, Tm, Yb, Lu and Y). Formation of hexagonal $LnPO_4 \cdot H_2O$ (La, Ce, Pr, Nd, Sm, Eu, Gd, Tb), tetragonal $LnPO_4 \cdot H_2O$ (Ho, Er, Tm, Yb, Lu) isostructural with YPO_4, and orthorhombic $DyPO_4 \cdot H_2O$ was observed.

A facile solution–precipitation process for the preparation of complex $LaPO_4$ nanostructures via oriented-attachment of small nanoparticles was adopted by *Zhanli Chai et al.*[36] They could obtain nanostructures with different shapes, including spherical ones, flake-like ones, star-shaped ones and short nanorods when the molar ratio of La^{3+}:H_3PO_4 or additional ionic surfactants: H_3PO_4 was adjusted. $LaPO_4$ nanostructures with different shapes (*Figure 5*) could be obtained by changing the molar ratio of La^{3+}:H_3PO_4.

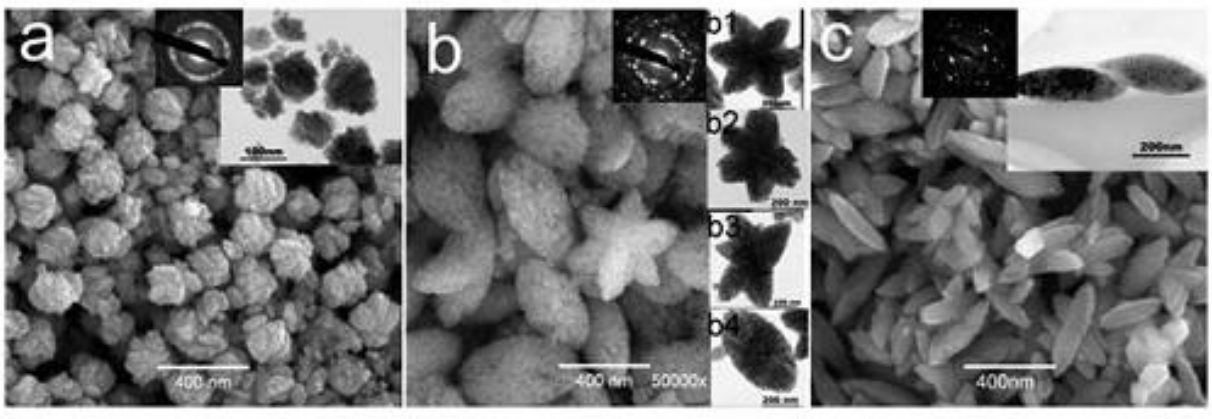

Figure 5) SEM images and TEM insets of $LaPO_4$ nanostructures obtained in a typical synthesis with different volumes of H_3PO_4–EG (*New J. Chem*, 33, **2009**, 1657)

Rare earth phosphate powders (Re=La, Ce or Y) were synthesized from an aqueous precipitation method by *Lucas and co-workers*.[37] The powders were prepared by an aqueous precipitation by adding rare earth chloride solution to either phosphoric acid or diammonium hydrogen phosphate. The pH was maintained at a constant value by the addition of an ammonium hydroxide solution. After the complete addition of the rare earth solution, the suspension was ripened for various times and the resulting precipitate was washed with distilled water, centrifuged three times**,** and finally dried at 80 °C. The precipitate crystallized in the hexagonal structure of rabhdophane $RePO_4$ $0.5H_2O$ and were having specific surface area of 80 m^2/g and the grains were agglomerated needle-like nanosized crystals.

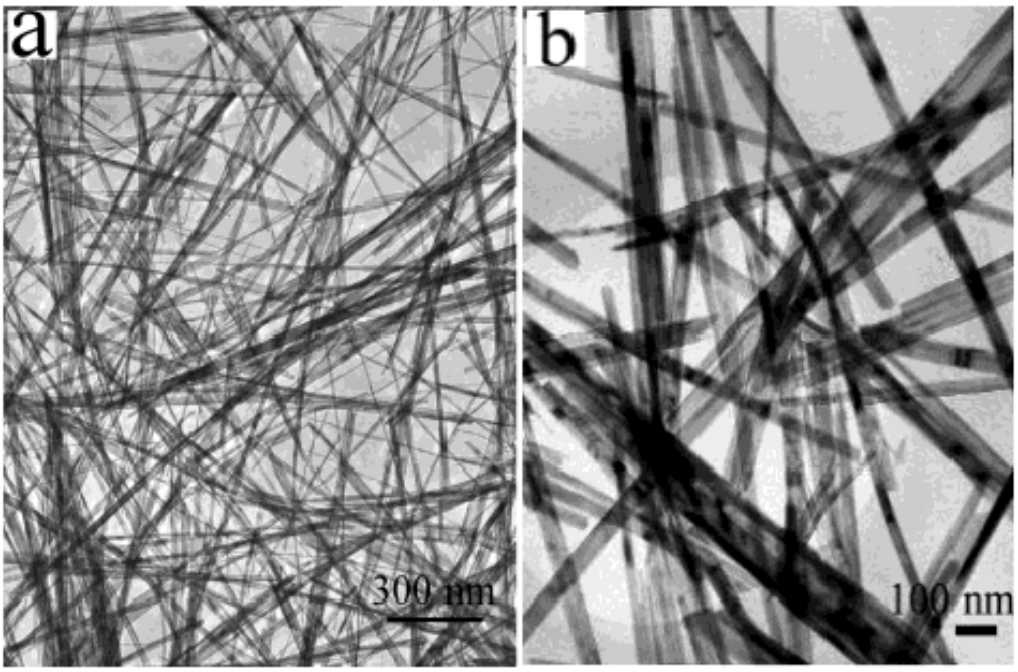

Figure 6) TEM images of the obtained hexagonal $LaPO_4$ (*J. Am. Chem. Soc.* **2003**, 125, 16025 - 16034)

Lanthanide orthophosphate crystals $LnPO_4$ crystallized with hexagonal or tetragonal structure depending on the ionic radius of the lanthanide ions. $LnPO_4$ (Ln= La→Dy) nanowires/nanorods crystallize in the hexagonal form, while (Ho → Lu, Y) $LnPO_4$ materials

exist in the hexagonal structure when synthesized using low-temperature hydrothermal conditions. From the X-ray analysis, the intensity of the (200) peak is found much stronger than those of the other peaks, which is different from bulk hexagonal $LnPO_4$ (Ln= La →Dy). This indicates that the obtained $LnPO_4$ (Ln= La→Dy) nanowires/nanorods grow preferentially along the [001] direction (the c axis). Based on the crystal structure of $LaPO_4$, *Fang et al.*[38] suggests that the growth of $LaPO_4$ nanowires is determined by its highly anisotropic character along the c axis.

Gunnar Buhler used microwave irradiation for synthesizing highly luminescent $LaPO_4$: Ce, Tb nanocrystals based on the use of ionic liquids (ILs) as reaction media.[39] During the synthesis, a solution of rare earth chlorides in Ionic Liquid of tributyl methyl ammonium triflylimide and a co solvent (for example, ethanol, dimethyl formamide (DMF), dimethyl sulfoxide (DMSO), or pyridine) was added to the phosphate precursor (phosphoric acid) similarly dissolved in the IL and a co solvent, at 70 °C. The IL was selected from a variety of candidates for its extraordinary thermal and chemical stability. Precipitation of $LaPO_4$: Ce, Tb occurs immediately, as indicated by the appearance of a slight opalescence. The crystallinity of the preformed nanoparticles was enhanced by heating the dispersion to 300 °C within 10 s in a microwave oven. After centrifugation and washing, the nanocrystals were collected. Transmission electron microscopy (TEM) images reveal spherical to slightly ellipsoidal particles with sizes of 9–12 nm and corresponding electron diffraction pattern and the lattice fringes observed in high-resolution images indicate that the particles are crystalline.

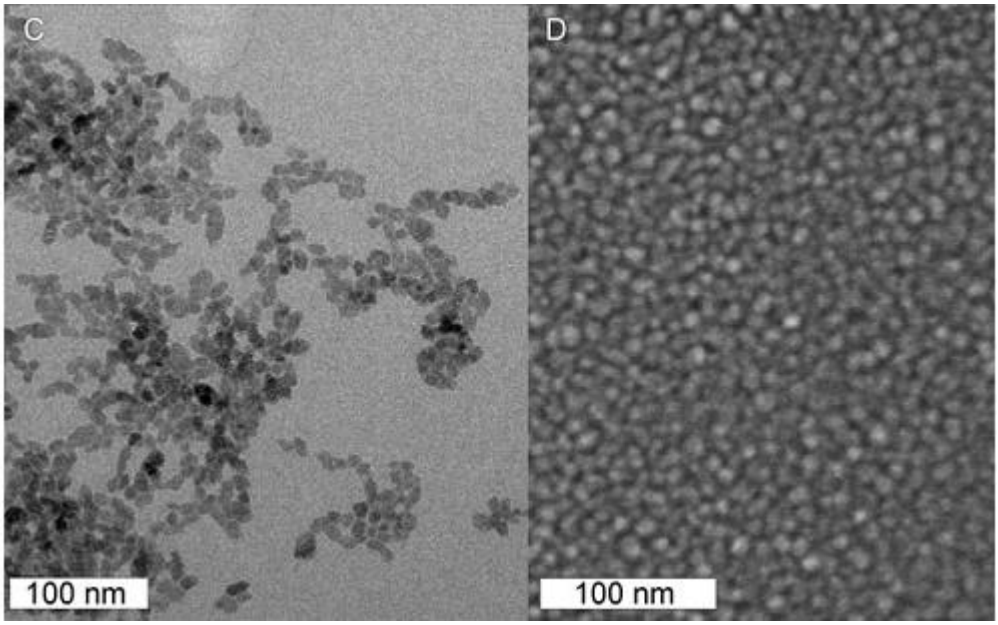

Figure 7) C) TEM and D) SEM images of as-prepared $LaPO_4$: Ce, Tb nanocrystals (*Angew. Chem. Int. Ed*. **2006**, 45, 4864 –4867)

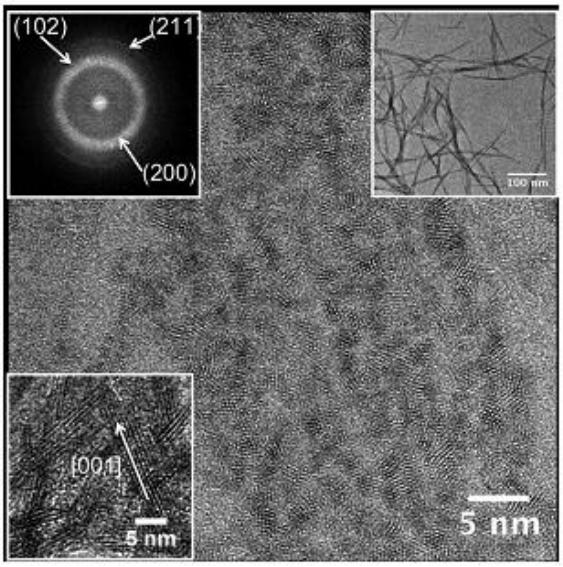

Figure 8) TEM micrographs of 1D nanowires of $LaPO_4$: Ce: Tb (*Dalton Trans*., **2011**, 40, 3122–3124)

Jie Fang et al. [40] developed a room temperature synthetic protocol to obtain high yields of crystalline lanthanide phosphate nanowires using a rotating tube microfluidic platform. They made use of the high surface energy SWCNTs as nucleation centres to potentially grow, stabilize and isolate well defined nanocrystals monomers before the fusion process into 1D

nanowires. They demonstrated that quantum yields close to the value of the bulk material for a nanocrystalline phosphor material can be achieved without the use of a passivating shell in the nanoscale.

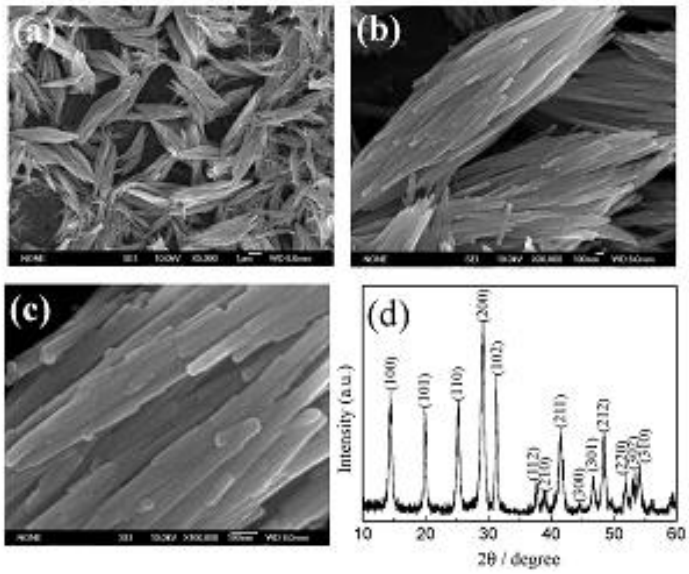

Figure 9) FE-SEM and XRD pattern of $LaPO_4$ (*Crystal Growth & Design*, **2007,** 7(11), 2305-2309)

In a typical *pechini* [41] process adopted by *Aleksandra Matraszek* and group for the synthesis of lanthanum phosphate, the citric acid and ethylene glycol were mixed with solutions of lanthanide nitrates in the following molar ratios: citric acid: La^{3+}—2:1, citric acid: ethylene glycol —1:1. The obtained solutions were heated at 80 °C under stirring until a viscous liquid was obtained. The $NH_4H_2PO_4$ in appropriate molar ratio was added under stirring. The heating was continued until foam appeared. Samples were then put in electric drier for 20 h at 120 °C. Further calcination of dried gels was per formed in a furnace preheated at 500 °C. The lanthanum, cerium, and praseodymium orthophosphates prepared by the above method were characterized by much smaller average crystallite size (about 16 nm) in comparison with that of the orthophosphates produced through precipitation from a phosphoric acid

solution at a temperature of 80 °C. Further increased mesopores and specific surface area were obtained.

A direct precipitation technique was used by *T.R. Herrero* [42] rabhdophane $LaPO_4$ was synthesized by mixing an aqueous solution of either 0.1 M $La(NO_3)_3.9H_2O$ or Nd $(NO_3)_3.9H_2O$ with an aqueous solution containing 0.1 M KH_2PO_4 and 0.09 M KOH.

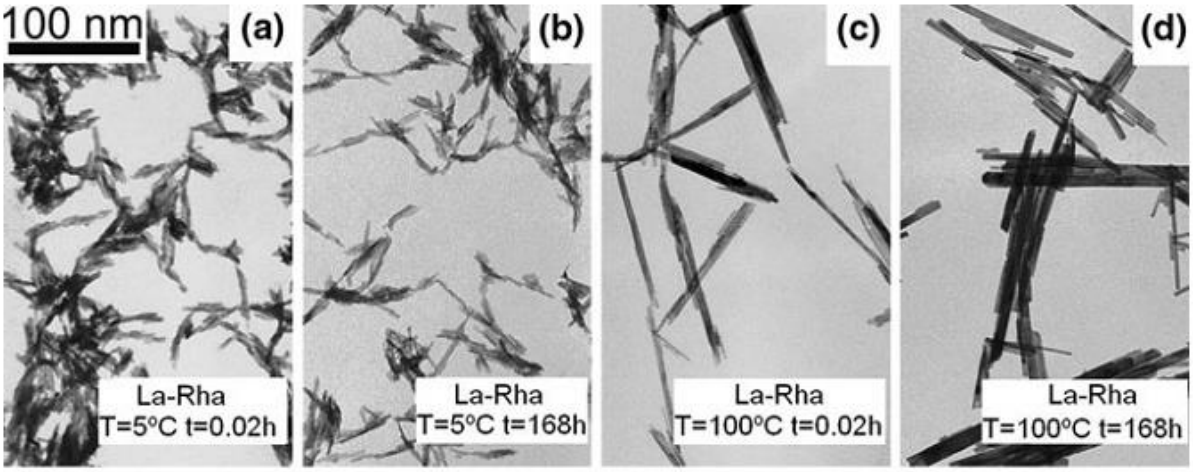

Figure 10) TEM micrographs of La- rabhdophane synthesized at different temperatures (*J. Nanopart. Res.* 13, **2011**, 4049)

More Recently *Yan li et al.* [43] successfully synthesized luminescent hydrogel $LaPO_4:Eu^{3+}$ by using insitu polymerization. The $LaPO_4$ hydrogel showed very high emission intensities than reported from conventional methods. *Xiao* synthesized hydrated and dehydrated Eu^{3+}/Tb^{3+}-doped $RePO_4$ (Re5Y, La, and Gd) nanophosphors via a solvo-thermal technology where they altered the temperature and solvents.[44] X-ray powder diffraction and scanning electron microscopy reveal that they have different structures and different morphologies.

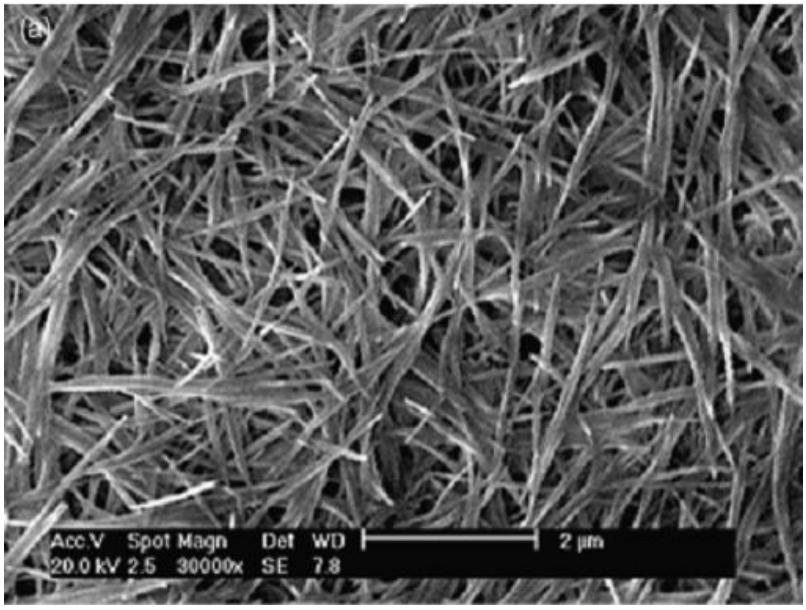

Figure 11) Scanning electron microscope image of hydrothermal synthesis - 1 day $LaPO_4$ nH_2O:$Eu3^+$ (J. Am. Ceram. Soc., 93 (**2010**) 2195

Fisher et al. successfully employed the sol gel template assisted synthesis method to produce $LaPO_4$: Eu nanotubes with sizes ranging from 20 to 200 nm.[45] Powder X-ray diffraction data indicate that the untemplated dried bulk powder is a mix of hexagonal and monazite phases, whereas the dried and sintered bulk powder is a pure monazite phase. *Guo et al.* prepared lanthanum phosphate using a sol gel route in both ethanolic and aqueous media.[46] The $LaPO_4$ gels prepared using this technique gave macro crystalline $LaPO_4$.

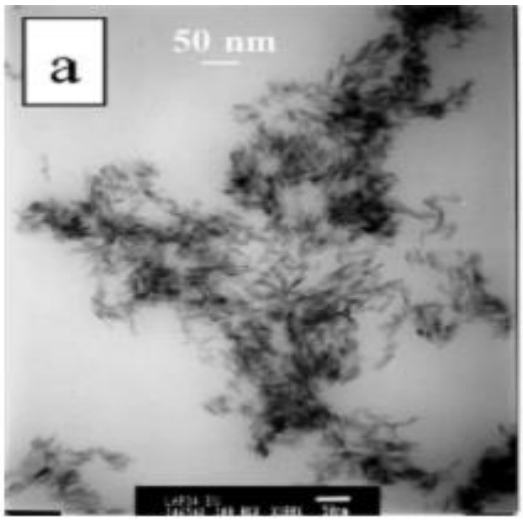

Figure 12) TEM image of $LaPO_4$: Eu bulk powder dried at 70 °C, showing rod like morphology (*J. Phys. Chem. C* 112, **2008**, 1901)

Rajesh et al. successfully employed room-temperature aqueous sol–gel process for Synthesis of rod-shaped nanocrystalline lanthanum phosphate.[47] Transmission electron microscopy shows that the sol and gel particles have rod-shaped morphology and comparable particle sizes. Precursor gel calcined at 400 °C possessed high specific surface area of 100 m^2/g, when measured using Brunauer–Emmett–Teller (BET) nitrogen-adsorption analysis. The results obtained from ammonia temperature-programmed desorption measurements, showed that the density of Lewis acid sites was four times higher than ever reported in the case of lanthanum phosphates.

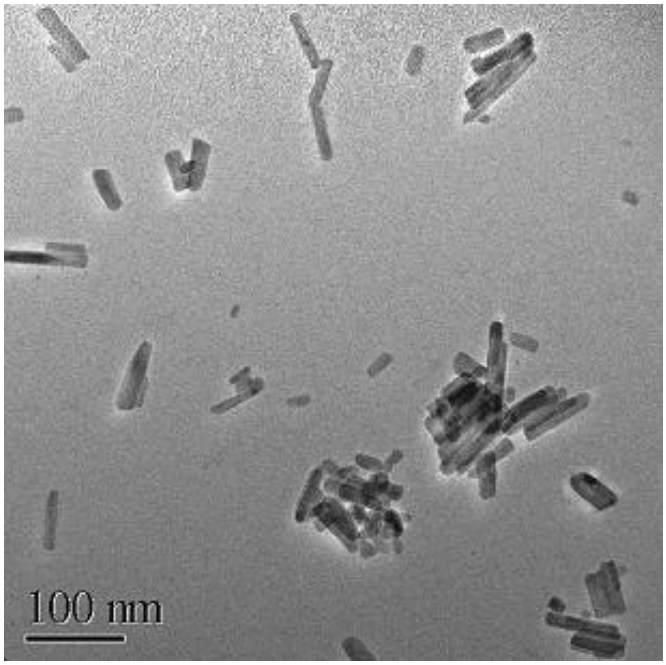

Figure 13) TEM of the lanthanum phosphate gel calcined at 70 °C (*Adv. Func Mater,* 17, **2007**, 1682)

Analysis of the reported literature available for the synthesis of lanthanum phosphate shows that most of the methods involve multiple steps, high synthesis temperature/pressure, and the products formed were in in the size range of micron/submicron range/size. Sol gel approach carried out in aqueous medium involving simple precipitation- peptization – gelation is not widely reported.

Maintaining stoichiometry of Lanthanum Phosphate ($LaPO_4$) has been one the problems reported which affects seriously its high temperature stability[8] and thereby limiting the utilisation of $LaPO_4$ in high temperature applications.[48] Synthesis of $LaPO_4$ by employing a modified sol gel process has been very effective to overcome such problem.[47]

Scaling up of the process for lanthanum phosphate particles starting from lanthanum nitrate has certain difficulties, especially with respect to safe disposal of nitrate containing effluents. The accumulation of nitrates in water is already well known to cause environmental problems like eutrophication.[49] For reducing the impact that is caused by disposal of effluents produced during the synthesis processes, alternative starting materials need to be identified, where the effluents or by-products are putting less pressure on the environment and one option is certainly lanthanum chloride. A suitable technique for the synthesis of nanosize lanthanum phosphate particles from lanthanum chloride precursors was found appropriate even for further scaling up for commercial purposes.

1.4 Lanthanum Phosphate based composites

Lanthanum phosphate ($LaPO_4$) has been realised as a potential material over the years because of its excellent thermal phase stability, high melting temperature, low thermal conductivity/diffusivity, thermal expansion coefficient comparable to common ceramic oxides such as alumina and zirconia, chemical inertness and hydrophobic character. Therefore, rare earth phosphates, especially lanthanum phosphate were investigated as a suitable interphase as well as reinforcement material for ceramic composites.[50, 51]

At higher temperature, $LaPO_4$ coatings behave as weak interface.[52] further, lanthanum phosphate has been found to be machinable[53] and this has supplemented its application in machinable ceramic composites. The layered structure and weak bonding nature of $LaPO_4$

with refractory oxides such as Al_2O_3, ZrO_2 and mullite help to prevent crack growth by interfacial debonding and crack deflection during machining.[54] Celaletdin Ergun reported lanthanum phosphate composite with hydroxyapatite or tricalcium phosphate for orthopedic applications.[55] $LaPO_4$ was used in alumina-lanthanum phosphate composites in order to control the grain growth effects.[56] Lanthanum phosphate is reported to be an effective constituent in thermal barrier coating (TBC) material due to its low thermal conductivity, matching coefficient of thermal expansion with conventional TBC materials like zirconia and high corrosion resistance.[57]

Synthesis of lanthanum phosphate based composites has been reported through various methods such as coating method[58], chemical precipitation[59], liquid precursor infiltration[60], mechanochemical[61] and sol gel.[62] In the synthesis of ceramic matrix composites like alumina – lanthanum phosphate composite, the alumina fiber is coated with precursor slurry through dip coating.[63] A colloidal route was adopted by *Boakye and co-workers* [64] to prepare colloidal rabhdophane phase lanthanum phosphate using lanthanum nitrate and phosphoric acid for coating on SiC and alumina fibers before fabrication of composites.

1.4.1 $LaPO_4$-Y_2O_3 Composite

Among the rare earth oxides, yttrium oxide is a thermodynamically stable, high temperature ceramic material and has been used as additive to zirconia for stabilizing tetragonal phase[65], in transparent ceramics[66], as host material for $Eu^{3+,}$ Tb^{3+}, $Er^{3+,}$ Yb^{3+}, Tm^{3+} ions in phosphor materials, and as a sintering aid to enhance densification[67] of ceramic systems during sintering. Yttrium oxide is also used in enhancing photoelectrical performance in dye – sensitized solar cells.[68]

A few properties of yttria certainly match with those of lanthanum phosphate. Yttrium oxide is also stable as lanthanum phosphate at high temperatures having high melting points of ~ 2410 °C and ~ 2072 °C respectively. Similarly Y_2O_3 has a thermal expansion coefficient (8.1 X 10^{-6} /°C) [69] close to that of $LaPO_4$. Theoretical density of $LaPO_4$ and Y_2O_3 are nearly identical and the values are 5.06 and 5.03 g/cc respectively. Yttrium oxide has higher hardness of about 10 GPa[70] compared to about ~ 5 GPa reported for lanthanum phosphate. Lanthanum phosphate – yttria composite is expected to result in many advantageous features such as controlled grain growth and fine microstructure. Further Y_2O_3 grains may impart synergistic effects of higher hardness and strength at higher temperatures. Y_2O_3 is often used as coatings in metal melting operations due to low reactivity and hence the composite may perform more efficiently.[71]

Lanthanum phosphate – yttrium oxide nano composite is not reported earlier. The properties of lanthanum phosphate especially the mechanical strength and hardness at high temperatures could be improved by the addition of yttria. Aqueous sol-gel process for the preparation of $LaPO_4$-Y_2O_3 composite is proposed where intimate mixing of the constituents is ensured by controlling the zeta potential (surface charge) in the precursor.

1.4.2 $LaPO_4$ - ZrO_2 Composite

Zirconia (ZrO_2) is a well-known and widely used material for many applications ranging from electrodes[72], fuel cells[73], catalysts [74,75] and as structural component. ZrO_2 is employed in TBCs and composites with its low thermal conductivity (3.0 W/mK at room temperature and 2.17 W/mK at 1000 °C) [76] and has a coefficient of thermal expansion value of $11x10^{-6}$/K, which is marginally higher when compared to that of Al_2O_3 as well as $LaPO_4$ ceramics. Also at low temperatures (below 1170 °C) the material transforms to the monoclinic structure. The

transformation from tetragonal to monoclinic is rapid and is accompanied by a 3 to 5 percent volume increase that causes extensive cracking in the material. This behaviour limits the mechanical properties of fabricated components and brings out the need for stabilization for high temperature application. Usual stabilizing agents are CaO/MgO and Y_2O_3. Yttria Stabilized Zirconia (YSZ) is reported to perform as thermal barrier coatings (TBC) and is used to protect as well as insulate hot-section metal components in advanced gas-turbine and diesel engines.[77] But again it has also got the major limitation of being used at much higher temperatures with the metastable tetragonal (t') phase partitioning by diffusion into the equilibrium tetragonal (t) and cubic phases (c) at high temperatures where the former will transform into monoclinic phase (m) during cooling, resulting disintegration and thereby damaging the coatings.[78] Of the available reports on the processing methods for synthesizing of YSZ, one problem is the inability to obtain the oriented grains there by causing destabilization of the material at high temperatures. Introduction of elongated particles as composite could be useful in obtaining the desired microstructure.

On the other hand, $LaPO_4$ possesses rod like morphology and has excellent high temperature properties while has tendency for grain growth above 1450 °C. This needs to be controlled to get a fine grained microstructure. Properly designed composite microstructure involving rod like particles of $LaPO_4$ compatible with zirconia is expected to improve the overall thermal properties. Sol gel based technique is used for the synthesis of $LaPO_4$- ZrO_2 composite and the results indicate the possibility of using $LaPO_4$- ZrO_2 as efficient thermal ceramics.

1.5 Lanthanum phosphate for biological/environmental applications.

Lanthanum phosphate, by virtue of its high chemical stability coupled with low toxicity and extremely low water solubility is reportedly suitable for a variety of applications in catalysis

and bio-functionalization.[31, 79] Further, lanthanum phosphate as promising sorbent material for uranium by a mechanism involving the formation of a mononuclear, polydentate surface complex[80] is also reported. Rare earth doped lanthanum phosphate phosphors are demonstrated to be candidate materials for bio-probe applications. Taking advantage of the excellent properties, porous lanthanum phosphate could be used for adsorbing harmful ions from water sources. Colloidal processing technique is reported for the synthesis of porous $LaPO_4$ for the first time, which could act as novel adsorbents of harmful perchlorate ions from drinking water sources.

1.6 Lanthanum phosphate and composites as non-reactive surfaces against molten metals.

As already seen from reports, $LaPO_4$ has very high thermal stability and melting point above 1900 °C. $LaPO_4$ based composites are reported to be useful in high temperature reactive environments as coatings.[10] *Sucharita Sinha et al.* suggest that a combination of a thick plasma based coating followed by a PLD based thin overcoat, both of lanthanum phosphates, would result in an effective protective coating that is dense enough to accomplish the function of isolating the substrate from a corrosive environment.[81] Ananthapadmanabhan and co- workers showed that $LaPO_4$ is thermally stable up to its melting point and also is resistant towards attack by molten uranium.[82] Adherent coatings of $LaPO_4$ could be deposited onto various substrates by atmospheric plasma spray technique.

This non reactivity can further be extended to develop suitable mould release agents for metal casting and moulding that are easy to synthesize and are relatively of low costs compared to existing prior art articles. No reports are also available for shaping of lanthanum phosphate to monoliths/ crucibles for metal melting applications. Hence the non-reactivity of lanthanum

phosphate with the molten metals relates to the process of preparation of lanthanum phosphate based coatings and monoliths as non-reactive surfaces for molten metals for high temperature applications such as mould release coatings and crucibles for metal casting.

1.7 Machinability of Lanthanum phosphate

Lanthanum phosphate being a soft ceramic is indicated to be easily machinable. However no detailed investigation is reported in this area. Machining effects of $LaPO_4$ and $LaPO_4$ composite using water jet cutting technique was conducted. A water jet cutter is an industrial tool capable of cutting a wide variety of materials using a very high-pressure jet of water, or a mixture of water and an abrasive substance.

1.8 Sol – Gel technique for material synthesis

Sol gel is a wet chemical synthesis used to synthesize nanomaterials which contains an intermediate stage called sol and a gel state. [83] Sol gel process is known for its superior quality to other preparation methods with respect to uniformity in mixing of components and the perfect homogeneity of phases in the final product. Sol-gel synthesis can be carried out at normal temperature and the process ensures the homogeneity of the product formed. Using this technique the applications using coatings to powders can be achieved in a single scheme as provided in the figure below.

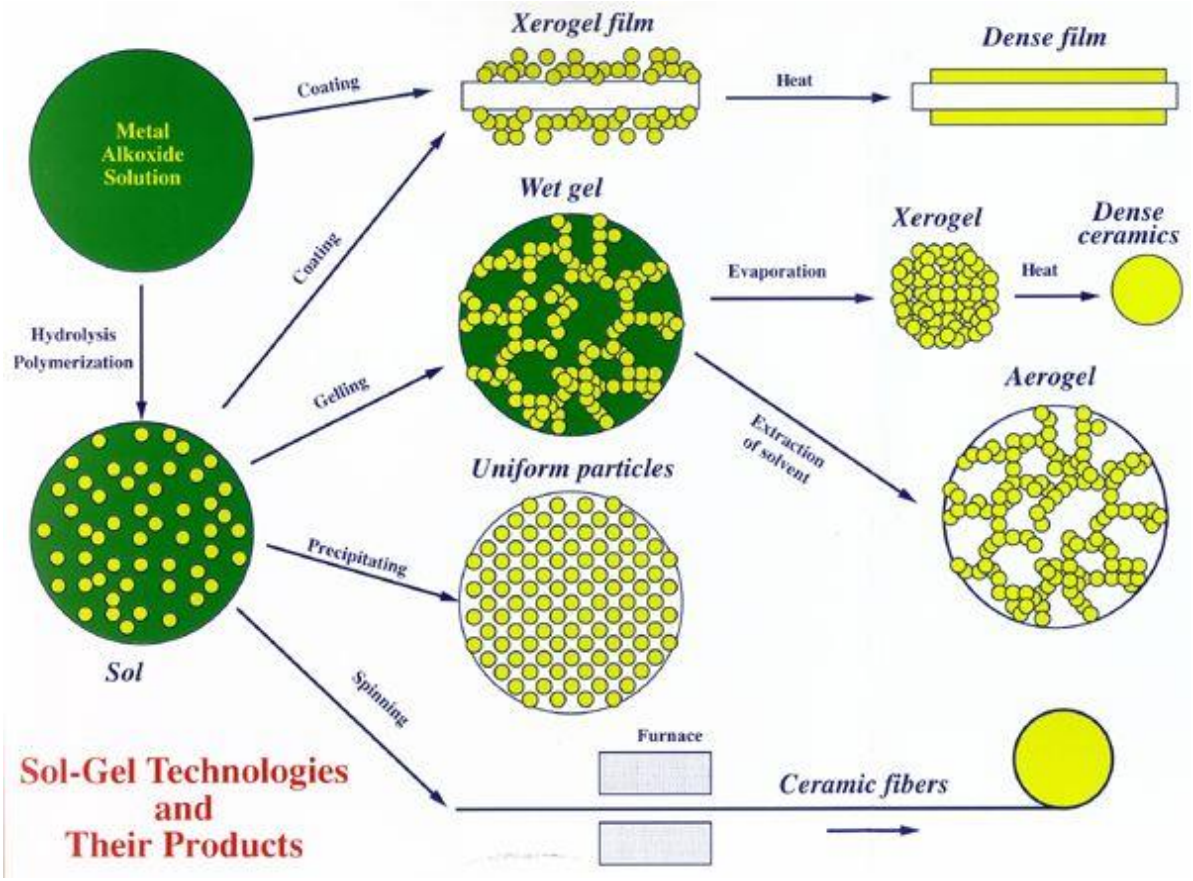

Schematic illustration showing the overview of sol-gel process with different steps and applications

Sol-gel processing of inorganic ceramic and glass materials began as early as the mid-1900s with *Ebelman,*[84] and *Graham*'s studies on silica gels**.** The motivation for sol-gel processing is primarily the potentially higher purity and homogeneity and the lower processing temperatures associated with sol-gels compared with traditional glass melting or ceramic powder methods**.** During the past decade there has been an enormous growth in the interest in the sol-gel process. This growth has been stimulated by several factors. *Yoldass* showed that large monolithic pieces of alumina could be made by sol-gel methods. On the basis of *Kistler's* early work, several teams have produced very low density silica monoliths, called aerogels, by hypercritical point drying.[85] *Zarzycki, Prassas, and Phalippou* demonstrated that

hypercritical point drying of silica gels could yield large fully dense silica glass monoliths. These demonstrations of potentially practical routes for production of new materials with unique properties coincided with the growing recognition that powder processing of materials had inherent limitations in homogeneity due to difficulty in controlling agglomeration.[86]

1.8.1 The sol- gel process

As the name implies, the evolution of inorganic networks through the formation of a colloidal suspension occurs first which is called **sol** followed by gelation into a continuous liquid phase which is the **gel**. [84] The basic mechanism of sol- gel process involves usually two major processes, hydrolysis and condensation respectively. The hydrolysis generally leads to the formation of a sol and condensation yield the gel state. **A sol** is a dispersion of solid particles in liquid phase in which the particles remain suspended by Brownian motion (or Brownian Diffusion). Sols are classified as lyophobic if there is a weak solvent/particle interaction and lyophilic if the solvent/particle interaction is strong**.** In order to counter the van der Waals interactions which cause agglomeration of small particles repulsive forces must be established by:

A) Electrostatic repulsion by adsorption of charged species onto the surface of the particles, repulsion between the particles will increase and agglomeration will be prevented which is most important for colloidal systems.

B) Steric hindrances by adsorbing a thick layer of organic molecules, the particles are prevented from approaching each other reducing the role of the van der Waals forces. This works well in concentrated dispersions. This is usual for nano materials particle being covered by organic layer.

A gel is a form that contains a continuous solid skeleton enclosing a continuous liquid phase. Gels form from particulate sols when attractive dispersion forces cause them to stick

together in such a way as to form a network.[83] The formation of gel influences the structure, pore volume and gel pore size and depends on the factors like pH, concentration of the medium as well as the chemical nature of the precursor. Aging of a gel is the long range maintenance along with the pore liquid. Four processes can occur, singly or simultaneously, during aging including polycondensation, syneresis, coarsening, and phase transformation.

The shrinkage of the gel and the resulting expulsion of liquid from the pores is called syneresis.[87] Syneresis in alcoholic gel systems is generally attributed to formation of new bonds through condensation reactions, which increases the bridging bonds and causes contraction of the gel network. In aqueous gel systems, or colloidal gels, the structure is controlled by the balance between electrostatic repulsion and attractive van der Waals forces. Therefore, the magnitude of shrinkage is controlled by additions of electrolyte.

The sol-gel process can be aqueous or alkoxide based, and this is based on the nature of precursors used for synthesis. Aqueous route has aqueous solutions of inorganic salts as precursors while non-aqueous route has metal alkoxides as precursors. Aqueous route is also known as the inorganic route involves the formation of a hydrated species from aqueous solutions of inorganic salts by pH adjustment and by increasing the temperature or changing the oxidation state. This could be used for synthesis of bulk powders with a proper control on experimental conditions so as to get materials with desired morphology. Alkoxide based process involves two main reaction types, hydrolysis and condensation. Here the chemical aspects plays an important role as the reactivity of metal alkoxides towards hydrolysis and condensation depends on the electronegativity of the metal atom, its ability to change the coordination number and also on the molecular structure of the alkoxide used.

1.8.2 Advantages of Sol-Gel Technique

- ✓ Can produce high purity products because the organo-metallic precursor of the desired ceramic oxides
- ✓ Can be mixed, dissolved in a specified solvent and hydrolysed into a sol, and subsequently a gel, the composition can be highly controllable
- ✓ Can produce thin bond-coating to provide excellent adhesion between the metallic substrate and the top
- ✓ Can produce thick coating to provide corrosion protection performance.
- ✓ Can easily shape materials into complex geometries in a gel state.
- ✓ Can have low temperature sintering capability, usually 200- 600 °C less than normal.
- ✓ Can provide a simple, economic and effective method to produce high quality coatings.
- ✓ Can ensure the higher purity of the product and better homogeneity of the reactants.
- ✓ Can get coatings from composite precursors for multifunctional coatings

Thus sol gel process evolves as a low temperature wet chemical method for the synthesis of inorganic nano materials. Synthesis of lanthanum phosphate and its composites using the room temperature sol gel process could be the method that could give the better stoichiometry and purity that is essential for developing materials for high temperature as well as functional applications. With the variety of organic, inorganic, and bio-organic materials that could be used in developing innovative and novel hybrids and composite materials we can realize that the potential of sol–gel technology is immense.[88]

1.9 Summary of literature- Gaps in current information and proposed research work

A detailed analysis of the literature shows that the synthesis and application of lanthanum phosphate has attracted increasing attention due to the excellent phase stability as well as

other properties. Various synthesis techniques reported for rare earth phosphate, especially lanthanum phosphate particulates include solid state reaction, precipitation, hydrothermal, solid–liquid reaction and colloidal synthesis. Further Lanthanum phosphate was characterized for high temperature stability, thermal conductivity, catalytic and photoluminescence properties, radioactive waste immobilization, and as excellent host to photoluminescent materials as well as in bio imaging and bio functionalization. Certain mechanical properties as well as preparation of composites are also covered in the literature. Investigations on the most promising properties are carried out in rare earth phosphates.

The reported synthesis techniques for lanthanum phosphate particles cover the particle size in micrometre or submicron meter range. Further stable nanoparticle suspensions and lanthanum phosphate having excellent stoichiometry are not covered. Particulate colloidal suspensions derived through hydrolysis – peptization route, stable for long time through strict control of surface charge are required for functional transparent coatings and no detailed report on such synthesis is available.

Although high temperature phase stability of lanthanum phosphate is studied, synthesis and properties of lanthanum phosphate composites are reported seldom. Only scanty reports are available on the reactivity of $LaPO_4$ with molten metals. The hydrophobic behaviour of lanthanum phosphate is not reported. Hence the present work addresses a few of the research challenges such as synthesis of nanosize particles of $LaPO_4$ and nano composites by aqueous sol-gel route, plasma sprayed coatings on steel substrates, investigation of reactivity with molten metals, wetting behaviour of $LaPO_4$ with water and investigation on the applicability $LaPO_4$ in biological systems. The thesis specifically covers a detailed study on the synthesis of $LaPO_4$ as well as $LaPO_4$- Y_2O_3 and $LaPO_4$- ZrO_2 composites using a modified aqueous sol

gel process. $LaPO_4$ functional coatings on glass surfaces were made and characterized. Thermal stability as well as thermal conductivity of $LaPO_4$ and composites is investigated. Biocompatibility of $LaPO_4$ is further extended to the possibility of removing harmful ions from drinking water sources. The following aspects are covered in detail.

- Synthesis of nano size lanthanum phosphate and composites based on Yttria (Y_2O_3) and Zirconia (ZrO_2) are carried out through aqueous sol-gel route. Morphological features of the particulates along with thermal properties are evaluated detail. The study on the applicability of $LaPO_4$, composites for developing coatings using plasma spray is investigated. $LaPO_4$-Y_2O_3 nano composite is studied as a nonreactive surface against molten uranium metal jointly with Bhabha Atomic Research Centre (BARC), Mumbai. Non-reactivity and non-wettability with some metals like Al, Zn and Ag with $LaPO_4$ are covered in the thesis.

- The inherent hydrophobic nature of $LaPO_4$ both as a monolith and as nano coatings is investigated. Nano coatings of $LaPO_4$ are developed over glass surfaces using dip coating technique. The contact angle values for the coatings and monolith with water are analysed. $LaPO_4$ reactivity with molten metals is investigated in detail.

- Porous bodies of $LaPO_4$ have been designed and prepared using an environmentally benign colloidal processing. The applicability of these monoliths for adsorbing harmful ions from water resources is investigated. The study on suitability of $LaPO_4$ monoliths and surfaces favourable for growth of specific perchlorate reducing bacteria is also envisaged.

- Structure - property correlation has been drawn in the case of hydrophobic and bio related behaviour of lanthanum phosphate.

REFERENCES

1. Y. Hikichi, K. Hukuo, J. Shiokawa, *Bull. Chem. Soc. Jpn.*, 51(12), **1978**, 3645.

2. Y.P. Fang, A.W. Xu, R.Q. Song, H.X. Zhang, L.P You, J.C. Yu, H.Q. Liu, *J. Am. Che. Soc.* 125,**2003**,16025.

3. R. C. L Mooney, *Acta Crystallogr.* 3, **1950,** 337.

4. G. W. Beall, L. A. Boatner, D. F. Mullica and W. O. Milligan, Z. Znorg, *Nucl. Chem 43,* **1981**,101.

5. D. F. Mullica, W. O. Milligan, D. A. Grossie , *Inorgania Chimica Acta,* 95, **1984,** 231**.**

6. D. F. Mullica, D. A. Grossie, L. A. Boatner, *J. Solid State Chem.,*58,**1985**,71.

7. A. Du, C. Wan, Z. Qu, W. Pan, *J. Am. Ceram. Soc*., 92 (11), **2009,** 2687.

8. Y. Hikichi, T. Nomura, *J. Am. Ceram. Soc*., 70 (10), **1987**, C-252.

9. P. E Stone, E.P Egan, J.R Lehr**,** *J. Am. Ceram. Soc*., 39, **1956**, 89.

10. Morgan Et al., *US pat.* (**1997**) 5 665 463.

11. M. R. Winter and D. R. Clarke, *J. Am. Ceram. Soc.*, 90 (2), **2007,** 533**.**

12. A. Du, C. Wan, Z. Qu, W. Pan, *J. Am. Ceram. Soc*., 92 (11), **2009,** 2687.

13. Y.Hikichi, T.Ota, T.Hattori, *Miner.j,* 19 (3), **1997,** 123.

14. Y. Hikichi, T. Nomura, Y. Tanimura, S. Suzuki, M. Miyamoto, *J. Am. Ceram. Soc.*, 73 (12), **1990**, 3594.

15. P. E. D. Morgan, D. B. Marshall, *J. Am. Ceram. Soc.*, 78, **1995**, 1553.

16. J. B. Davis, D. B. Marshall, R. M. Housley, P. E. D. Morgan, *J. Am. Ceram. Soc.*, 81, **1998,** 2169.

17. D.G Grossman, *J. Am. Ceram. Soc.*, 55 (9), **1972**, 446.

18. M.W Barsoum, T.EI Raghy**,** *J. Am. Ceram. Soc.*, 79 (7), **1996**, 1953.

19. W. Min, K. Daimon, T. Matsubura, Y. Hikichi, *Mater. Res. Bull.*, 37, **2002,** 1107.

20. S. Phadke, J. C. Nino, M. S. Islam, *J. Mater. Chem.,* 22, **2012,** 25388.

21. N. Kitamura, K. Amezawa, Y. Tomii and N. Yamamoto, *Solid State Ionics,* 162-163, **2003**, 161.

22. B. Narasimha, R. N. P. Choudhary, K.V. Rao, *J.Mater.Sci*, 23 **(1988),** 1416.

23. Y. Takita, K. Sano, T. Muraya, H. Nishiguchi, N. Kawata, M. Ito, T. Akbay , T. Ishihara, *Appl. Catal., A,* 170, **1998**, 23, K. Ramesh, J. Zheng, E.G.Y. Ling, Yi-Fan Han, A. Borgna, *J. Phys. Chem. C* 113, **2009,** 16530, H. Furuno, T. Kambara, Y. Tanaka, T. Hanamoto, T. Kagawa, J. Inanaga, *Tetrahedron Letters* 44, **2003**, 6129.

24. R. Riwotzki, H. Meysammy, H. Schnablegger, A. Kornowski, M. Hasse, *Angew. Chem. Int. Ed*., 40, **2001**, 573.

25. M. Yu, J. Lin, J. Fu, Y.C Han, *Chem. Phy. Letts*., 371, **2003**,178.

26. P. Schuetz, F.Caruso, *Chem. Mater.*, 14, **2002**, 4509.

27. M. Yang, H. You, K. Liu, Y. Zheng, N. Guo, H. Zhang , *Inorg. Chem., 49* (11), **2010**, 4996.

28. V. Buissette, M. Moreau, T. Gacoin, J-Peirre Boilot, *Adv. Funct. Mater*., 16, **2006**, 351.

29. J. Shen, L-Dong Sun, C-Hua Yan, *Dalton Trans.*, 42, **2008**, 5687.

30. F. Meiser, C. Cortez, F. Caruso, *Angew. Chem.* 116, **2004**, 6080.

31. J. Woodward, S. J. Kennel, A. Stuckey, D. Osborne, J. Wall, A. J. Rondinone, R. F. Standaert, S. Mirzadeh, *Bioconjugate Chem*. 22, **2011**, 766.

32. C. Guy, F. Audubert, J.E Lartille, T. Adocat, C. Fillet, *C.R Acad. Sci. Paris Phys.*,3, **2002**,827.

33. O. Terra, N. Clavier, N. Dacheux, R. Podor , *New J. Chem*., 27, **2003**, 957.

34. W. Ruigang, P. Wei, C. Jian, F. Minghao, C. Zhenzhu, L. Yongming, *Mater. Chem. and Phy.*, 79, **2003**, 30.

35. R Kijowska, *J. Mater. Sci.*,38, **2003**, 229.

36. Z. Chai, L. Gao, C. Wang, H. Zhang, R. Zheng, P. A. Webley , H. Wang, *New J. Chem.*, 33, **2009**, 1657.

37. S. Lucas, E. Champion , D. Bregiroux, D. Bernache- Assollant, F Audubert, *J. Solid State Chem.*, (4-5), **2004**, 1302

38. Y.-Ping Fang, A-Wu Xu, R-Qi Song, H-Xin Zhang, L-Ping You, J.C. Yu, H-Qin Liu, *J. Ame Chem Soc.*, 125, **2003**, 16025.

39. G. Buhler, C. Feldmann, *Angew. Chem. Int. Ed*., 45, **2006**, 4864.

40. J. Fang, Y. Guo, G. Lu, C. L. Raston , K. S. Iyer, *Dalton Trans*., 40, **2011**, 3122.

41. A. Matraszek, E. Radominska, I. Szczygiel, *J. Therm. Anal. Calorim.*, 103**, 2011**, 813.

42. T. Roncal-Herrero, J. D. Rodrıguez-Blanco, E. H. Oelkers, L. G. Benning, *J. Nanopart. Res.* 13, **2011**, 4049.

43. Y.li, Y. Zheng, Q. Wang, W. Cai, Y. Yu, *Optical Materials*, 34(7), **2012**, 1019.

44. X. Xiao, B. Yan, *J. Am. Ceram. Soc.*, 93 (8), **2010**, 2195.

45. M. J. Fisher, W. Wang, P.K. Dorhout, E. R. Fisher, *J. Phys. Chem. C*, 112, **2008**, 1901.

46. Y. Guo, P. Wozniacki, A. Barkatt, *J. Mater. Res.*,11 (3), **1996**, 639.

47. K. Rajesh, P. Shajesh, O. Seidel, P. Mukundan, K. G.K.Warrier, *Adv. Func Mater*, 17, **2007**, 1682.

48. W Pan, S. R Phillpot, C. Wan, A. Chernatynskiy, Z. Qu, *MRS Bulletin*, 37, **2012,**917.

49. D. W. Schindler, Science, 4139, **1974**, 897.

50. D.B. Marshall, P.E.D Morgan, R.M Housley, JT Cheung, *J. Am. Ceram. Soc*., 81**, 1998**, 951.

51. P.E.D Morgan, D.B Marshall. *Mater. Sci. Eng., A-Structural Materials Properties Microstructure and Processing*, 162, **1993**, 15.

52. J.R. Mawdsley, D. Kovar, J.W. Halloran, *J. Am. Ceram. Soc*. 83, **2000**,802.

53. J.B. Davis, D.B. Marshall, P.E.D. Morgan, *J. Eur. Ceram. Soc*. 20, **2000**, 583.

54. a) K.K Chawlaa, H. Liu, RJ Janczak, S. Sambasivan. *J. Eur. Ceram. Soc*. 20, **2000,** 551. b) A. Majeed, L. Vijayaraghavan, S.K .Malhotra, R. Krishnamurthy, *Int. J. Mach. Tools Manuf.*, 48 ,**2008**, 40.

55. C. Ergun, *J. Mater. Process. Technol.*, 199, **2008**, 178.

56. R. Wang, W. Pan, J. Chen, M. Jiang, Y. Luo, M. Fang, *Ceram. Inter*., 29, **2003,** 19.

57. J.B. Davis, D.B. Marshall, R.M. Housley, P.E.D. Morgan, *J. Am. Ceram. Soc*., 81, **1998**, 2169.

58. Q. Zheng, X. Wang, X. Liu, Y. Yin, *Adv. Mater. Res.*, 79, **2009**, 2227**.**

59. C. Ergun, H. Liu, T.J. Webster, *Biomed. Mater. Res. Part A.*, 89, **2009**, 727.

60. Z. Zhou, Z. Yang, Q. Yuan, X. Li., *J. Rare Earths.*, 20**, 2002,**197.

61. W. Min, K. Daimon, T. Matsubara, Y. Hikichi., *Mater. Res. Bull.*, 37**, 2002**, 1107.

62. K. Rajesh, K.V. Baiju, M. Jayasankar, K.G. Warrier., *J. Am. Ceram. Soc*., 91, **2008**, 2415.

63. R.S. Hay, E. Boakye, M.D. Petry., *J. Eur. Ceram. Soc*., 20, **2000**, 589.

64. E.E. Boakye, P. Mogilevsky, T.A Parthasarathy, R.S. Hay, J. Welter, R.J. Kerans., *J. Am. Ceram. Soc*., 89, **2006**, 3475.

65. X. Zhu, Z. Lu, B. Wei, X. Huang, Y. Zhang, W. Su, *J. Power Sources*, 196, **2011**,729.

66. H. Yihua, J. Dongliang, Z. Jingxian, L. Qingling, *J. Am. Ceram. Soc.*, 92, **2009,** 2883.

67. I.K. Lloyd, *Ceram. Trans*., 221, **2010,** 115.

68. J. Wu, G. Xie, J. Lin, Z. Lan, M. Huang, Y. Huang, *J. Power Sources*, 195, **2010**, 6937.

69. C.E. Curtis, *J. Am. Ceram. Soc.*, 40, **1957**, 274.

70. S. Erdei, R. Roy, G. Harshe, H. Juwhar, I, D. Agrawal, F.W. Ainger, W.B. White, *Mater. Res. Bull.*, 30, **1995**, 745.

71. N. Alangi, J. Mukherjee, P. Anupama, M.K. Verma, Y. Chakravarthy, P.V.A. Padmanabhan, A.K. Das, L.M. Gantayet, *J. Nucl. Mater., 410*, **2011**, 39.

72. N.L. Wu, S.Y. Wang, I.A. Rusakova, *Science*, 285, **1999**, 1375.

73. S. Park, J.M. Vohs, R.J. Gorte, *Nature*, 404, **2000**, 265.

74. V. Grover, R. Shukla, A.K. Tyagi, *Scripta Materialia*, 57, **2007**, 699.

75. W. Li, H. Huang, H. Li, W. Zhang, H. Liu, *Langmuir*, 24, **2008**, 835.

76. X.Q. Cao, R. Vassen, D. Stoever. *J. Eur. Ceram. Soc.* 24, **2004**, 1.

77. K. W. Schlichting, N. P. Padture, P. G. Klemens, *J. Mater. Sci.*, 36, **2001**, 3003.

78. A. M. Limarga, S. Shian, M. Baram, D. R. Clarke, *Acta Materialia*, 60, **2012**, 5417.

79. F. Meiser, C. Cortez, F. Caruso, *Angew. Chem.*,43,**2004**, 5954

80. E. Ordonez-Regil, R. Drot, E. Simoni, J. J. Ehrhardt , Langmuir,18,**2002,** 7977.

81. S. Sinha, T.R.G. Kutty, P.V.A. Padmanabhan, K.G.K. Warrier, *J. Laser Appl.* 21, **2009**, 149.

82. P.V. Ananthapadmanabhan, K.P. Sreekumar, T. K. Thiyagarajan, R.U. Satpute, K. Krishnan, N.K. Kulkarni, T.R.G. Kutty, *Mater. Chem. Phy.*, 113(1), **2009**,417.

83. A.C. Pierre, *Introduction to sol-gel processing*, Kluwer Academic Publishers,**1998**

84. C. J. Brinker, G. W. Sherer, *Sol-Gel Science, Academic Press*, **1990**.

85. S. S. Kistler, *Nature*, 127, **1931,** 742.

86. L. L. Hench, J. K. West, *Chem. Rev.*, 90, **1990**, 33

87. R. K. Iler, *The Chemistry of Silica*; Wiley: New York, **1979.**

88. A. V. Vinogradov, V. V. Vinogradov, *RSC Adv.*, 4, **2014**, 45903.

Chapter 2

Nanosize Lanthanum Phosphate and Composites through Sol Gel Approach –Synthesis, Characterization and Applications

Part 1- Experimental

2.1 Synthesis of Stoichiometric Lanthanum Phosphate Particles

An attempt has been made here to prepare lanthanum phosphate nano particles starting from lanthanum chloride for the first time through modified aqueous sol-gel process. The synthesized powder is characterized and reported in detail. A precipitation - peptization method followed by electrostatic stabilization is adopted and lanthanum phosphate particles having size in the range of 25-100 nm are prepared and characterized.

2.1.1 Experimental

Lanthanum Phosphate was precipitated from lanthanum chloride hexa hydrate prepared from lanthanum chloride (99%), (Supplied by Indian Rare Earths Ltd, Alwaye, India) by adding ortho phosphoric acid (sd-fine sp grade 1.75 AR) with continuous stirring and was further flocculated by addition of 25% ammonia (sd- fine) solution.

As a typical case, for synthesis of 20gm $LaPO_4$, the following procedure was adopted. 0.05M lanthanum chloride hexa hydrate ($LaCl_3.6H_2O$) solution was prepared using deionized water (~1710 ml). 5.4 ml of 88% H_3PO_4 was added drop wise to the chloride salt solution with continuous stirring. The pH was brought down to ~2. After stirring for 2hr, 25% ammonia solution was added drop wise to flocculate the lanthanum phosphate which formed was complete at a pH 7. The pH value was determined at the point were all the phosphate had flocculated and the clear solution was on the top till no further flocculation was observed by the addition of ammonia solution. The precipitate formed was then washed with luke warm water (~60 °C) and centrifuged (~4000 rpm) several times (5-6 times) to remove Cl^- ions

and the excess phosphate from the medium. The completion of chloride removal was confirmed by silver nitrate test. The washed precipitate was then filtered and redispersed in de-ionized water and was further **peptized** to form lanthanum phosphate sol using 20% nitric acid at a pH of 1.75-1.85 with continuous, vigorous stirring for nearly 5 hr followed by ultrasonication (Ultra sonic processor P2, Vibronics, India) for 15 minutes. The sol particles were allowed to self-assemble in ammonia atmosphere for approximately 24 hr and thick lanthanum phosphate gel was obtained. The ammonia atmosphere was created by keeping ammonia solution in closed dessicator.The gel obtained was then dried at 70 °C overnight in an oven, ground well and was then heated at temperature range of 100 - 1300 °C and further characterized. The flow chart for the preparation of lanthanum phosphate is provided in *figure 1*.

2.1.2 Characterization

The particle size and stability of the sol (zeta potential) as well as the $LaPO_4$ precipitate was measured using dynamic light scattering method with Zeta Sizer (Malvern Instruments Ltd, UK). Thermal decomposition study was conducted in air atmosphere using thermo gravimetric analyser (Shimadzu 50H, Japan). A rate of heating of 10 °C/min was followed. FT-IR spectra were recorded on a FT-IR Spectrophotometer (Thermo Nicolet Magna 560, USA). The measurements as done on pellets made from the mixture $LaPO_4$ powder and KBr at resolution of 4 between 400 cm^{-1} and 4000 cm^{-1}. After heating the dried gel at different temperatures, the resultant powders were subjected to x-ray diffraction and corresponding patterns were obtained. Cu Kα radiation was used at a scanning rate 2°/min with an increment/ step size of 0.06° in the 2θ range 20-60°. Philips X'pert Pro Diffractometer was engaged for measurement. The crystallite size was calculated using Scherrer equation.

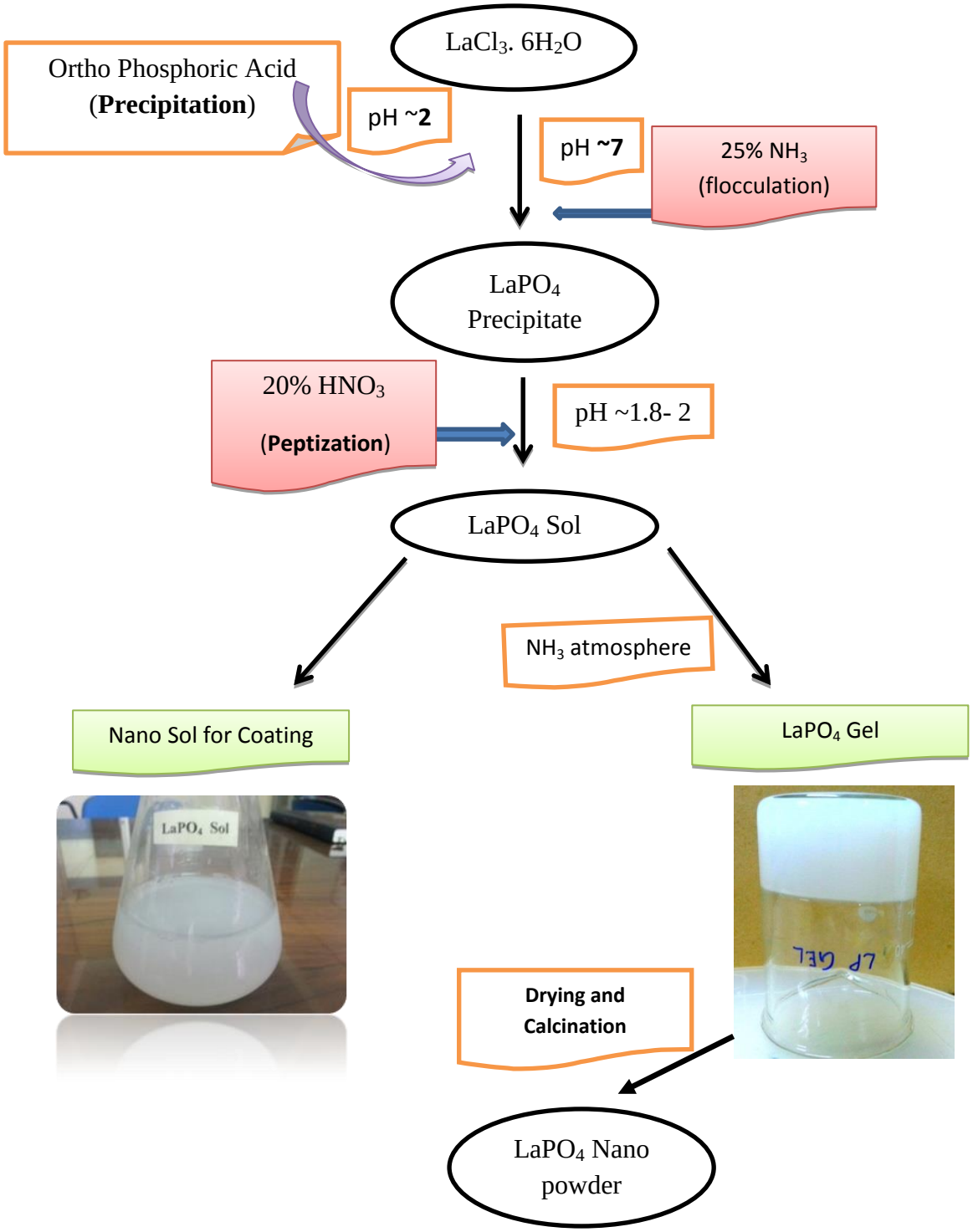

Figure 1) *Flow chart of sol gel preparation method of $LaPO_4$*

Samples for transmission electron microscopy were prepared by mounting the samples over copper grids. The powder samples were mixed with acetone and ultrasonicated for about 15 minutes before drop casting over the TEM grids. The grids were kept for drying overnight.

TEM micrographs of the particles were taken using JEOL 3000EX (with an accelerating voltage of 300 kV) and JEOL 200CX electron microscopes respectively. Scanning Electron Microscopic images of the particles were taken using JEOL JSM-6700F electron microscope. The samples were placed over conducting carbon tape before getting coated with gold. The surface area of particles pre-heated at 400 °C was measured using surface area analyser (Micromeritics Gemini 2375 V5.01, USA) after degassing the powder at 200 °C for 2 hr. The affinity of lanthanum phosphate particles with water was measured using Tensiometer (Data physics, Germany). Filter paper was inserted into the perforated sample tubes provided along with the instrument. $LaPO_4$ powder of definite weight was uniformly packed using tapping method ensuring definite packing density. For knowing the constant c (material factor of the powder dependent on the powder porosity) the powder is wetted using a total wetting liquid, n-hexane in this case. The sample stage with water is lifted till the bottom of the tubes with powder and the measurement is carried out automatically. Size measurements for the lanthanum phosphate particles as well as sol were performed at 25 °C by static light scattering (also referred to as Photon Correlation Spectroscopy, PCS) on a zetasizer 3000 HSA, (Malvern, UK).The samples are ultrasonicated in deionized water for 15 minutess to avoid agglomeration that can hinder the analysis.

2.2 $LaPO_4$-Y_2O_3 Composite

The preparation of $LaPO_4$-Y_2O_3 composite was also done by aqueous sol- gel route where intimate mixing of the constituents is ensured by controlling the zeta potential (surface charge) in the precursor. The homogeneity of the two phases was ensured by dispersing yttrium nitrate solution in the sol of lanthanum phosphate.

2.2.1 Experimental

Yttrium nítrate hexahydrate (99.9%), Y $(NO_3)_3$. $6H_2O$ (CDH Pvt. Ltd, New Delhi, India) was used as starting material for yttrium oxide. In a typical synthesis of 5gm $LaPO_4$- 20 wt%Y_2O_3 nanocomposite, 17gm of yttrium nitrate dissolved in minimum amount of distilled water was added to 0.05 M lanthanum phosphate sol prepared as reported above under constant stirring using a mechanical stirrer. The stirring was continued for approx. 2h for the homogeneous mixing of lanthanum phosphate sol and the yttrium nitrate solution. The precipitation of $Y(OH)_3$ as well as flocculation of $LaPO_4$ was achieved slowly by adjusting the pH to 8 using 25% NH_3 (sd- fine) solution and the composite precursor was kept for stirring for 3 h.

The precipitate obtained was later dried over water bath and further calcined to different temperatures (100- 1300 °C) for further characterisation.

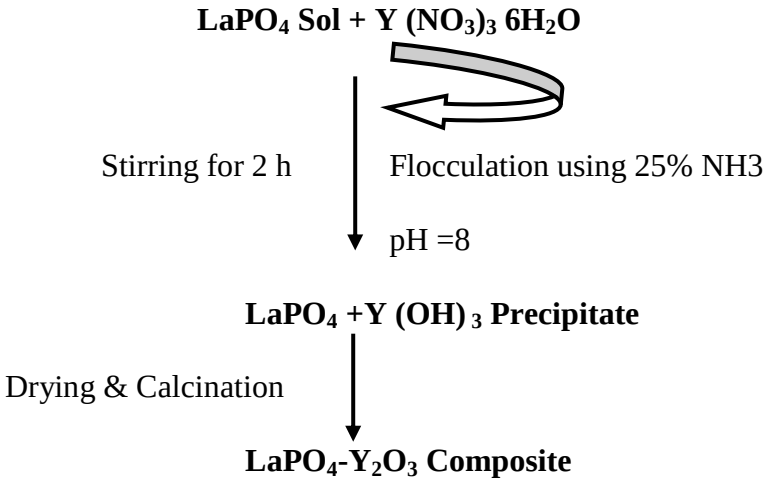

Figure 2) *Flow chart of preparation method of $LaPO_4$-Y_2O_3 nanocomposite*

2.2.2 Characterization

Particle size distribution and zeta potential of composite precursor powder were measured using photon correlation spectroscopy also known as dynamic light scattering (Zeta Sizer, Malvern Instruments Ltd., UK). The composite precursor powder dried at 70 °C was subjected to thermal decomposition using a Shimadzu thermal analyser, Japan (model 50H)

in air at a heating rate of 10 °C min^{-1} at a temperature range of 100 – 1000 °C. The characteristic functional groups present in composite were identified by FTIR analysis using a Nicolet Magna-IR 560 spectrophotometer. The samples were prepared for measurement by mixing with KBr, making pellets and spectrum recorded in the range of 400-4000 cm^{-1}. The precursor powder was subjected to calcination over a temperature range of 400-1600 °C and phase identification was carried out by X-ray diffraction technique (Philips PW 1710) in the 2θ range of 20–60° using Cu Kα radiation at a scanning rate 2°/min with an increment/step size of 0.06°. Transmission electron microscopy of the calcined composite powder was performed on a JEOL 3000EX microscope operating at an accelerating voltage of 300 keV. Samples were mounted on carbon coated copper grids for observation after ultrasonication in acetone medium for 15 minutes.

The precursor composite heated at 600 °C was well powdered and compacted uniaxially at a pressure of 200 MPa to form cylindrical pellets with dimensions 10 mm diameter and 2 mm thickness and were sintered in the range 1400-1600 °C in a high temperature furnace (Nabertherm, Germany) at a heating rate of 3°/min and a soaking time of 3 hr. The relative density of sintered pellets was measured in accordance with Archimedes principle. The sintered samples were polished and thermally etched at 50 °C less than the sintering temperature and hold time of approx. 20 min. The polished and thermally etched surface of sintered composite pellets after providing gold coatings was observed under a scanning electron microscope (Hitachi, 2240 Japan). BET surface area of the composite was measured by nitrogen adsorption using a (Micromeritics Gemini 2375 V5.01, UK) surface area analyser after degassing the powder at 200 °C for nearly 2 hr.

The photopyroelctric (PPE) technique was used to determine the thermal parameters of the samples. A 120 mW He–Cd laser of wavelength λ = 442 nm has been used as the optical

heating source, and the intensity modulation was accomplished with a mechanical chopper (Stanford Research Systems Model SR 540). A PVDF film of thickness 28 μm, with Ni–Cr coating on both sides, with a pyroelctric coefficient P = 0.30 × 10^{-8} V cm^{-1} K^{-1}, is used as the pyroelctric detector. The output signal was measured with a dual-phase lock-in amplifier (Stanford Research Systems Model SR 830). Modulation frequency was kept above 30 Hz in all our experiments to ensure that the detector, the sample and the backing medium are all thermally thick during measurements. The dielectric properties dielectric constant ε_r and the coefficient of temperature variation of resonant frequency τ_f of the materials were measured in the microwave frequency range (3–13 GHz) using a network analyser HP 8510C (Hewlett-Packard, Palo Alto, CA).

2.3 $LaPO_4$-ZrO_2 Composite

A facile wet chemical approach involving precipitation- peptization mechanism was successfully adopted to synthesize $LaPO_4$–ZrO_2 composites with ZrO_2 percentages varying from 5-20 wt%.

2.3.1Experimental

Zirconium oxy chloride (99.9% purity) (M/s Indian Rare Earths Ltd. India) solution of 0.05 M concentration and with different weight percentages (5-20 wt%) was added to the Lanthanum Phosphate ($LaPO_4$) sol synthesized by modified sol gel process (section 2.1.1) The solution adjusted for pH 1.8-2 and stirring was continued for couple of hours for homogenous mixing. 25% ammonia solution (sd- fine) was added dropwise with stirring up to ~ pH 8. The precursor precipitate was under stirring for another couple of hours. The flocculated precipitate was washed in warm water (70 °C), dried over water bath followed by calcination at 800 °C and characterized.

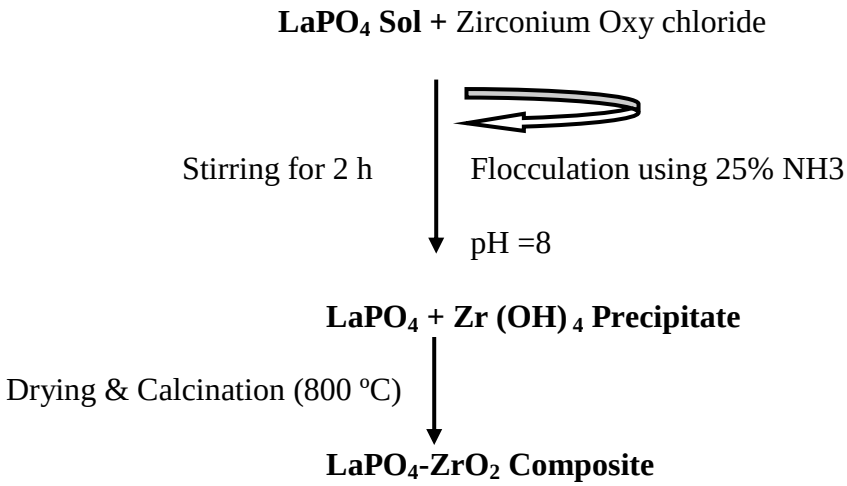

Figure 3) *Flow chart of preparation method of $LaPO_4$- ZrO_2 nanocomposite*

Thermal decomposition analysis (Perkin Elmer STA 6000) of composite precursor after drying at 100 °C was done at a heating rate of 10 ^{o}C/min upto 1000 in air atmosphere. X-ray diffraction patterns were recorded for the precursor as well as the sample calcined above 1000 °C in the 2θ range of 20–60 using Cu Kα Radiation using Philips PW 1710 X-ray Diffractometer. Transmission Electron Microscopic images were taken using a JEOL 3000EX microscope operating at an accelerating voltage of 300 keV for analysing the morphological behaviour of the composite with respect to temperature. The samples were mounted on carbon coated copper grids for observation.

The composite powder prepared was compacted uniaxially at a pressure of 200 MPa to pellets of 11 mm diameter and 2-3 mm thickness. The samples were sintered in the temperature range of 1400-1600 °C. Densification studies of the sintered pellet samples were completed by using Archimedes method. The sintered pellets were characterized using X-ray diffraction for the phase stability. Microstructural evaluation including grain growth pattern of the composites were done using scanning electron microscopy on polished and etched specimen after coating gold. Laser flash technology (Vikram Sarabhai Space Centre, Trivandrum) was used to determine the thermal conductivity of the samples.

Chapter 2

2.4 Coatings

2.4.1 $LaPO_4$ Nanocoatings

The coatings were obtained starting from stock sols of lanthanum phosphate. For the synthesis of 20gm Lanthanum Phosphate, 37.0198gm Lanthanum chloride was initially dissolved in 1710 ml de-mineralized water. Lanthanum phosphate particles were precipitated from by adding 88% ortho phosphoric acid (sd- fine) (5.44 ml) drop by drop and the precipitate formed was further flocculated by addition of 25% ammonia solution. pH was maintained between 6.8 -7.8. The precipitate was then washed with warm water, filtered and redispersed in de-ionized water and further peptized to form lanthanum phosphate sol (pH 1.9 – 2) using 20% nitric acid with continuous, vigorous stirring for about 5 h followed by ultrasonication for 15 minutes. The stability of the sol was checked using zeta potential measurement. The sol thus obtained was coated over surfaces and annealed to different temperatures (100- 400 °C) to get the coatings.

The $LaPO_4$ nano coatings were made on glass substrate using a dip coater supplied by KSV Instruments (Netherlands) with different advancing and receding rates and soaking times. Parameters are optimized to obtain a good adherent coating. The coated glass slides were dried at 50 °C for 5 hours and then annealed at a temperature range 100- 400 °C. The morphology of the samples was observed under a scanning electron microscope. The viscosity of the sol was measured with varying shear rates in the range of 100 to 1000 s^{-1} using Rheolab MC1, Physica, Anton Paar (Germany).

2.4.2 Plasma Spray coating

Thermal and chemical stability of monazite ($LaPO_4$) and composites was studied by plasma spheroidization experiments using a DC thermal plasma reactor set up at Bhabha Atomic Research Centre (BARC), Mumbai. Atmospheric plasma spraying (APS) technique is generally used for depositing ceramic materials due to the high enthalpy and temperature available in the plasma jet. Depending on the process parameters, the temperature at the core of plasma jet can be as high as 10,000–15,000 K and any metal or ceramic powder injected into the plasma jet can be melted and spray coated.[1,2] The injected spray grade powder particles are rapidly melted, accelerated and propelled at high velocity to the substrate surface.

Lanthanum phosphate and composite powders were coated by atmospheric plasma spraying technique on stainless steel (SS304) substrates at different power levels. The powder was stored in a powder feeder and injected into the plasma jet through a side port located 3 mm inside the plasma torch nozzle exit. A mixture of argon and nitrogen was used as the plasma gas. The coatings on substrates were carried out at 16 and 20 kW plasma power. Plasma spheroidization and melting experiments showed that monazite phase melted congruently without decomposition. Plasma spray deposition on stainless steel substrates was carried out by atmospheric plasma spray system. Adherent coatings of $LaPO_4$ and the coatings could be obtained with reasonably good deposition efficiency. Plasma coated portions were cut from the coated piece and metallographically (mounted and polished) prepared and examined using scanning electron microscopy.

2.5 Sintered $LaPO_4$ and $LaPO_4$ -Y_2O_3 for machinability and reactive metal melting studies

The $LaPO_4$ and $LaPO_4$- Y_2O_3 composite powders were synthesized as detailed in sections 2.1.1 and 2.2.1 respectively. The powders were initially heated to 800 °C. 65 wt% slurries of $LaPO_4$ as well as the $LaPO_4$- Y_2O_3 composite were prepared using isopropyl alcohol (IPA) and ball milled for approximately 12 hr. The pH of the slurry was maintained at ~2 using 20% HNO_3. After the milling, 2 wt% polyvinylpyrrolidone (PVP) was added and again milled for couple of hours for better dispersion. The slurry was then dried, powdered and sieved for obtaining uniform size particles. The obtained powders were compacted uniaxially to form discs of approx. 50mm diameter as well as bar shapes with a length of 40 mm and thickness of 10mm. The green samples of $LaPO_4$ were sintered at 1400 °C and $LaPO_4$- Y_2O_3 at 1600 °C to its maximum density at a heating rate of 3 °C/min in a high temperature furnace at a soaking time of ~ 3 hr.

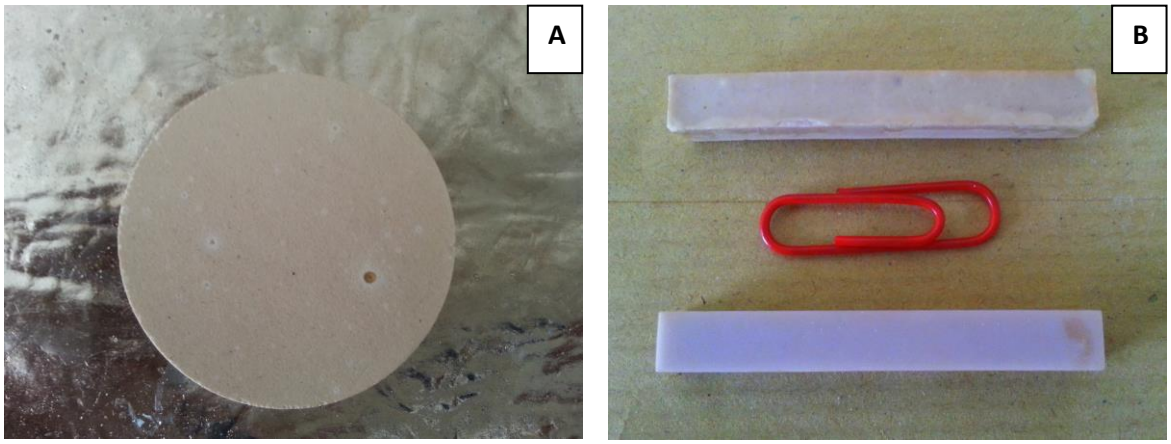

Figure 4) A) $LaPO_4$ sintered disc and **B**) bars of $LaPO_4$- Y_2O_3 processed

Chapter 2

Part 2- Results and Discussion

2.6 Stoichiometric Lanthanum Phosphate

One of the main issues in the synthesis of stoichiometric lanthanum phosphate is the removal of anions from the precipitation medium. In the case of nitrate, thermal decomposition during calcination removes the excess nitrate.[5] Any excess phosphate remaining in the precipitate may seriously affect the temperature stability of the $LaPO_4$. Addition of ammonia solution (NH_4OH) facilitates the formation of ammonium salts with anions which can be easily removed through filtration/centrifuging/washing as well as easy decomposition during thermal treatment. During initial precipitation of lanthanum phosphate from lanthanum chloride using phosphoric acid, HCl is formed as by product. By addition of ammonia solution, HCl formed gets converted to ammonium chloride at the pH of 6.8–7.8. The ammonium chloride thus formed is removed from the precipitate using centrifugation. This has considerably reduced the number of filtration steps in obtaining chloride free lanthanum phosphate.

The particle size distribution of lanthanum phosphate in as-precipitated as well as in the sol was measured using photon correlation spectroscopy technique and is presented in figure 5. The distribution obtained for the precipitated and the $LaPO_4$ sol was monomodal in nature. The particle size of precipitated $LaPO_4$ was around 110 nm with a wide distribution pattern while that of the sol was around 88 nm with a narrow distribution as indicated by polydispersity index (PDI) value of 0.327 obtained during the analysis. A zeta potential value of +46 mV obtained indicates good stability of the sol prepared in the pH range 1.75-1.85.the particle size reported from nitrate is nearly identical (~50 nm) and hence the present process confirms the narrow particle size distribution.

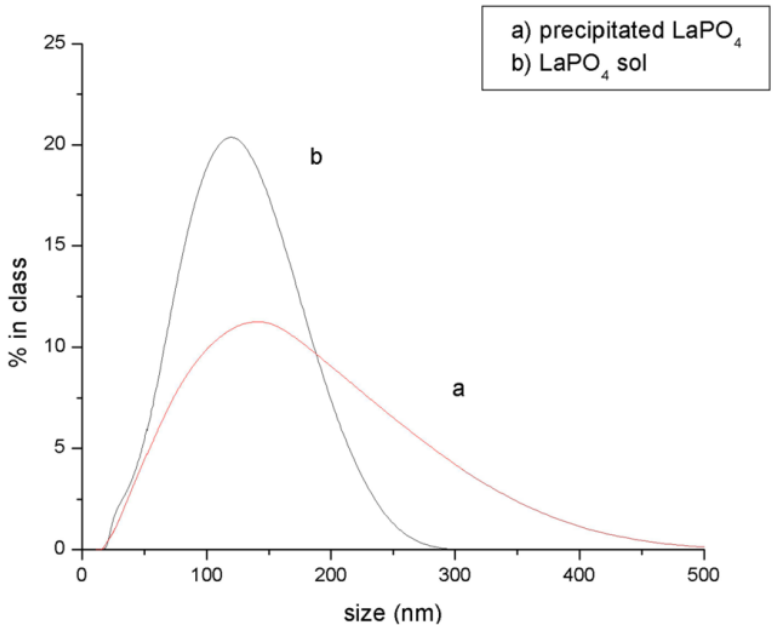

Figure 5) Particle size distribution curves of as prepared $LaPO_4$ and the sol

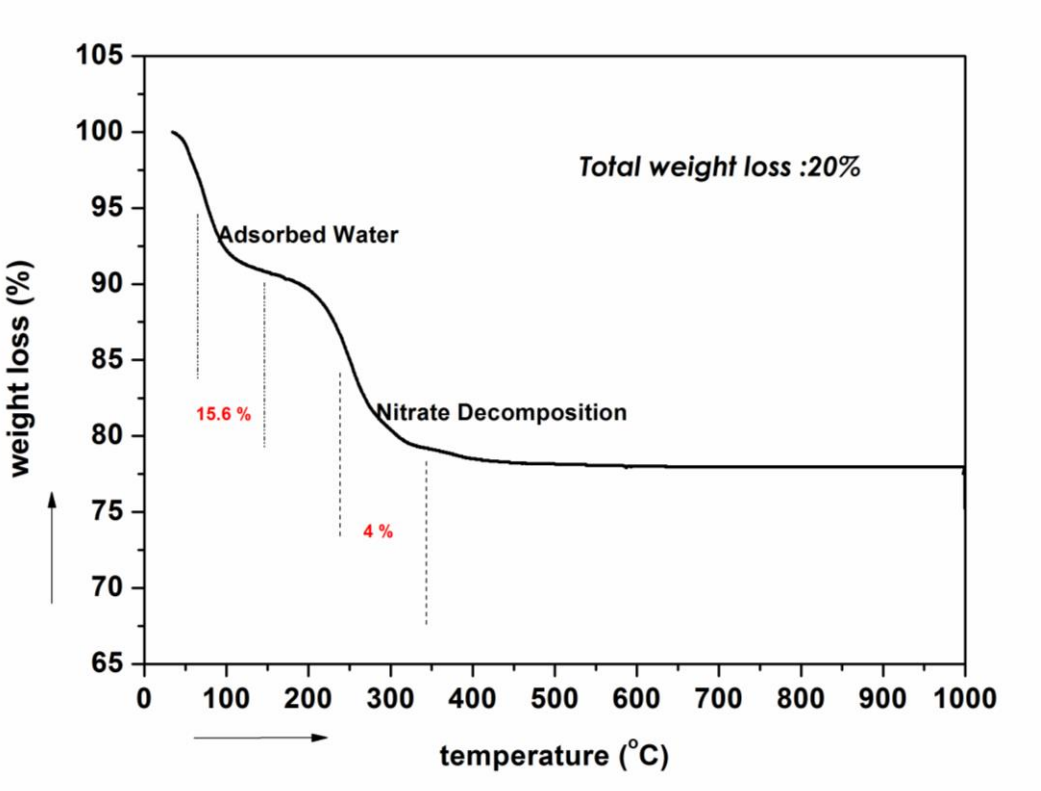

Figure 6) Thermo gravimetric analysis curve of $LaPO_4$ gel dried at 100 °C

The thermo gravimetric analysis curve (*Figure 6*) of the $LaPO_4$ gel after initial drying at 100 °C shows a total weight loss of 20% during the entire analysis of which 15.6 % was

below 250 °C which is due to the physically adsorbed water. The weight loss (4%) between 250 and 600 °C is due to the nitrate decomposition from the gel powder which was added during peptization of the sol using nitric acid. After the temperature of 650 °C no weight loss was observed which shows no excess phosphate was formed during the process which indicates stoichiometric formation of the particles.

Powder X-ray Diffraction pattern (Figure 7) obtained for the $LaPO_4$ gel powder heated at 70 °C indicates that the peaks are indexed well and are found matching with the pattern for hexagonal rabhdophane phase (JCPDS File No: 46-1439). The crystallite size was calculated using Scherer equation to be 8 nm. The intensity for the (200) peak is greater than the intensity of the (102) peak. This is certainly in accordance to the growth patterns reported for lanthanum phosphate nano rods in one direction[2] unlike for bulk hexagonal lanthanum phosphate.[3]

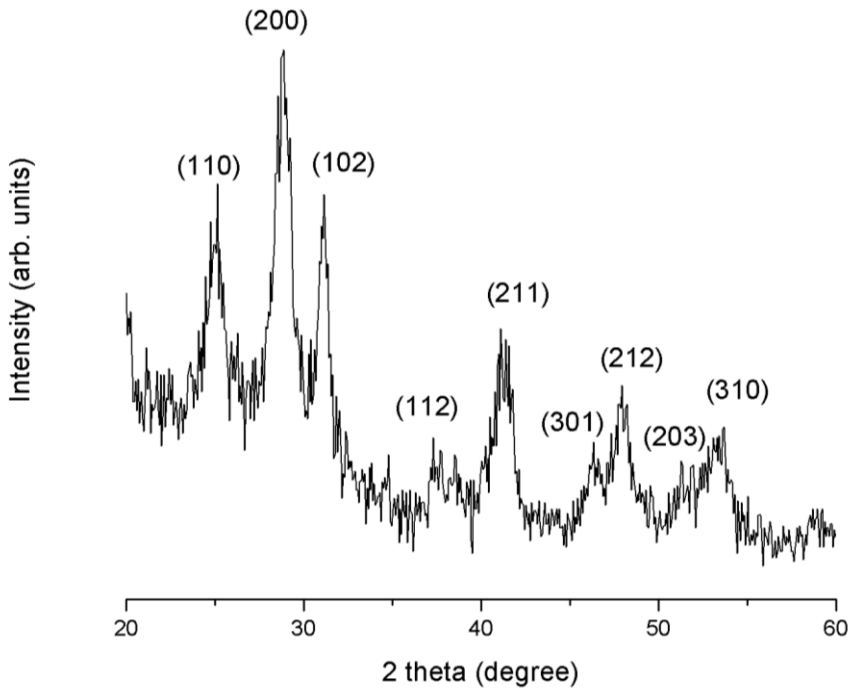

Figure 7) X-ray diffraction pattern of lanthanum phosphate gel dried at 70 °C

The XRD patterns obtained for the $LaPO_4$ particles heated at different temperatures are shown in the Figure 8. The change from hydrated form (Figure 7) to hexagonal phase with less hydrate is seen to occur on heating of the particles at 400 °C (Figure 8). The pattern obtained matches with the JCPDS file no: 04-0635. The particles also seem to acquire good crystalline nature. The transformation from hexagonal phase to monoclinic phase could be seen at 800 °C (Figure 8) (JCPDS file no.35-0731). From the pattern obtained for sample heated at 1200 °C, the transformation to monoclinic phase for the lanthanum phosphate is very much evident. The formation of the monoclinic phase is also confirmed by the FT-IR spectra (Figure 9).

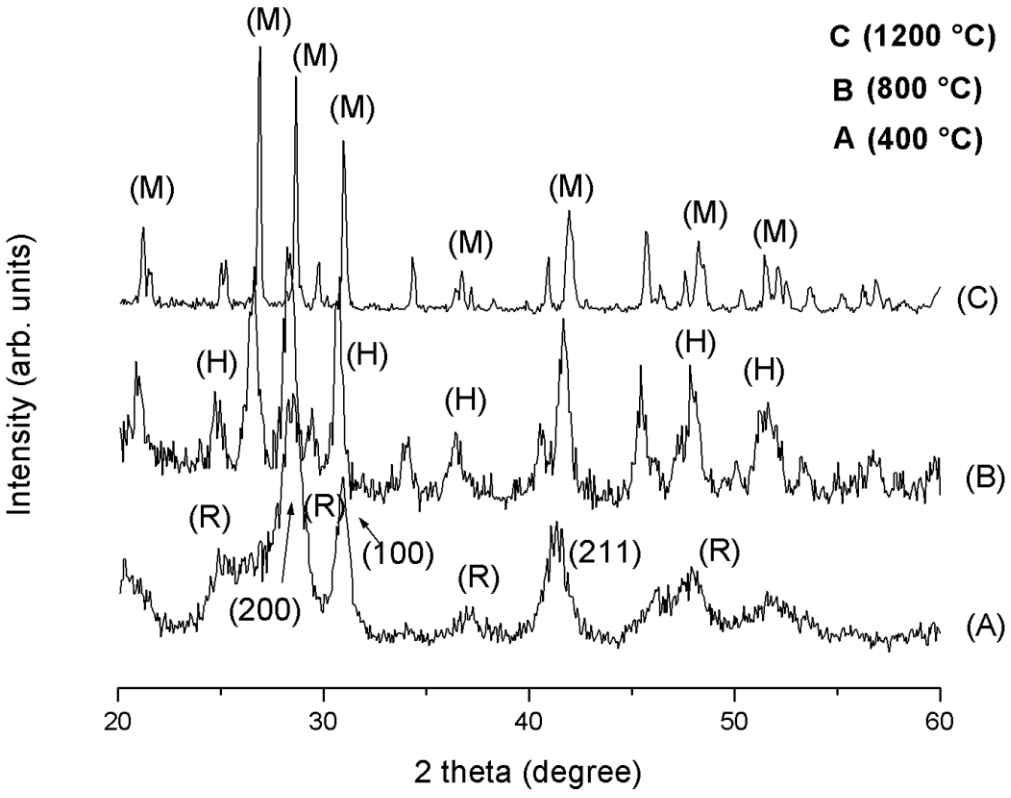

Figure 8) XRD patterns of lanthanum phosphate gel heated 400, 800 and 1200 °C.

The Fourier Transform infra-red spectra of gel heated at temperatures 70, 400, 600, 800 and 1200 °C are represented in Figure 9. The peak at 1040 cm^{-1} corresponds to the P-O stretching and the phosphate vibrations are characterized by peaks at 616 and 540 cm^{-1} respectively.[4] The broad band in the region 3700–3450 cm^{-1} is due to the water OH stretching vibrations and the corresponding bending vibration is seen at 1650 cm^{-1}. The splitting of stretching peak at 1040 cm^{-1} after 800 °C is characteristic of monoclinic lanthanum phosphate phase.[5] *Lucas et al.*[4] had reported non-stoichiometric lanthanum phosphate with formation of excess phosphate with corresponding absorbance at 770 and 1259 cm^{-1} of FT-IR spectra which is not obtained for the present analysis.

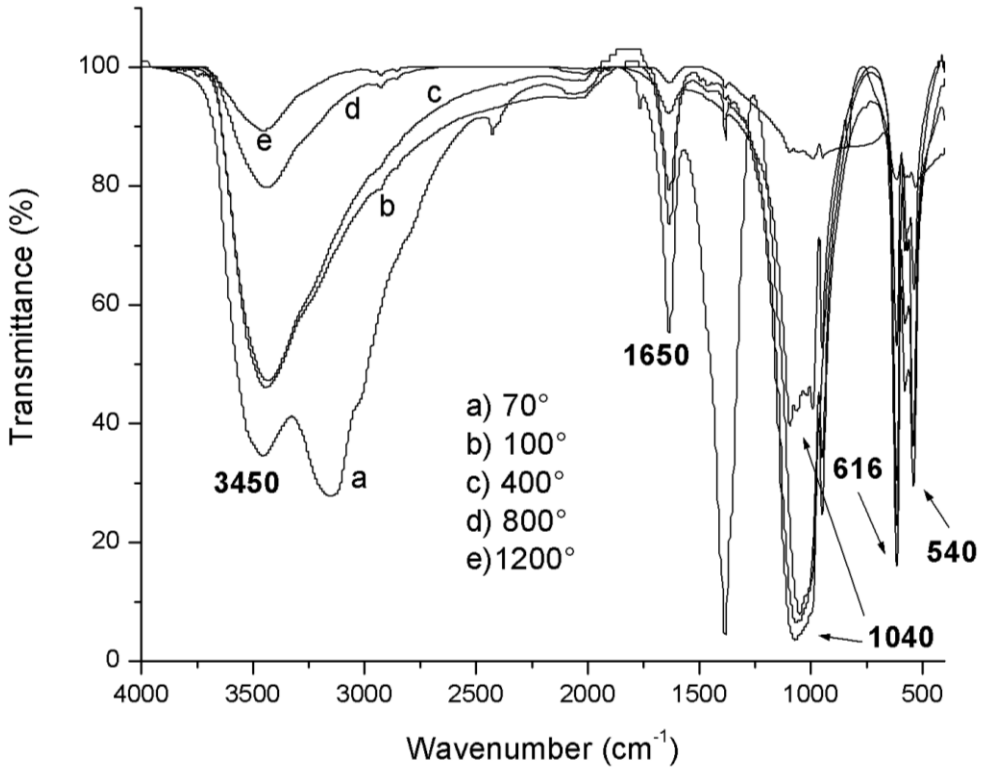

Figure 9) FT-IR spectra of $LaPO_4$ gel powders heated at different temperatures.

Earlier *Rajesh et al.*[5] had reported a BET surface area of 100 m^2g^{-1} for lanthanum phosphate particles heated at 400 °C starting from lanthanum nitrate. A reasonably high surface area (BET) was obtained (85 m^2g^{-1}) for 400 °C calcined gel powder in the current

synthesis where as the $LaPO_4$ precipitated initially after the removal of chloride ions, dried and calcined at same temperature, produced a surface area of 60 m^2g^{-1}.

The nature of the $LaPO_4$ precipitated immediately from Lanthanum chloride using phosphoric acid was examined using TEM (Figure 10). The micrographs obtained reveal an elongated and very long rod like morphology of the particles during this precipitation stage. Some of the rods are found agglomerated. These micrographs show that the unidirectional growth of lanthanum phosphate particles takes place from the initial state of precipitation in the present sol–gel approach. The unidirectional precipitation of $LaPO_4$ could be due to the spherical diffusion model growth as explained by *Fang et al.* [6] and the structure can also be is envisaged as infinite linear chains extending along the c axis and such a structure results in favour of growth along one direction.[7]

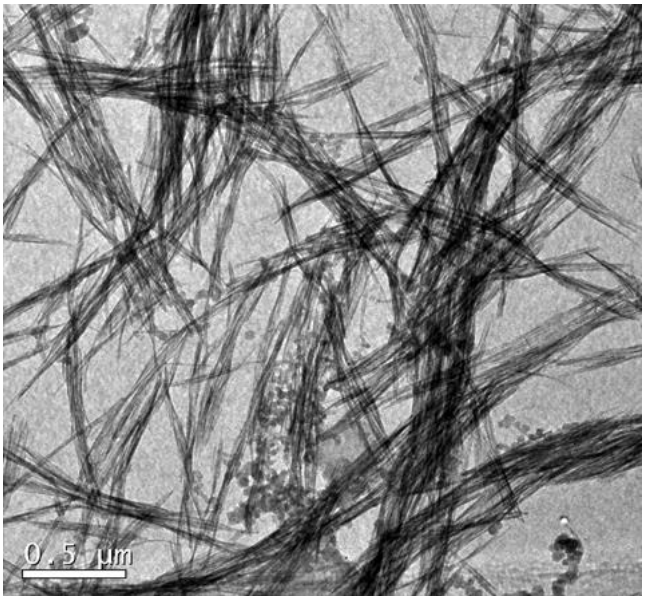

Figure 10) Transmission electron micrograph obtained for $LaPO_4$ as precipitated.

Transmission electron micrographs (Figure 11) reveal the rod like morphology obtained for the phosphate particles prepared (Sol dried and calcined). The samples were dried at 70 and 100 °C and later calcined at 800 °C with soaking for 3 hr. We can see from

the micrographs that the average length of ~50 nm and diameter ~15 nm is obtained after heat treatment of particles at 800 °C. This shows that the morphology is retained even at higher temperatures. Since the micrographs indicates that the particles are reasonably in un-agglomerated state and retains the shape, the particle size obtained for the sol using PCS should be due to the elongated morphology.

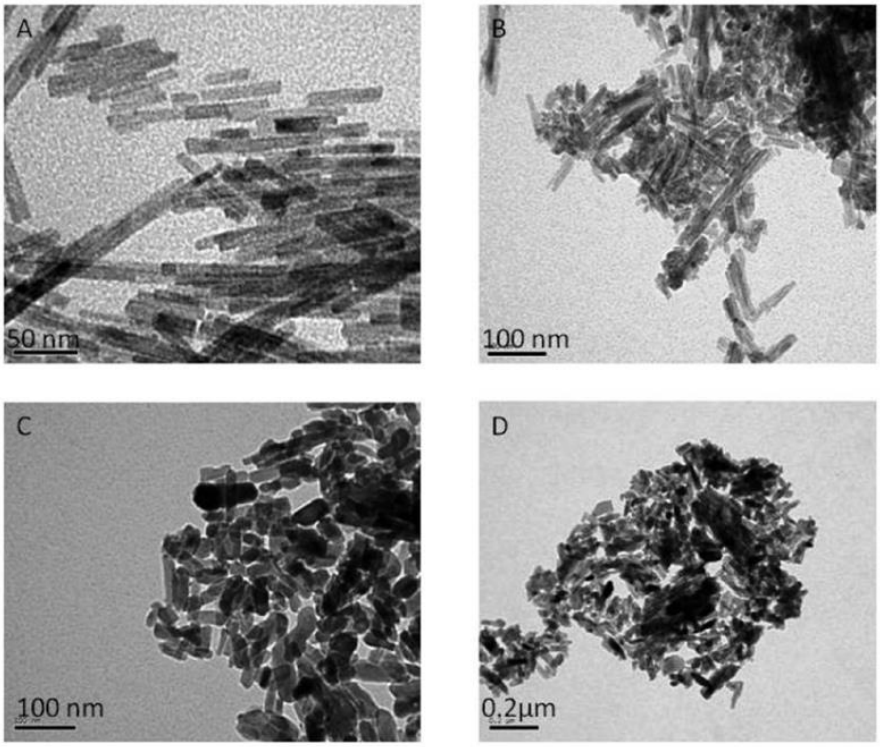

Figure 11) TEM micrographs of Lanthanum Phosphate (A) 70 °C, (B) 100 °C, (C) and (D) 800 °C

The scanning electron micrographs of lanthanum phosphate gel calcined phase as well as for $LaPO_4$ pellet sintered at 1300 °C are shown in Figure 12 (A&B). The micrograph presented indicates that phosphate particles get sintered on calcination at this temperature with the formation of well distinguishable grain boundaries. The sintering of $LaPO_4$ was followed by dialotometric measurements. $LaPO_4$ powder compacts could be sintered to >99% density at 1300 °C and sintered microstructure revealed average grain size of ~1 µm with occasional grains of 2 µm.

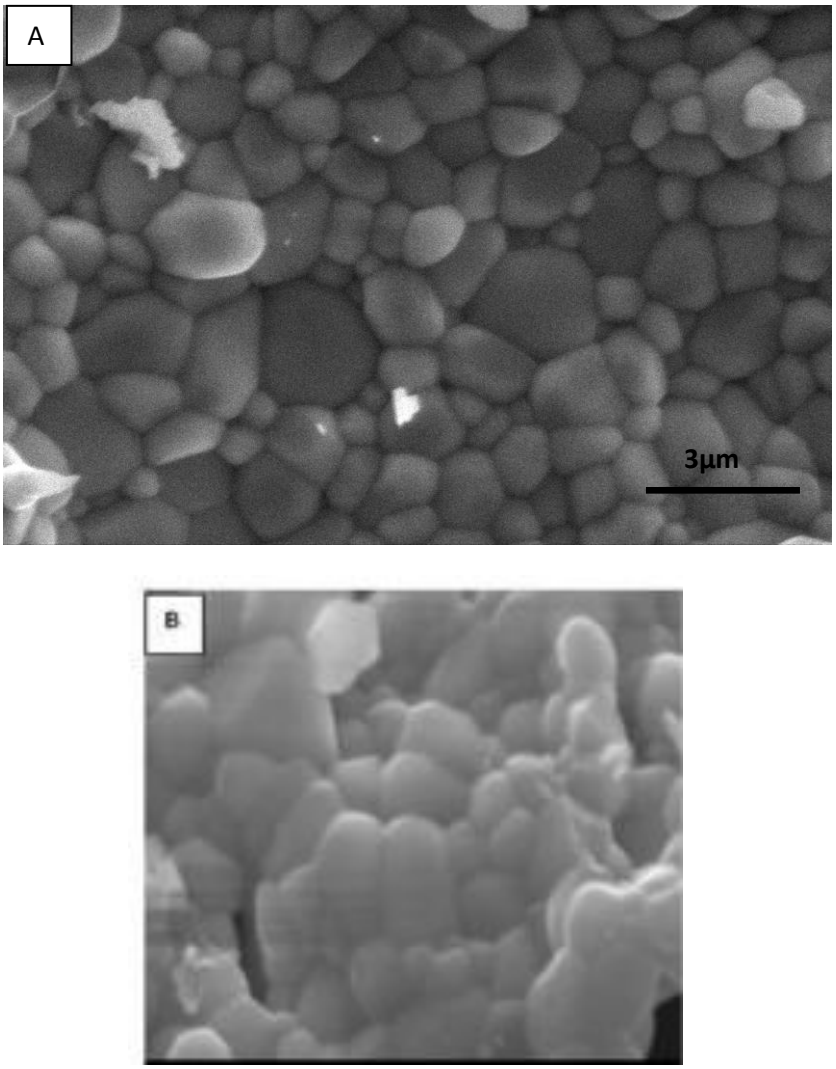

Figure 12) A) $LaPO_4$ pellet sintered at 1300 °C **B)** scanning electron micrographs of lanthanum phosphate dried gel dried and calcined at 1300 °C

$LaPO_4$ pellet sample uniaxially pressed was subjected to TMA (dialotometric) measurement at a heating rate of 10 °C /min to analyse the sintering behaviour as well as the coefficient of thermal expansion behaviour and the corresponding results were recorded. The corresponding thermograms are provided in the figure 13. It was seen that the densification occurs in three steps and the sintering starts at around 800 °C and finishes at 1300 °C as evident from figure 13A. Density as high as >99% was obtained on sintering at 1300 °C .The sinterability at low temperature was achieved for the $LaPO_4$ compared to conventional methods[8], is certainly due to fine particle size, good surface area for the particles obtained in the current study which

enhances the surface diffusion. The co-efficient of thermal expansion (figure 13B) for $LaPO_4$ was obtained to be 8.6 $x10^{-6}$/°C in the temperature range of 100 – 1300 °C which is close to reported values obtained for $LaPO_4$ [9, 10] which is 9.6 $x10^{-6}$/°C.

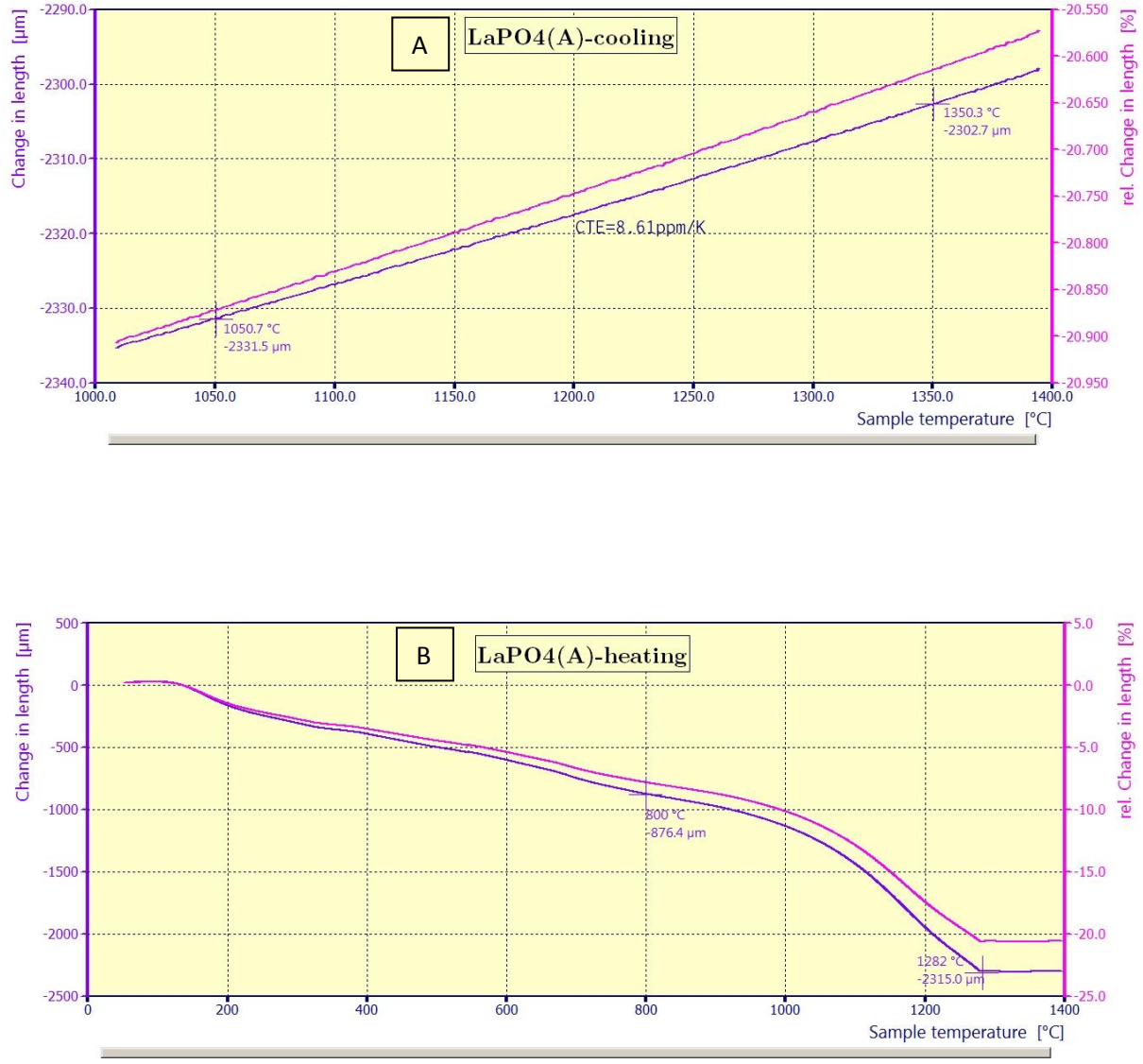

Figure 13) Thermo mechanical analysis of $LaPO_4$ **A**) sintering behaviour of $LaPO_4$ and **B**) Co-efficient of thermal expansion study

Contact angle data measured in aqueous media for the $LaPO_4$ powder samples heated for 3 hr duration at different temperatures ranging from 70 °C to 800 °C are given in Table 1. The contact angle values for $LaPO_4$ particles dried at 70 °C and calcined at 400° C are nearly

identical while there is a marginal decrease in the value for particles heated at 800 °C. The inherent hydrophobic character of $LaPO_4$ could be the reason for the minimal difference in values at different temperatures. The hydrophobic behaviour possibly arises due to the electronic structure of the lanthanide series where unfilled 4f orbitals of the rare earth atoms are shielded from interactions with the surrounding environment by the full octet of electrons in the $5s^2p^6$ outer shell.[11] The values obtained from repeated measurements indicate the possibility of using $LaPO_4$ as a hydrophobic material and in coatings which could perform at higher temperatures. These nano coatings could involve pure lanthanum phosphate or as nano composites with other oxides such as Al_2O_3, ZrO_2, La_2O_3 which are hydrophilic in nature to impart higher non-wetting characteristics.

$LaPO_4$ samples	Temperature (°C)	Contact angle (°)
Hydrated	70	88.87
Calcined	400	87.36
Presintered	800	83.80

Table 1) Contact angle values for $LaPO_4$ dried at different temperatures

2.6.1 Mechanical properties

Machinability

Hardness is an important parameter as an indication of ceramic machinability and in general less hardness means excellent machinability. Lanthanum phosphate being a soft ceramic could be easily machinable. Abrasive water jet cutting is successfully used to machine $LaPO_4$ as shown in figure 14. The hardness of the sintered $LaPO_4$ was measured to be 3.8 GPa (388 kgf/m^2) which is close to the machinable mica glass ceramic[12] which has as a hardness value of 3GPa and also close to Ti_3SiC_2 compounds.[13] Machinability for $LaPO_4$ discs sintered at 1300 °C was successfully carried out using abrasive water jet cutting technique (figure 14)

without any cracking or chipping. The microstructure of the portion indicates appreciable ductile morphology. Report by *Ruigang et al.*[14] suggests that the excellent machinability of $LaPO_4$ is due to the layered structure and also due to the deformation bands observed between the grains, beneath hertizian contact sites which are rather similar to sites of dislocation and twinning, martensitic transformation of ceramic materials.

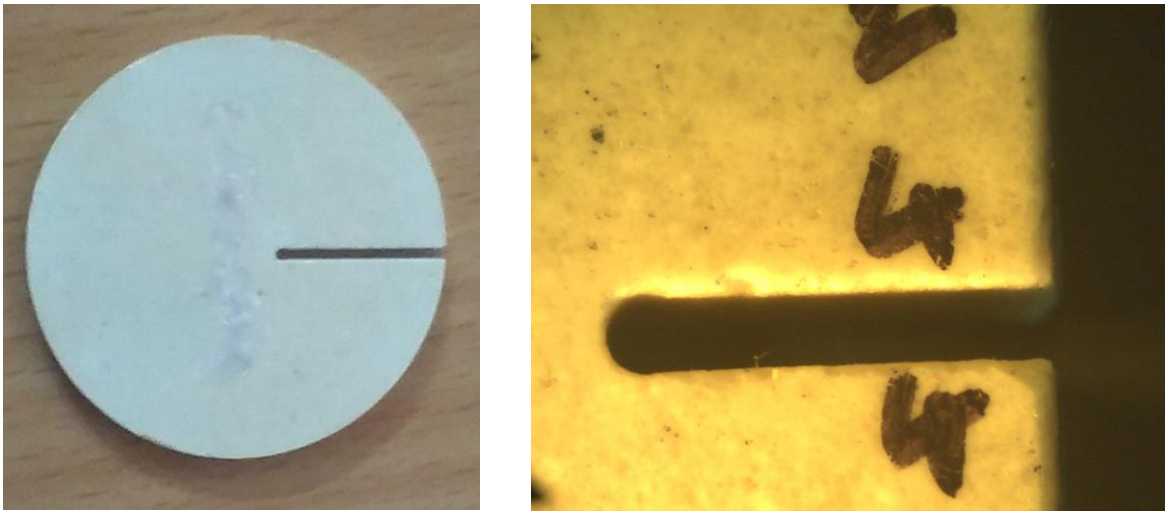

Figure 14) Photographs of $LaPO_4$ discs machined using water jet cutting

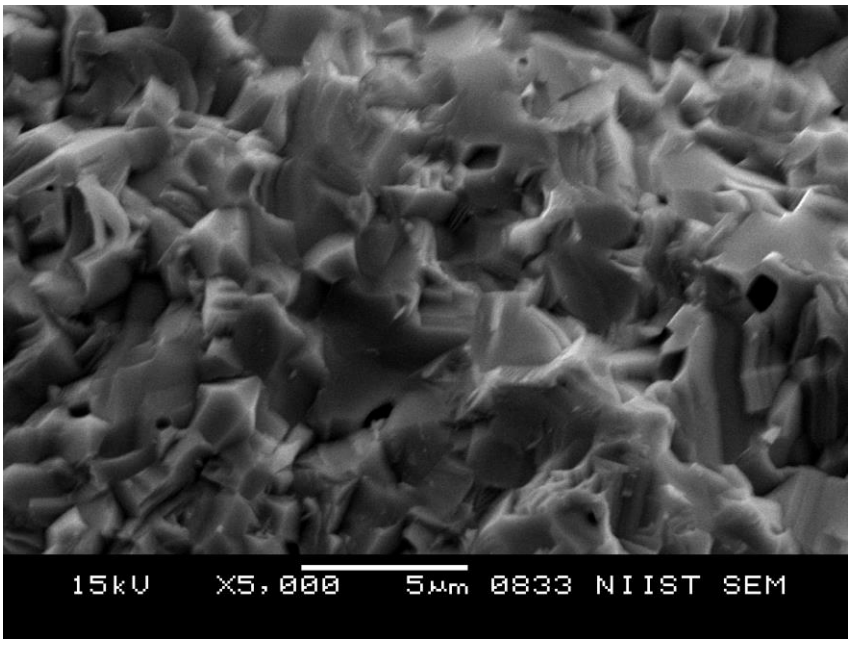

Figure 15) Microstructure of machined portion of $LaPO_4$

Flexural Studies

Flexural tests aid in understanding the mechanical properties as well as the underlying atomic structures that cause the properties of ceramic materials. Flexural strength is defined as a material's ability to resist deformation under load. It represents the highest stress experienced within the material at its moment of rupture. For a rectangular sample under a load in a three-point bending setup

Bending strength $\sigma = 3FL/2bd^2$

Where,

F is the load (force) at the fracture point (N),

L is the length of the support span (mm),

b is width (mm) and ***d*** is thickness (mm)

Here the bending strength for lanthanum phosphate sintered at 1300 °C was measured to be 95 MPa with a displacement of 0.3 mm and this value is at par with the reported value of 100 ±29MPa.[13]

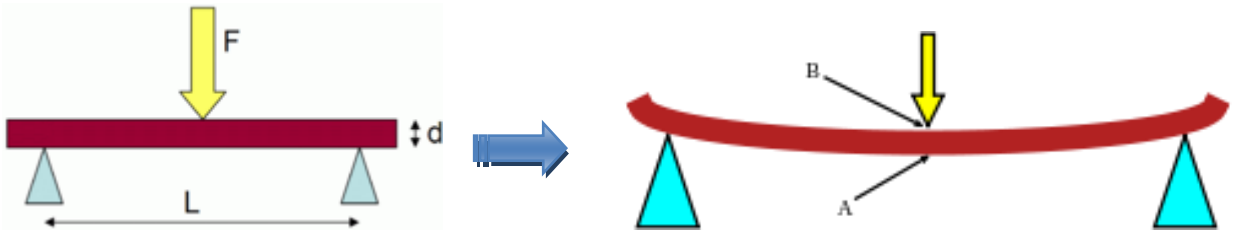

Scheme showing the flexural/bending strength measurement

2.7 $LaPO_4$- Y_2O_3 Nano Composite

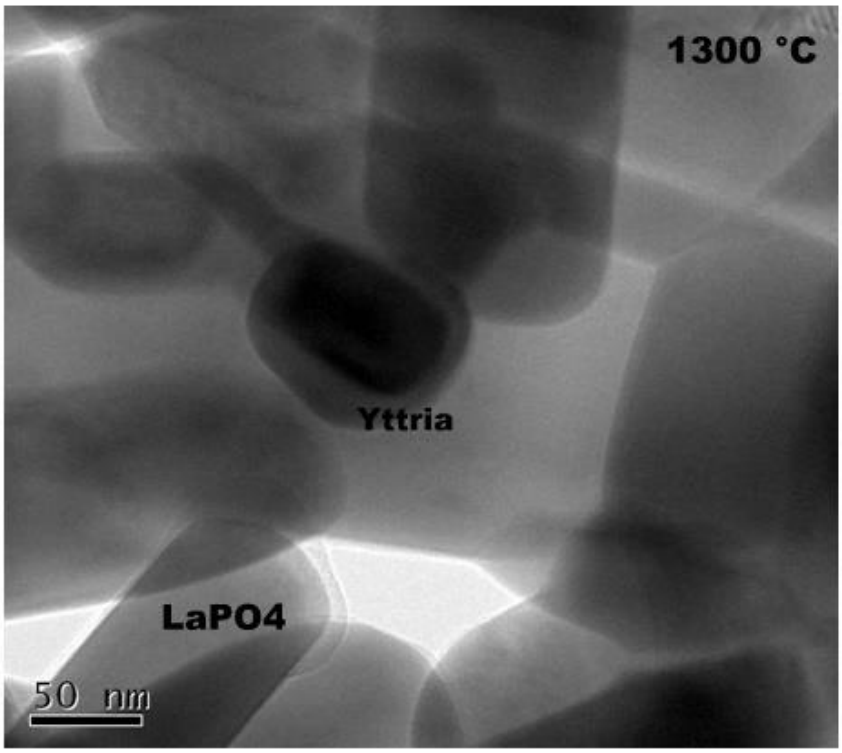

$LaPO_4$- 20wt% Y_2O_3 nanocomposite sintered at 1300 ºC

A facile aqueous sol-gel route involving precipitation – peptization mechanism followed by electrostatic stabilization is used for synthesizing nanocrystalline $LaPO_4$ –Y_2O_3 nano composite. Average particle size of ~ 70 nm after heat treatment of precursor at 600 °C is observed. $LaPO_4$ –Y_2O_3 composite through sol gel process is reported for the first time. TG-DTA analysis reveals that stable phase of the composite is formed on heating the precursor at 600 °C. The TEM images of the composites show rod shape morphology of $LaPO_4$ while yttria appears in near round shape. Phase identification of the composites as well as the phase stability at higher temperatures was carried out using X-ray Diffraction technique. With the phases being stable at higher temperatures, the composite synthesized should be a potential material for high temperature applications like thermal barrier coatings and metal melting applications.

The thermal decomposition characteristics of the lanthanum phosphate (80 wt %) – yttria (20 wt %) composite precursor can be observed from the *figure 16*. During the analysis a total weight loss of 41% was observed of which ~12 % occurred below 200 °C corresponding to the loss of physically absorbed water. A corresponding sharp endothermic peak can be noticed in the DTA curve. Above 200 °C the loss of hydration appears as a weight loss in theromogravimetric analysis and as an intense endothermic peak centred around 270 °C in the DTA curve. An intense exothermic peak around 323 °C is a strong indication of removal of nitrate ions added during the lanthanum phosphate sol synthesis and a weight of loss 13.14 % in the temperature range of 260-315 °C is observed from the TGA curve. Above 250 °C, $Y(OH)_3$ gets transformed to its oxyhydroxide form YOOH and then gets further decomposed to Y_2O_3. A weight loss of 9.62% occurs between 310 - 570 °C due to the formation of Y_2O_3 by de-hydroxylation of YOOH and corresponding endothermic peak appears in DTA curve. The TGA pattern obtained is similar to the pattern obtained for pure $LaPO_4$ showing the purity of the composite formed.

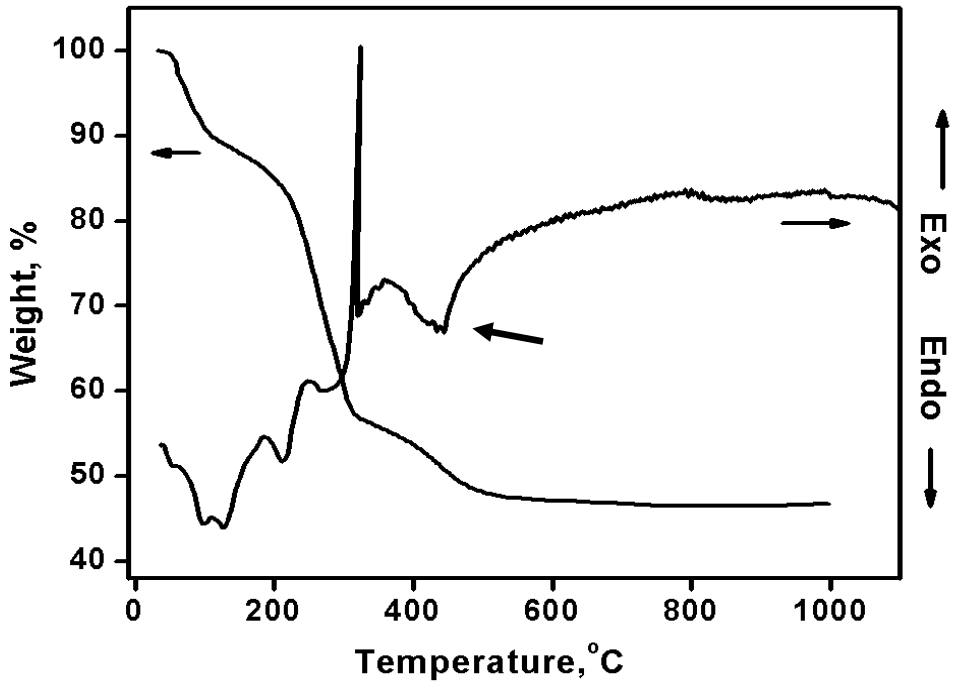

Figure 16) TG-DTA curve of $LaPO_4$–20wt%Y_2O_3 composite precursor dried at 70 °C

Figure 17 shows the X-ray diffraction pattern obtained for $LaPO_4$ -20 wt% Y_2O_3 gel precursor heated at 600° C. In the present case the peaks are well indexed with monoclinic $LaPO_4$ (JCPDS file No.46-1326) and cubic Y_2O_3 (JCPDS file No.44-0399).The identity of the phases are distinct and there appears to have no reaction between the two constituents at the heat treatment temperature. Earlier reports[15] however indicate that cubic yttrium oxide formation occurs when the hydroxide is heated at 500 °C. The composites were further heated to temperatures of 1300 °C and the corresponding X-ray diffraction pattern obtained is represented in *figure 18*. There appears no reaction between the $LaPO_4$ and Y_2O_3 and the composite is phase pure with respect to its constituents. The X-ray diffraction peaks are well indexed with monoclinic $LaPO_4$ (JCPDS File No.84-0600) and Cubic Y_2O_3 (JCPDS File No.82-2415).

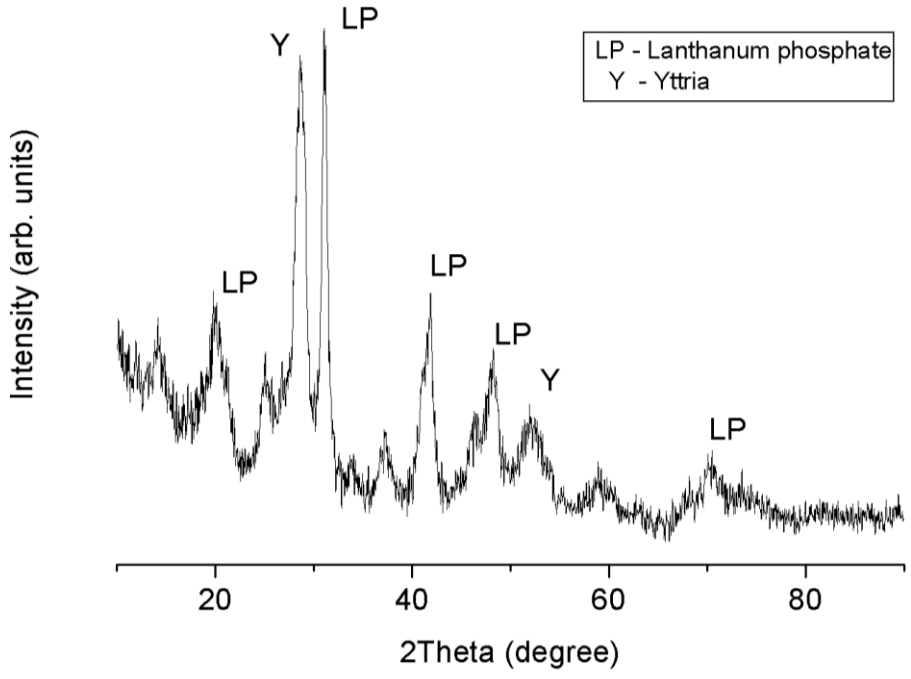

Figure 17) X-ray diffraction pattern for $LaPO_4$–20wt%Y_2O_3 nano composite precursor heated at 600 °C

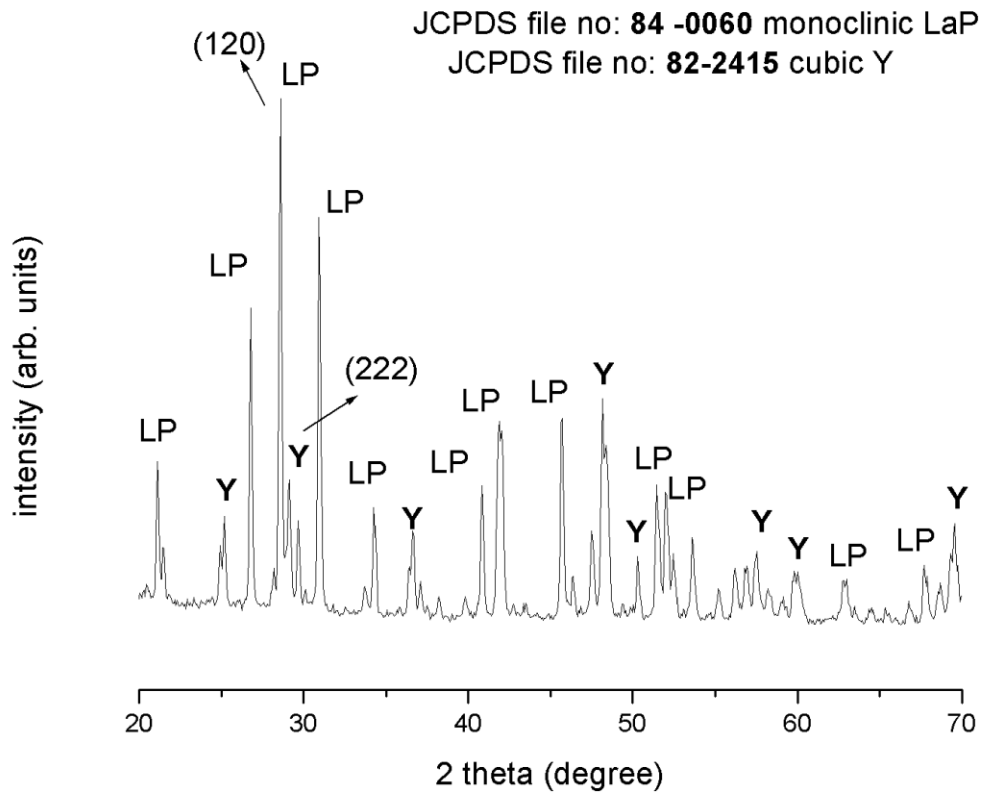

Figure 18) X-ray diffraction pattern for $LaPO_4$–20wt%Y_2O_3 nano composite precursor calcined at 1300 °C

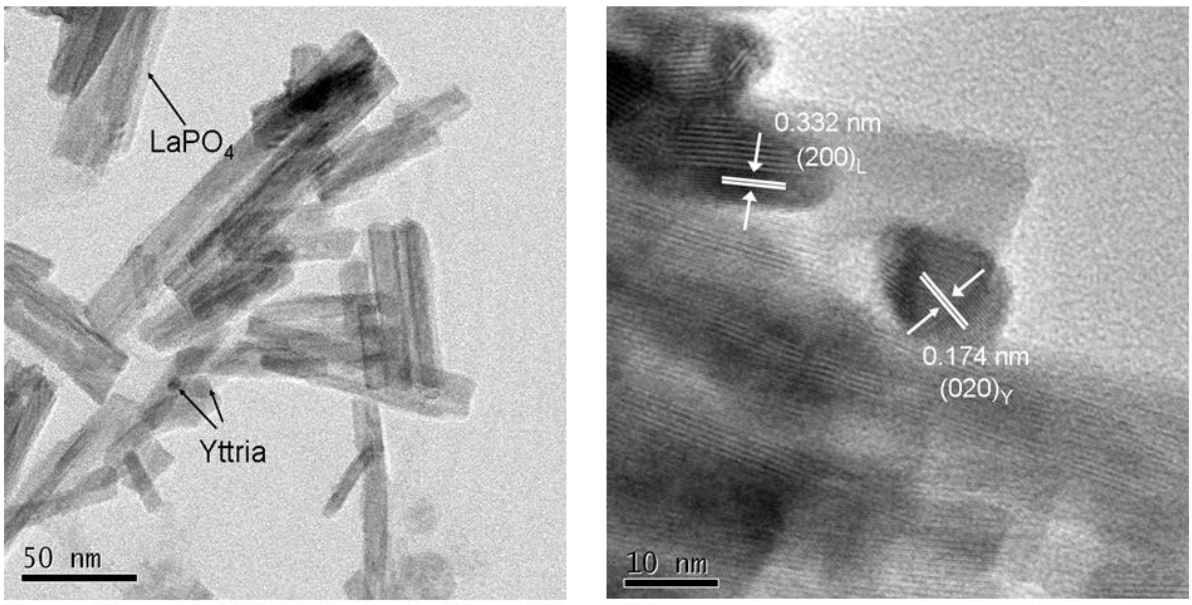

Figure 19) TEM micrographs of Lanthanum Phosphate –20wt%Yttria composite calcined at 600 °C

The $LaPO_4$- 20wt%Y_2O_3 composite precursor powder calcined at 600 °C was observed under transmission electron microscope and the corresponding micrographs obtained are presented in *Figure 19.* The $LaPO_4$ is found to possess rod shape[16] morphology and yttria appears spherical.[15] Micrograph reveals that the lengths of $LaPO_4$ nano rods are ~70 – 80 nm with a width of ~5 nm. The spherical yttria particles have average diameter of ~10 nm. The corresponding EDAX spectrum confirms the phases of $LaPO_4$ and Y_2O_3.

TEM micrograph of Lanthanum phosphate –Yttria nanocomposite calcined at 1300 °C is presented in page 59. The FFT (figure 20) obtained for the micrograph clearly indicates the presence of two phases with its corresponding planes. As evident from XRD obtained and supported by TEM image the composite is found phase pure at higher temperatures and could be used for high temperature applications.

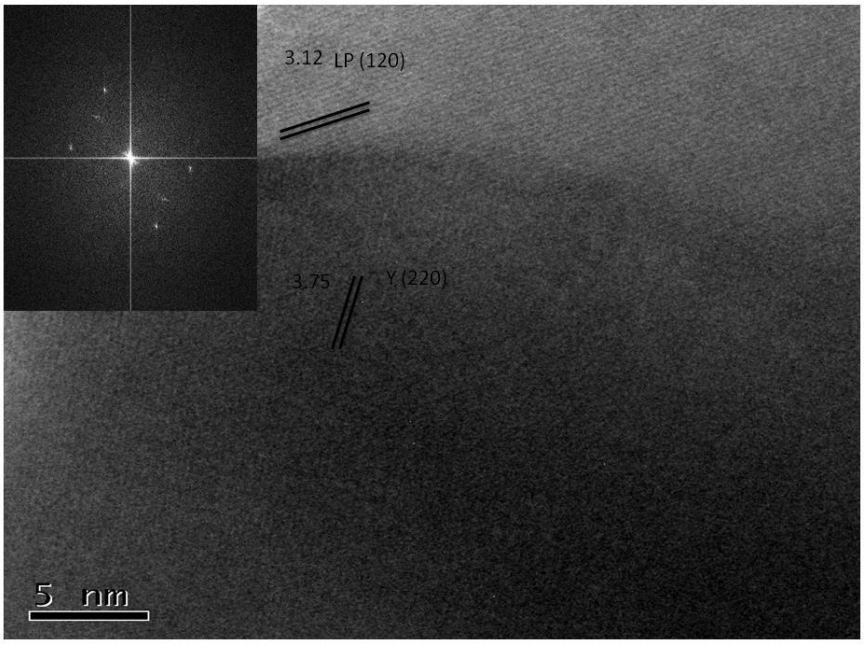

Figure 20) HRTEM micrograph of $LaPO_4$–20wt%Y_2O_3 composite calcined at 1300 °C

The FTIR spectra of LaP_4-20 wt% Y_2O_3 composite calcined at different temperatures were measured and are given in the figure 21 provided below. The broad band in 3500-3450 cm^{-1} range represents the O-H stretching frequency of water and corresponding bending vibration is seen at 1638 cm^{-1} The IR band between 3100-3000 cm^{-1} is due to the N-H stretching. Corresponding bending vibration is present around 1772 cm^{-1}. The N-H vibrations originate from ammonia used for flocculation. The peaks around 1467 and 1380 cm^{-1} indicate the presence of nitrate ion. These peaks are weak in 400 °C heated sample.

The peak at 1090 cm^{-1} is due to the phosphate P-O stretching and those around 616 and 540 cm^{-1} correspond to the O=P-O bending and O-P-O bending modes respectively. In figure 21b the P-O stretching band at 1090 cm^{-1} is split at higher temperatures and is a characteristic of monoclinic $LaPO_4$. In the monoclinic form the tetrahedral phosphate groups are distorted in the nine fold coordination of La atoms and the phosphate absorptions are split accordingly.[19, 20] Further, the polytrioxophosphate was also identified as absorbing at 770 and 1250 cm^{-1} both of which are absent in the IR spectrum in the present case, which shows there is no excess phosphate in the system

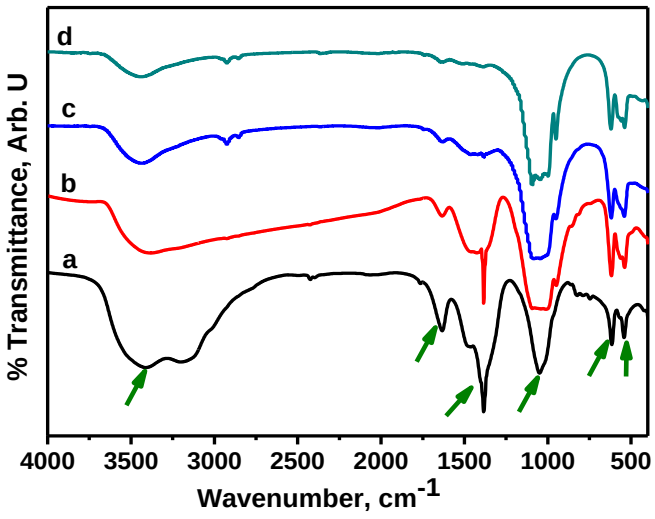

Figure 21) FT-IR spectra of $LaPO_4$-20 wt%Y_2O_3 composite **a**) dried at 70 °C **b**) heated at 400 °C **c**) calcined at 600 and **d**) 1000 °C

The sintering schedule of $LaPO_4$-20%Y_2O_3 composite was carried out in the range 1250-1600 °C with 3 h soaking time. The rate of heating from room temperature to 1000 °C was set at 5 °C/min, and from 1000 °C to high temperature at 10 °C/min. Densification behaviour of $LaPO_4$ as well as $LaPO_4$-20 wt% Y_2O_3 pellets which were uniaxially pressed and heated at 400 °C was monitored using dilatometry upto a temperature of 1400 °C as shown in *figure 22*. The shrinkage schedule also could be observed from the figure provided. The shrinkage curve shows that the rate of shrinkage in composite is less compared to pure $LaPO_4$. As discussed earlier and from the current data obtained for pure $LaPO_4$, it is evident that sintering starts around 1200 °C and finishes at 1300 °C while the composite ($LaPO_4$-20%Y_2O_3) would require still higher temperature to get sintered due to the presence of a second phase and also the schedule shows sintering has just started around 1200 °C.

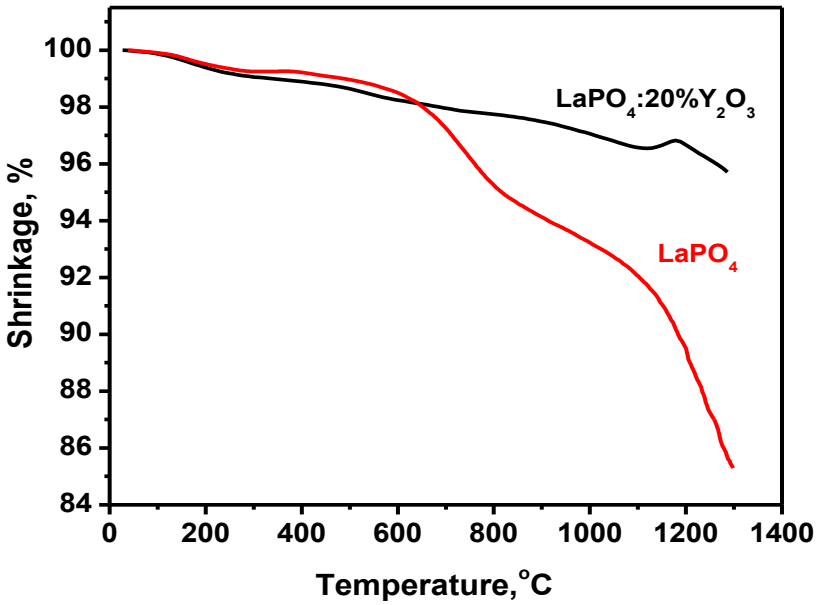

Figure 22) Shrinkage schedule obtained for $LaPO_4$-20%Y_2O_3 composite and $LaPO_4$

The relative density of sintered samples was calculated by rule of mixtures. The theoretical density of $LaPO_4$ is 5.06 g/cc and that of yttrium oxide is 5.03 g/cc.The comparative study of sintering of different compositions and temperatures are represented in figure 23. The

sintered density is measured in accordance with the Archimedes' principle. It could be observed that the sintered density is increasing along with temperature in every composition. The relative density of $LaPO_4$ - 5 wt% Y_2O_3 was found to be 98.6% where as $LaPO_4$-20 wt% Y_2O_3 has 93% density at a sintering temperature of 1600 °C. $LaPO_4$ synthesis through sol-gel method attained sintered density of 99.8 wt% at 1300 °C (section 2.6). The decrease in density of $LaPO_4$ on the addition of Y_2O_3 is due to distribution of fine yttria particles on the grain boundaries of $LaPO_4$.[21]

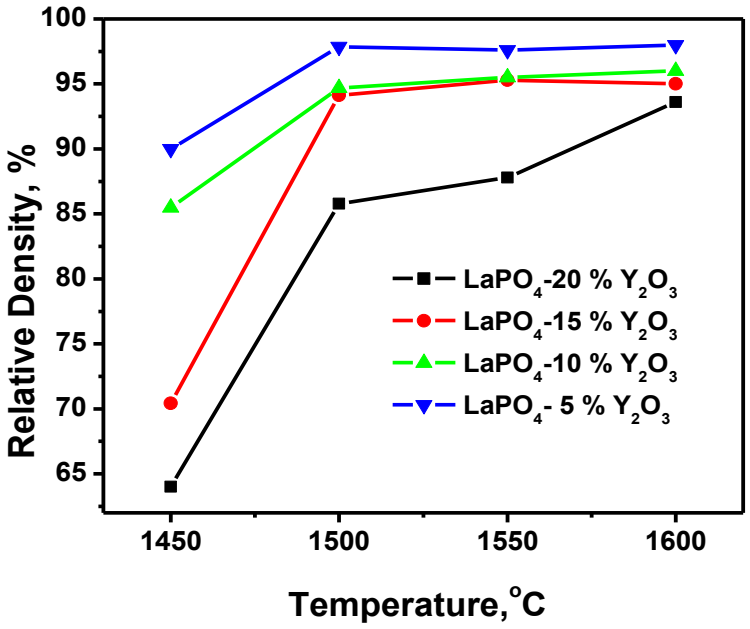

Figure 23) Plot of relative density of $LaPO_4$-Y_2O_3 composite versus temperature

The microstructural investigation on sintered composite pellets calcined at different temperatures was done. The sintered pellets were polished and were washed thoroughly with distilled water and thermally etched below the sintering temperature. The figure 24 shows the SEM of 1600 °C sintered $LaPO_4$-Y_2O_3 composite with varying concentration of yttria content. Average grain size is found to be ~ 2 μm for $LaPO_4$.The EDAX spectrum obtained shows the presence of Yttria which is found in along the grain boundaries.

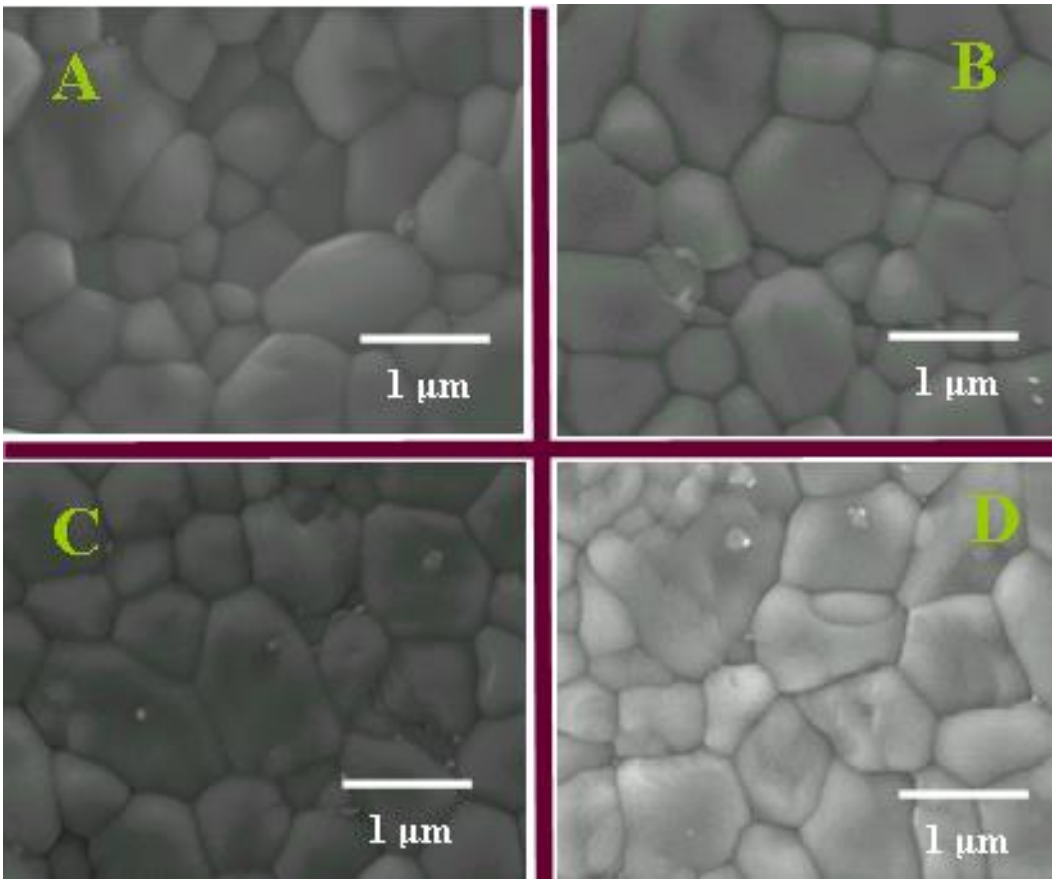

Figure 24) SEM image of composite sintered at1600 °C, polished and etched pellets of $LaPO_4$-Y_2O_3 A) 5, B) 10, C) 15 and D) 20 wt% of yttria

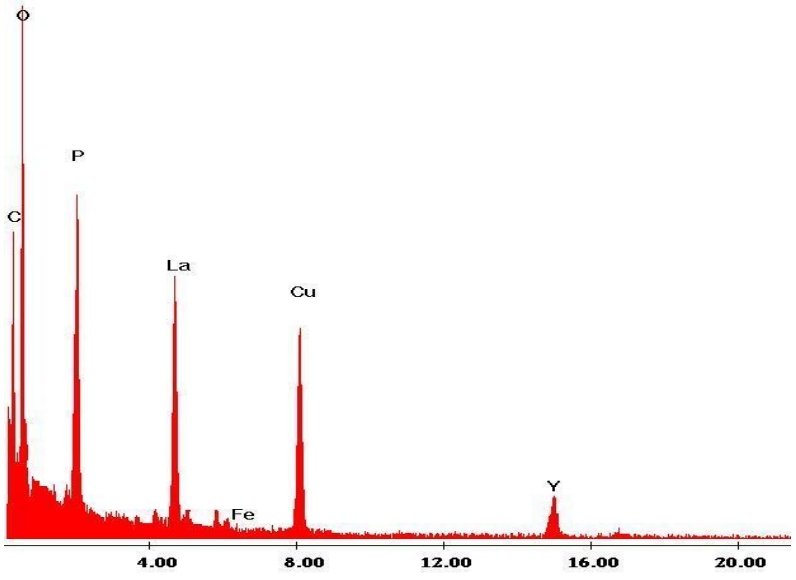

EDAX spectrum obtained for $LaPO_4$-20wt%Y_2O_3 sintered at 1600 °C

2.8 $LaPO_4$– ZrO_2 composite

A facile wet chemical approach involving precipitation- peptization mechanism is successfully adopted to synthesize $LaPO_4$–ZrO_2 composites with ZrO_2 percentages varying from 5-20 wt%. The composite precursor heated to ~650 °C develops rod like morphology for $LaPO_4$ were as ZrO_2 phase appears in near spherical morphology as was evident from TEM micrographs. ZrO_2 addition to $LaPO_4$ has resulted in considerable grain growth inhibition in $LaPO_4$, thus finding a solution to one of the major issues in obtaining fine grain sintered $LaPO_4$ at higher temperature. Grain growth reduction as much as ~50% was achieved by the addition of ZrO_2. Densification of >98% TD was achieved for $LaPO_4$ on heat treatment at 1400 °C while similar density is obtained by sintering at 1600 °C for the $LaPO_4$ - 10% ZrO_2 composite. In addition, $LaPO_4$-ZrO_2 composite possesses low thermal conductivity values compared to ZrO_2 especially at higher temperatures. There is no reactivity between $LaPO_4$ and ZrO_2 and the fine grain sintered composite could be a promising high temperature thermal insulation with excellent non-reactive property.

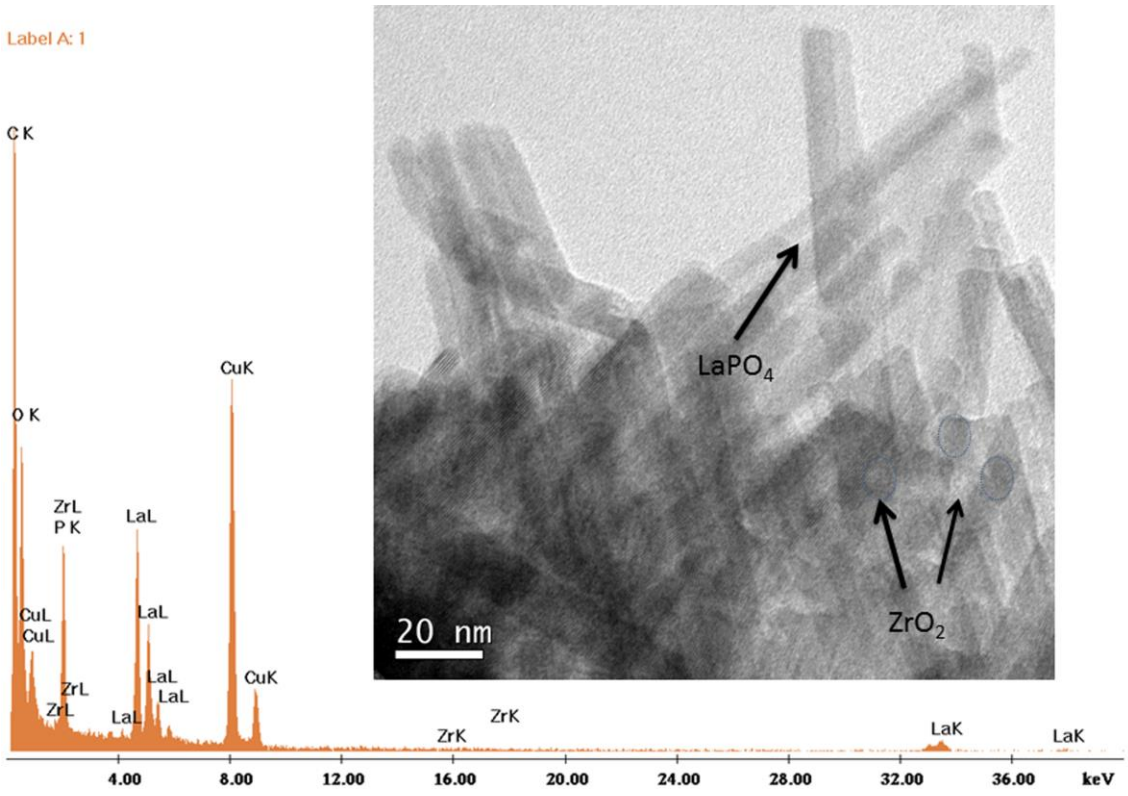

Thermal decomposition data obtained from for *$LaPO_4$*-10% ZrO_2 composition indicate that there is a total weight loss of ~10% (figure 25). Nearly ~5% weight loss was below 200 ^oC and could be attributed due-to the loss of physically adsorbed water. A weight loss of ~ 4% between 200 ^oC and 400 ^oC was partially attributed to residual nitric acid that came from $LaPO_4$ sol used for preparation. The endothermic DTA peak due to loss of water of hydration is at 230 ^oC while that of nitrates is found around 320 ^oC. An endothermic peak appears in DTA curve is certainly due to the formation of ZrO_2 (tetragonal phase) from $Zr(OH)_4$ at ~650 ^oC and this low temperature formation is due to the low average particle size obtained in comparison to higher particle sizes during solid state synthesis were monoclinic phase is formed initially and is converted only at ~1100 ^oC.[22]

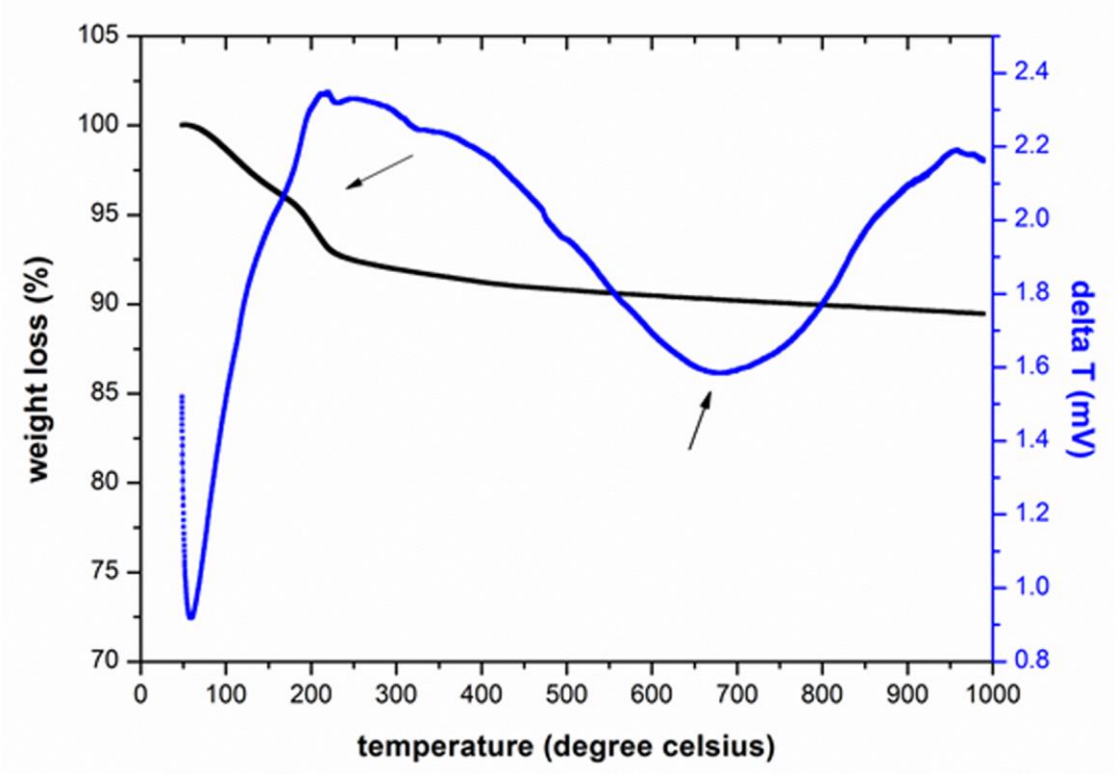

Figure 25) TG-DTA curve obtained for $LaPO_4$-10% ZrO_2 composite

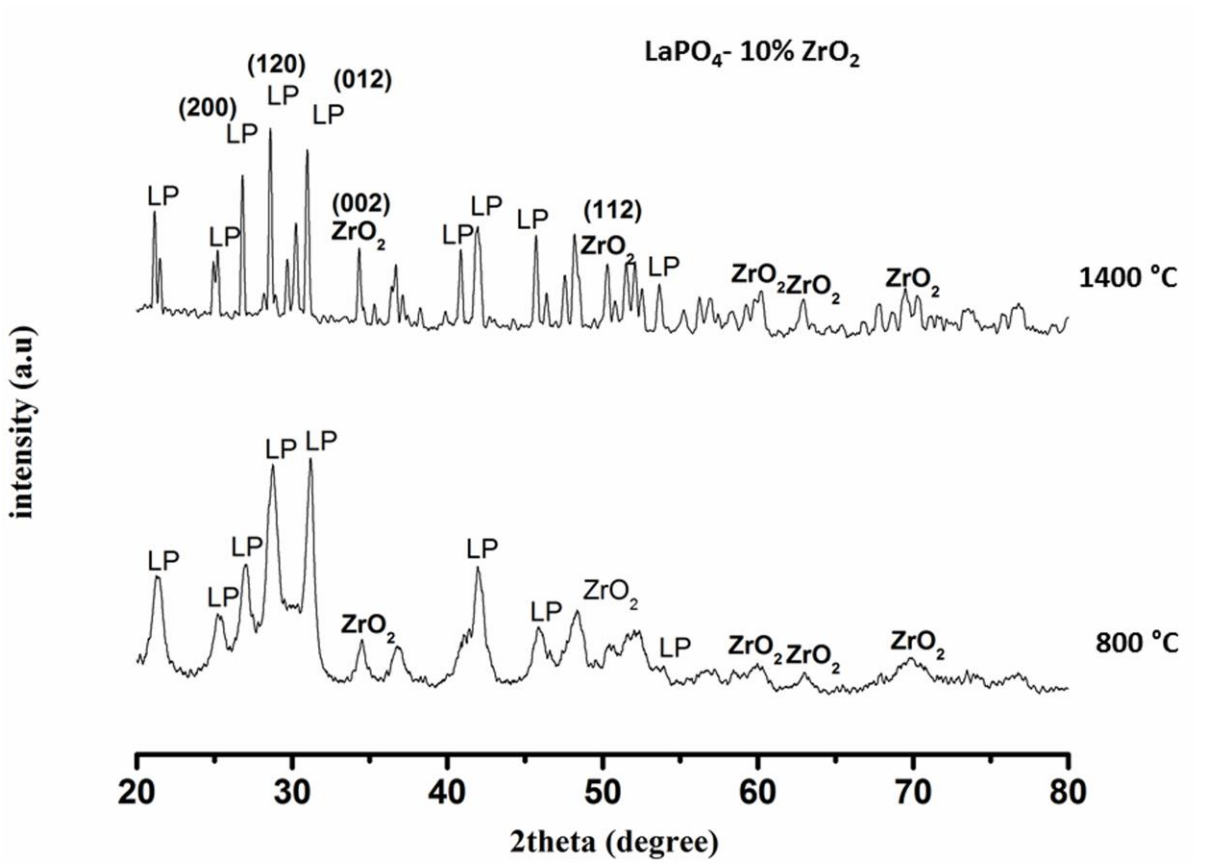

Figure 26) X-ray diffraction pattern for the composite calcined at 800 and 1400 °C.

Figure 26 shows X-Ray Diffraction patterns obtained for $LaPO_4$-ZrO_2 composite precursor calcined at 800 ºC and composite sintered at 1400 ºC. The peaks are well indexed with monoclinic $LaPO_4$ (JCPDS file no. 35-0731) and tetragonal ZrO_2 (JCPDS file no. 81-1544) for the sample heated at 800 ºC which are in accordance with the TG-DTA analysis for the formation of the composite. The diffraction peaks indexed to (200), (120) and (012) crystal planes of monoclinic $LaPO_4$ appear at 26º, 28º and 30º 2θ. The composite was further heated to a temperature of 1400 ºC, and the results show no reaction as well as formation of new phases. Therefore possibility of using the composite at higher temperatures is feasible. TEM micrographs along with EDAX spectrum obtained for 800 (*figure 27*) and 1400 ºC heated composite precursors also provide clear indication to the formation of the composite as well

as the stability at higher temperatures.The rod like morphology of the $LaPO_4$ is retained at

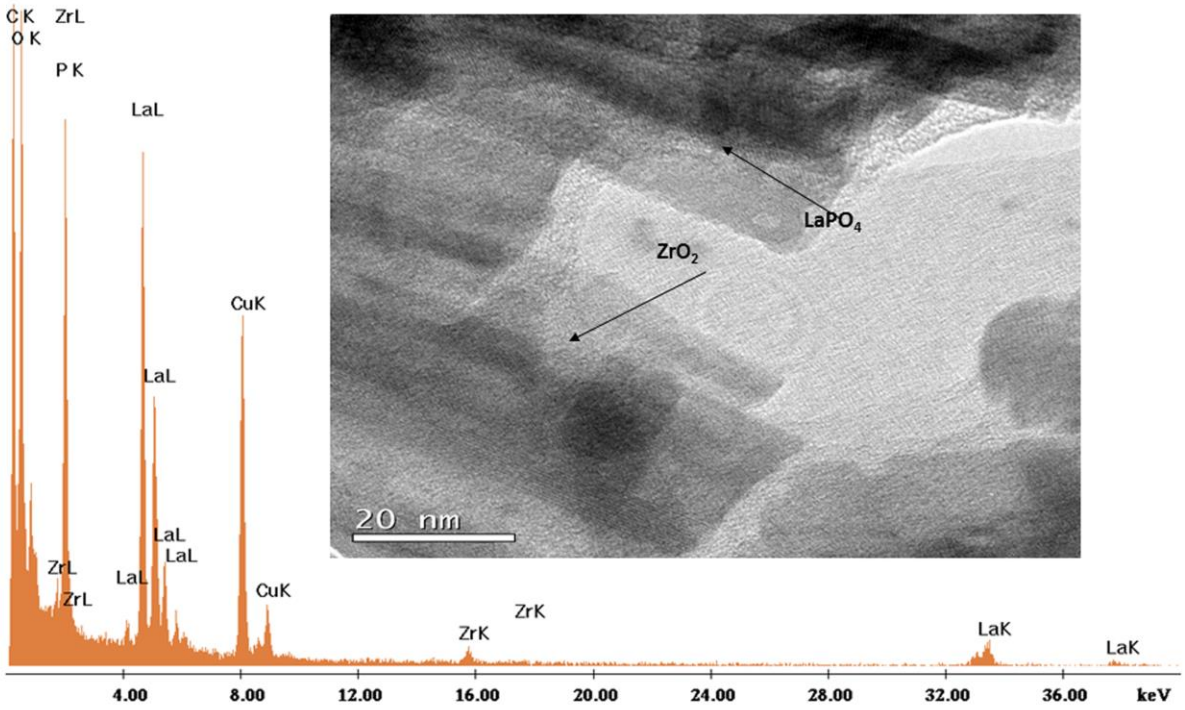

1400 ºC (TEM micrograph provided in page 32)

Figure 27) TEM image of the 800 °C calcined precursor powder and the corresponding edax spectrum

Density measurements were carried out using Archimedes principle and are presented in *figure 28*. The composite precursor calcined at 100 °C was compacted to pellets of 11 mm diameter uniaxially which were sintered at rate of 3°C/min over a temperature range of 1400-1600 °C with soaking time of 3h. From the graph we can see that, on sintering at 1400 °C composite samples with 5 and 10wt % ZrO_2 yielded >90 % TD density while $LaPO_4$ - 20% ZrO_2 had a poor sinterability. Sintering at 1600 °C with the same conditions, all the four compositions yielded greater than 90 % of the theoretical density. $LaPO_4$-10% ZrO_2

composite yielded a good theoretical density of greater than 98% with 5 and 15 % compositions having >95% TD. Although lanthanum phosphate gets sintered at ~ 1300 °C, the decrease in density on the addition of ZrO_2 could be attributed to the distribution of fine ZrO_2 particles on the grain boundaries of $LaPO_4$ which is evident from the SEM observation.

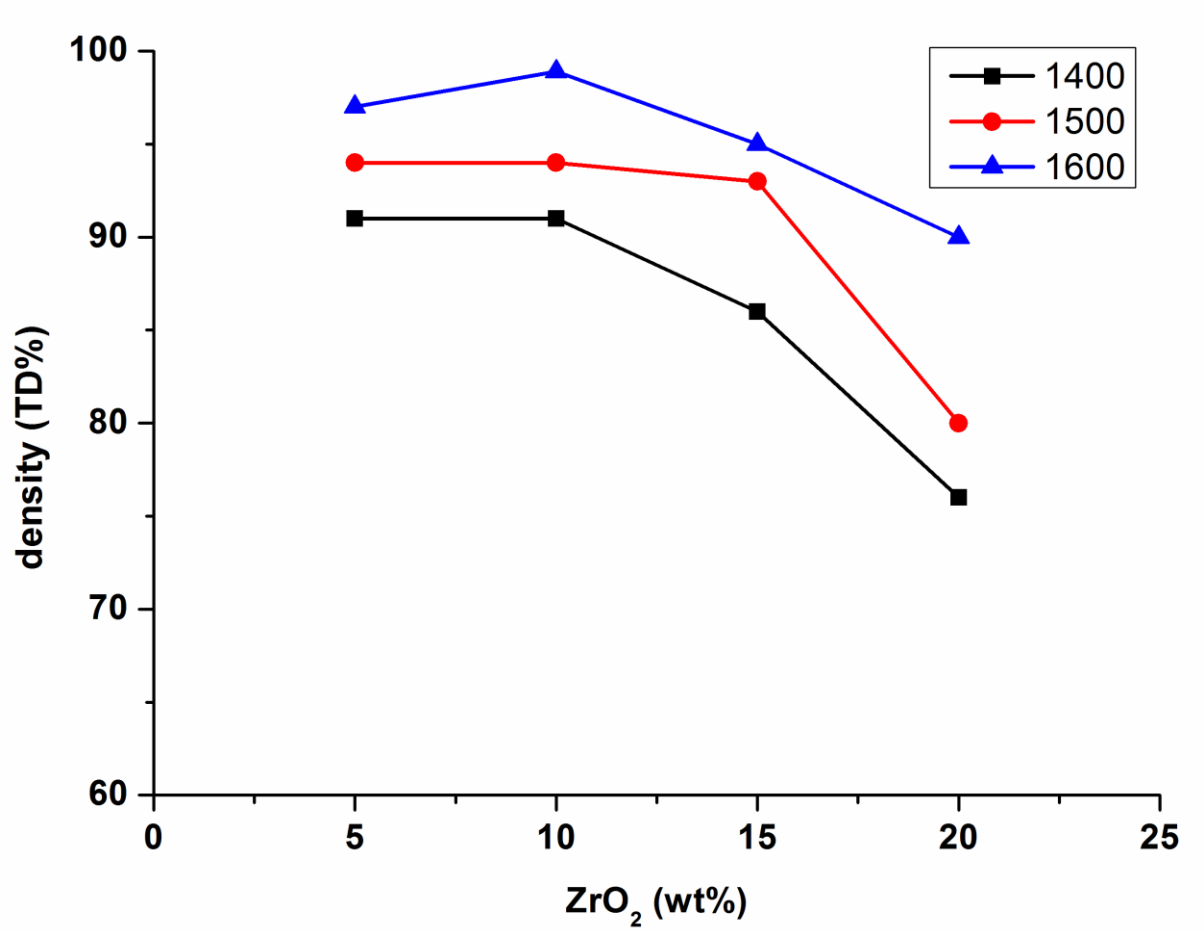

Figure 28) Plot showing densities acquired for the composite samples with respect to sintering temperature and ZrO_2 addition

The pellets were mirror polished, thermally etched and were observed under scanning electron microscope for the microstructural evaluation. The SEM micrographs obtained for composite samples, sintered at 1600 °C,with addition of 5% - 10 % ZrO_2 presented in figure 26 reveals that the size of $LaPO_4$ grains gets reduced when compared to that of pure $LaPO_4$ (> 4 µm, Figure 30).With the increase in content of ZrO_2 to 20%, the grain growth of $LaPO_4$ has been inhibited to nearly 50% with an average grain size of ~1-2 µm as seen in *figure 29d*

($LaPO_4$-20% ZrO_2). The distribution of ZrO_2 in the composite samples is evident from the micrographs obtained. The reduction in grain size of $LaPO_4$ with increasing ZrO_2 content is also given as a table *(table 2)*.

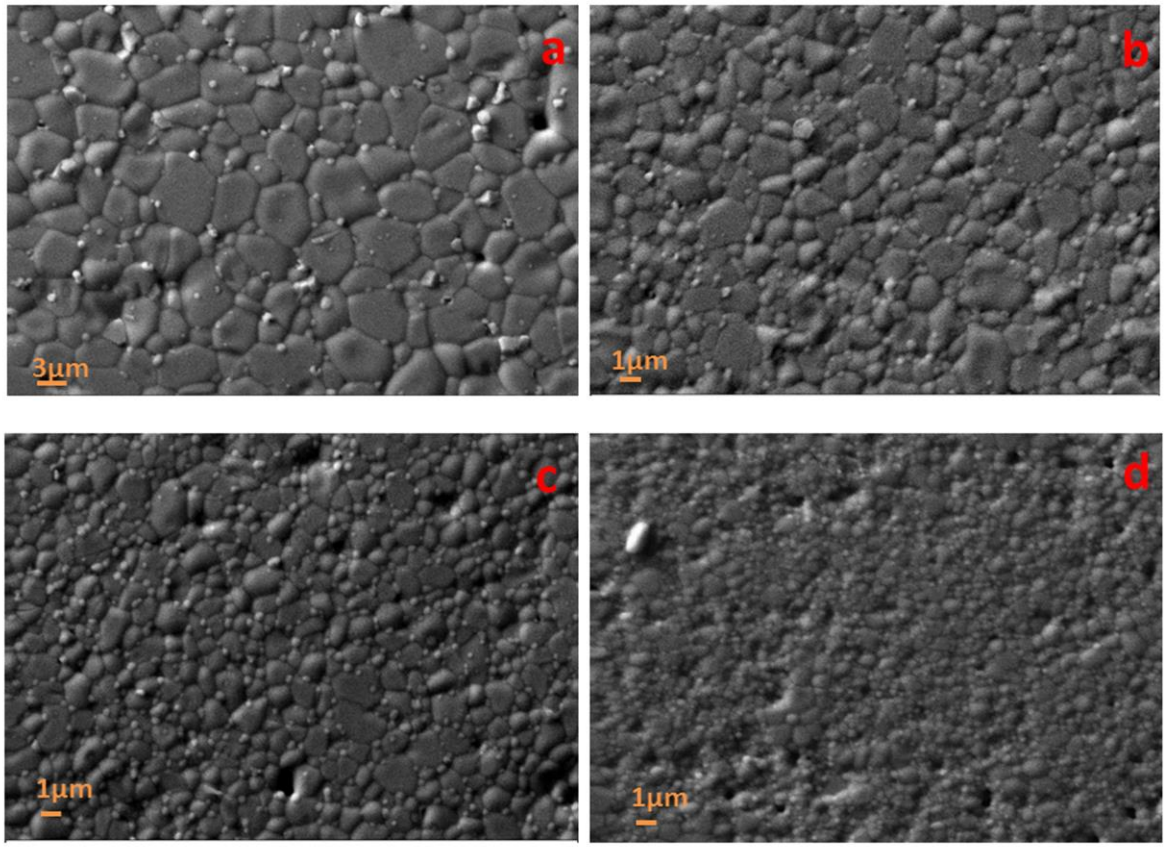

Figure 29) SEM micrographs of $LaPO_4$-ZrO_2 composites sintered at 1600 °C **a)** $LaPO_4$- 5% ZrO_2 **b)** $LaPO_4$-10% ZrO_2 **c)** $LaPO_4$-15% ZrO_2 **d)** $LaPO_4$-20% ZrO_2.

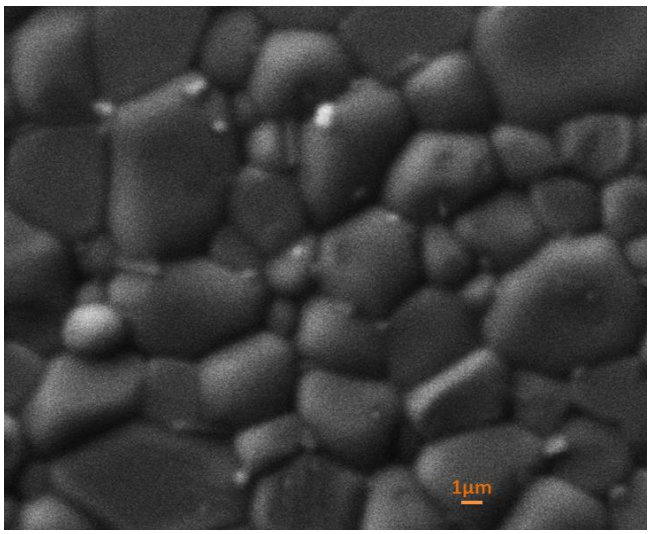

Figure 30) SEM image of the 1600 °C sintered and etched $LaPO_4$ sample

Although there are reports[20] on ZrO_2 acting as grain growth inhibitor, we hypothesize in this case, that ZrO2 will restrict the growth of phosphate grains at their grain boundaries due to the higher thermal expansion coefficient of ZrO_2 in comparison with $LaPO_4$. The reduction in sintered grain size will definitely improve the $LaPO_4$ stability to higher temperatures. Further, the presence of La^{3+} induces oxygen vacancies and strain in zirconia which stabilizes tetragonal phase and decreases the concentration of monoclinic phase with poor mechanical properties.[23]

Composition	Average Grain Size
$LaPO_4$	**4 µm**
$LaPO_4$ + 5% ZrO_2	**3.8µm**
$LaPO_4$ + 10% ZrO_2	**2.9µm**
$LaPO_4$ + 15% ZrO_2	**2.5µm**
$LaPO_4$ + 20% ZrO_2	**1.9µm**

Table 2) Grain reduction pattern for the compositesamples.

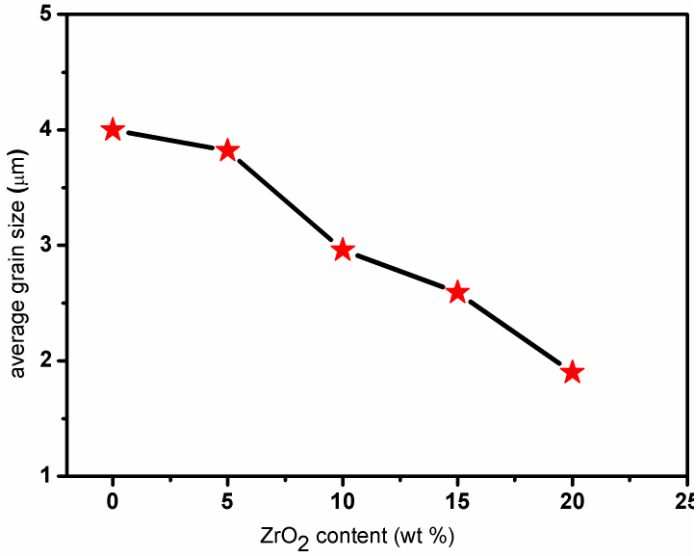

Figure 31) Grain size reduction with respect to ZrO_2 content.

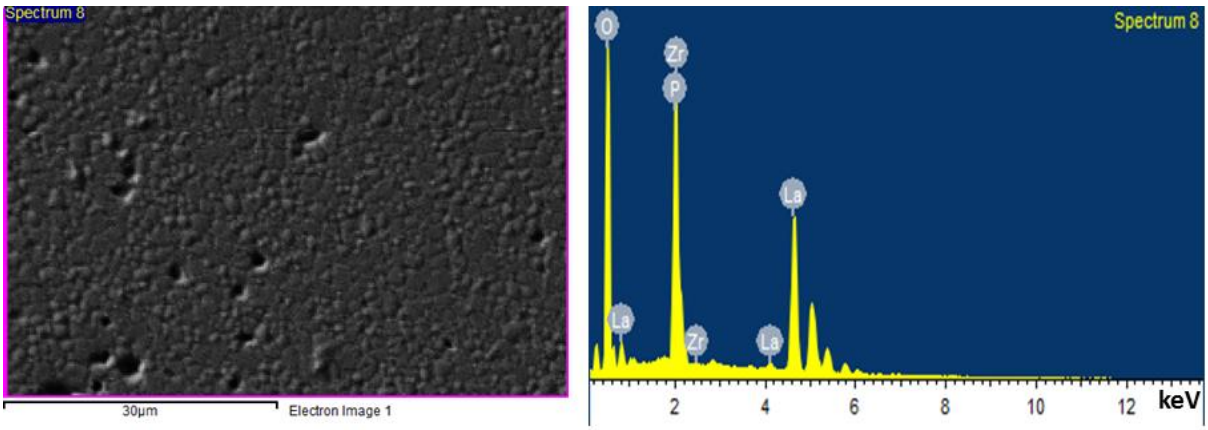

Figure 32) SEM image of the 1600 °C sintered $LaPO_4$- 10% ZrO_2 pellet sample and the corresponding EDX spectrum

2.8.1 Thermal conductivity

Thermal behaviour of the composite was analysed using a laser flash method and *figure 33* explains the trend in thermal conductivity for the composite with respect to temperature. Lanthanum phosphate shows a thermal conductivity value of 3.2 W/mK at 25 °C which is less than the previous reports[24] (3.61 W/mK) and shows a decreasing trend with increase in temperature in accordance to literature [21] and this is primarily due to the nanocrystallanity and high surface area obtained for the $LaPO_4$ obtained using the wet chemical method.[18] In the composite samples, $LaPO_4$-10 wt% ZrO_2 showed low conductivity values of 2.1 W/mK and 1.4 W/mK at room temperature and 200 °C respectively which can be ascribed to the reduction in grain size of the phosphate with ZrO_2 addition since the relation between thermal conductivity and grain size of a material is known to be linear. The grain size of a material decreases, the number of grain boundaries increases. The low thermal conductivity is due to the enhanced phonon scattering arising from the presence of numerous closely spaced grain boundaries.[27] So, the thermal conductivity of material decreases with increasing the GBs and this is the reason for low thermal conductivity in $LaPO_4$-ZrO_2 composite material. Thermal conductivity value for $LaPO_4$- 20% ZrO_2 was found out as 1.2 W/mK at 25 °C and on increasing the temperature to 400 °C, the value obtained was ~ 1 W/mk. The very low

thermal conductivity for the composite could be due to the combined effect of the reduced grain size as well as the porosity induced.

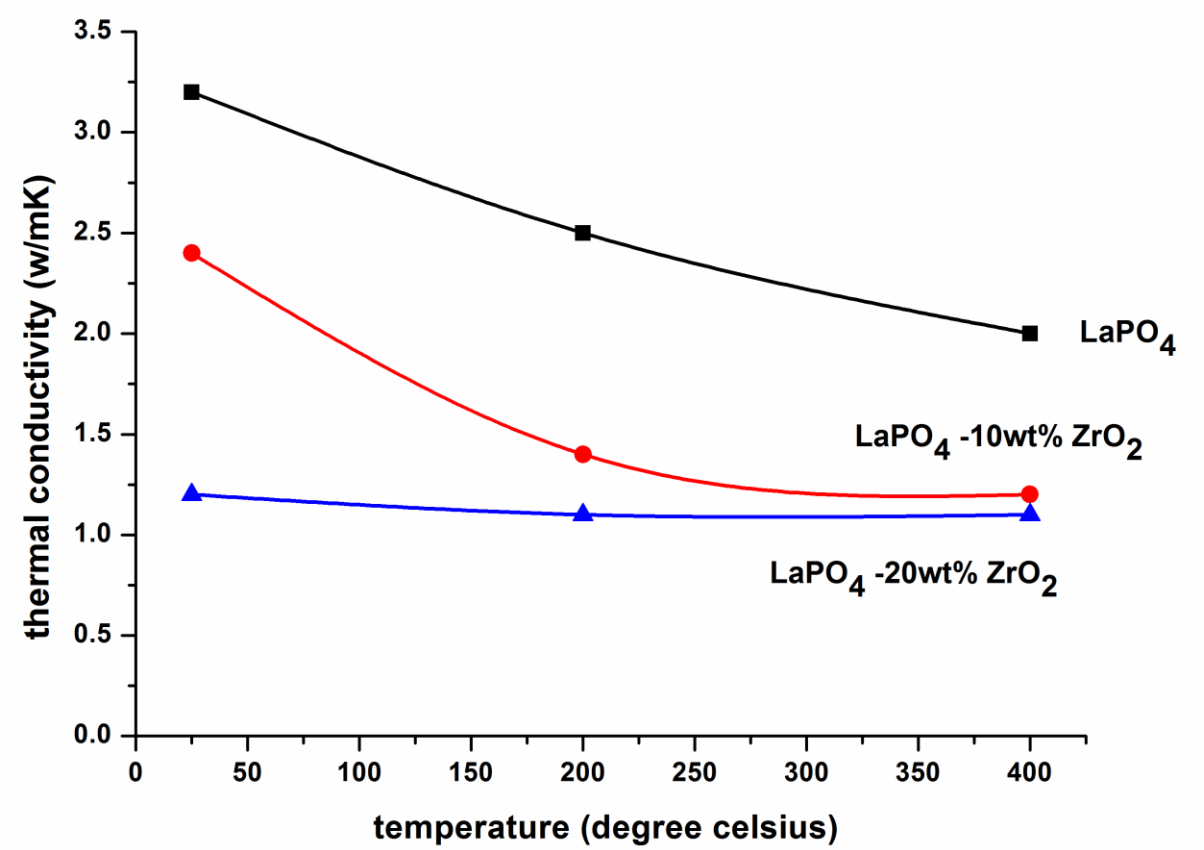

Figure 33) Thermal conductivity values obtained for the samples sintered at 1600 °C with varying composition and increase in the temperature range 25- 400 °C

2.9) Plasma Spray coating

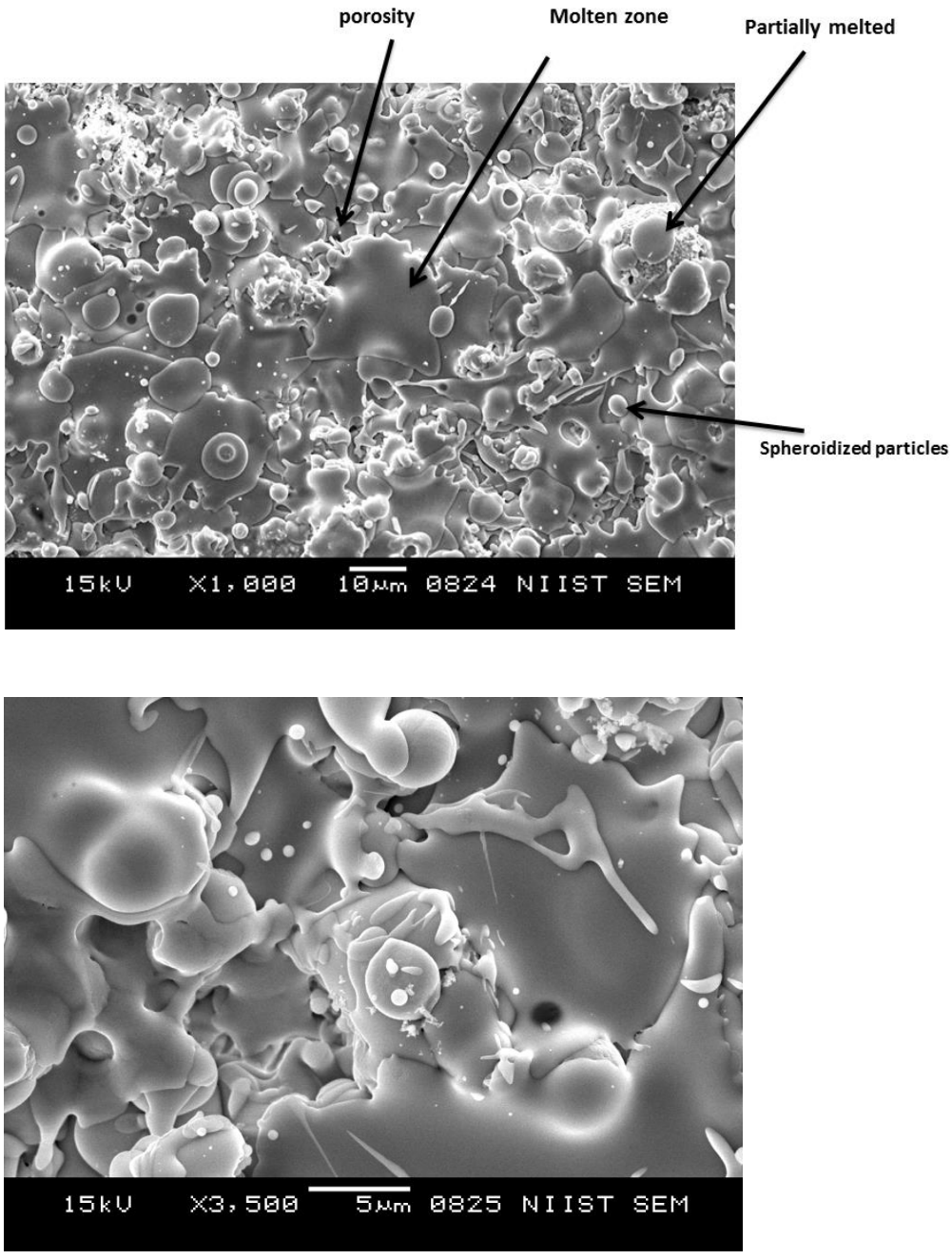

Figure 34) Microstructures of $LaPO_4$ plasma sprayed coating at 16 kW

Thermal and chemical stability of $LaPO_4$ and $LaPO_4$ -20%Y_2O_3 coating was studied by plasma spheroidization experiments using a DC thermal plasma reactor set up. Plasma

spheroidization and melting experiments showed that monazite phase melted congruently without decomposition. Plasma spray deposition on stainless steel substrates was carried out by atmospheric plasma spray system. Adherent coatings of $LaPO_4$ as well as $LaPO_4$ - 20%Y_2O_3 could be obtained with reasonably good deposition efficiency. Plasma coated samples of required dimensions were cut from the coated piece and metallographically prepared and examined. Typical microstructures of the coatings are provided.

The microstructure (figure 34) across the coating cross-section shows fully molten lamellae, craters, un-melted particles and molten spherical particles characteristic of plasma spray deposited coatings. Porosity of the coatings was determined from the surface morphology and cross-sectional microstructures of the coatings. Less porosity was observed indicating good deposition efficiency. The thickness of the coatings is about 100µm (figure 35). The microstructural features at the coating–substrate interface did not show any de-lamination indicating good adhesion of the coating to the substrate. The micrographs obtained clearly indicate that the microstructural features depend on the plasma power as decrease in porosity and increase in molten lamellae zone is observed (*figure 36*).

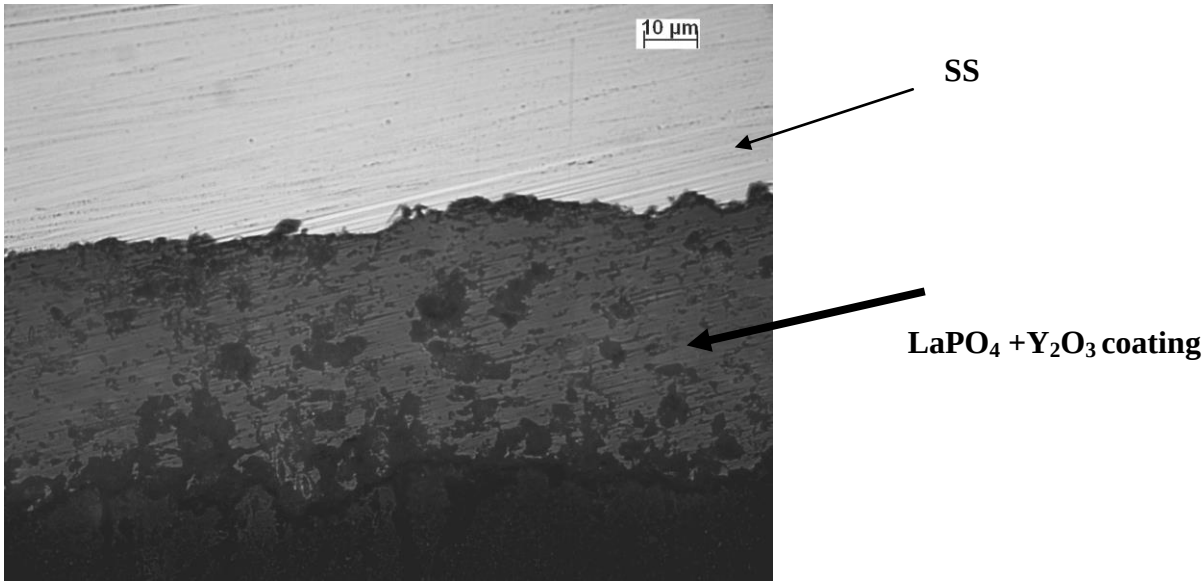

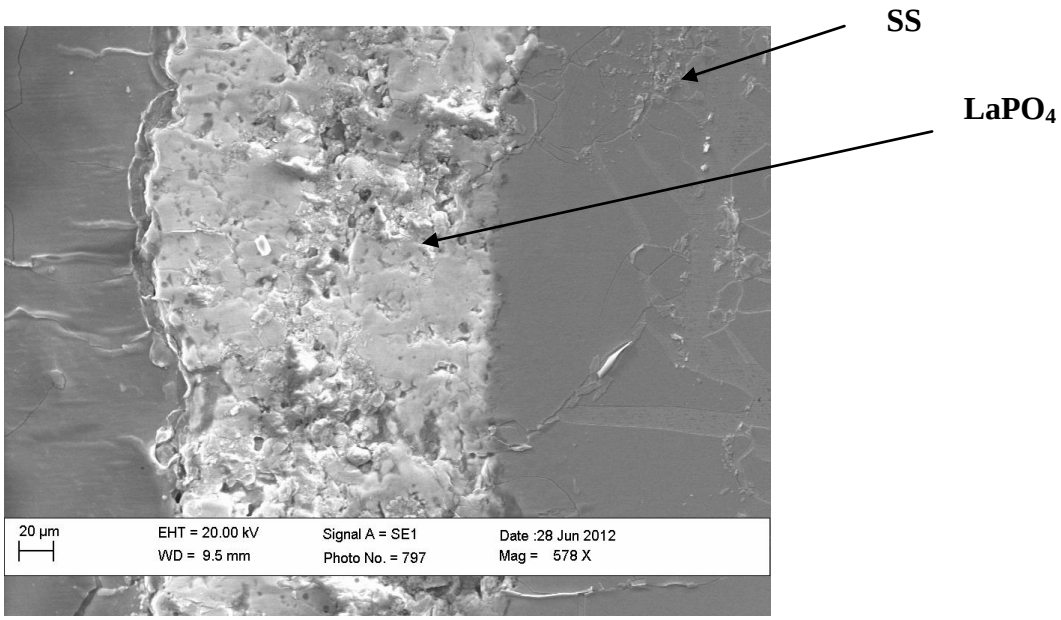

Figure 35) SEM images showing thickness of plasma sprayed coatings

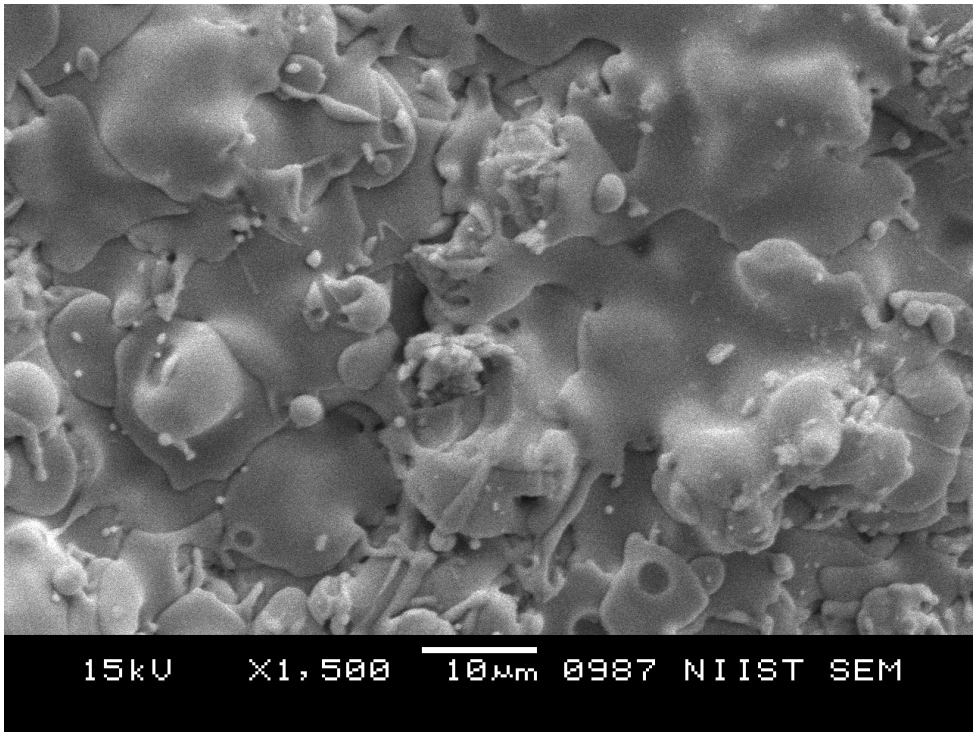

Figure 36) Microstructure of $LaPO_4$ plasma sprayed coating at 20 kW

Chapter 2

Conclusions

Synthesis of stoichiometric lanthanum phosphate nano particles from lanthanum chloride through an environment friendly aqueous sol-gel method was done and the resultant compositions were characterized. The nano rod morphology was found to happen in the initial step of the current sol-gel process and this morphology is retained even at higher temperature. The average particle size of the $LaPO_4$ after precipitation was ~110 nm and was further reduced to ~80 nm and the size distribution was narrow. The lanthanum phosphate was compacted and sintered at temperature as low as 1300 °C due to the fine size and was characterized using TGA, FTIR, XRD, High Resolution Transmission Electron Microscopy, Scanning electron microscopy and contact angle measurements. The contact angle values obtained in the range of 80° - 90° for the $LaPO_4$ particles indicate the potential for further applications in high temperature hydrophobic non-wetting coatings and composites. Lanthanum phosphate has a thermal expansion co-efficient of 8.6 x 10^{-6}/°C nearly identical to alumina. Lanthanum phosphate was successfully machined using abrasive water jet cutting and has good flextural strength of 95Mpa which is close the reported value.

Lanthanum phosphate based yttria ($LaPO_4$-$Y_2O_{3)}$ and zirconia composites ($LaPO_4$-ZrO_2) are successfully prepared extending the precipitation-peptization mechanism. Both Yttria and Zirconia content of 5-20 wt% were used to synthesize the composites and with $LaPO_4$-10% ZrO_2 and $LaPO_4$- 5% Y_2O_3 helped in achieving >98% TD on sintering at 1600 °C. The stability of the composites at higher temperature was confirmed using phase identification as well as microstructural evaluation which showed no reaction between the phases. Microstructural evaluation confirmed the grain growth inhibition of lanthanum phosphate by the addition of ZrO_2. The excellent insulation property obtained for the composite could prove to be advantageous in developing $LaPO_4$- ZrO_2 based composites as thermally

insulating material and for high temperature application including thermal barrier coatings and prove advantageous over the existing oxide based TBC materials.

Plasma spray coatings of $LaPO_4$ and $LaPO_4$-Y_2O_3 composites on metallic substrate could be achieved with good deposition efficiency and adherence which will enable it for being used for high temperature applications. Microstructal evaluation showed an average thickness of 100 μm with good deposition and adherence to the SS substrate.

Chapter 2

REFERENCES

1. R.B. Heimann, Plasma-spray coating principles and applications, *VCH Verlagsgesellschaft* mbH, **1996**.

2. A. Pragatheeswaran, P.V. Ananthapadmanabhan, Y. Chakravarthy, Subhakar Bhandari, T.K. Thiyagarajan, N. Tiwari, T.K. Saha, K. Ramachandran, *Ceramics International*, 40, **2014**, 10441.

3. Z. Chai, L. Gao, C. Wang, H. Zhang, R. Zheng, P. A.Webley , H. Wang, *New J. Chem.*, 33, **2009**, 1657.

4. A. Hezel and S.D. Ross, *Spectrochimica Acta* 22**, 1966**, 1949.

5. K. Rajesh, P. Shajesh, O. Seidel, P. Mukundan, K. G.K.Warrier, *Adv. Func Mater.* 17,**2007,**1682.

6. Y.P Fang, A.W Xu, R.Q Song, H.X. Zhang, L.P You, J.C Yu, H.Q Liu, *J. Am. Chem. Soc.*,125, **2003**,16025.

7. K.E Murphy, M.B Altman, B. Wunderlich, *J. Appl. Phy.*, 48, **1977**, 4122.

8. W. Min, D. Miyahara, K. Yokoi, T. Yamaguchi, K .Daimon, Y. Hikichi, T Matsubura, T. Ota, *Mater. Res. Bull.*, 36, **2001**, 939.

9. M. R. Winter and D. R. Clarke, *J. Am. Ceram. Soc.*, 90 (2), **2007,** 533**.**

10. A. Du, C. Wan, Z. Qu, W. Pan, *J. Am. Ceram. Soc*., 92 (11), **2009,** 2687.

11. G. Azimi, R. Dhiman H-M. Kwon, A.T. Paxson, K. K. Varanasi, *Nature Mater*. 12, **2013**, 315

12. H.H.K Xu, S. Jahangir, *J. Am. Ceram. Soc.*, 78, **1995,** 497.

13. M.W Barsoum, W. Michel, *Scripta Mater*., 36, **1997**,535.

14. W. Ruigang, P. Wei, C. Jian, F. Minghao, C. Zhenzhu, L. Yongming, *Mater. Chem. Phys.*, 79, **2003**, 30.

15. Y.Hikichi, T.Ota, T.Hattori, *Miner.j*, 19 (3), **1997,** 123.

16. S. Lucas, E. Champion , D. Bregiroux, D. Bernache- Assollant, F. Audubert, *J. Solid State Chem*., 4-5, **2004,** 1302.

17. H. Gong, D.Y. Tang, H. Huang, T.S. Zhang, M. Jan., *Mater. Chem. Phys.* 112, **2008**, 423.

18. S. Sankar, K.G. Warrier. *J. Sol-Gel Sci. Technol.*, 58, **2011**, 195.

19. D.F. Mullica, W.O. Milligan ,D.A. Grossie, G.W. Beall, L.A. Boatner,*Inorg. Chimica Acta*., 95, **1984**, 231.

20. S. Lucas , E. Champion, D. B. Assllant, G. Leroy, *J. Solid State Chem*., **2004**,1774, 1312.

21. S.R. Kumar, S. C. Pillai, U.S. Hareesh, P. Mukundan, K.G.K. Warrier, *Mater. Letters*, 43, **2000**, 286.

22. K. Prasad, D.V. Pinjari, A.B. Pandit, S.T. Mhaske, *Ultrasonics Sonochemistry,* 18, **2011**, 1128.

23. J-Tsiar Lin, H-Yang Lu. *Ceramics International*, 14, **1988**, 251.

24. X. Ren, S. Guo, M. Zhao, W. Pan. *J. Mater. Sci.*, 49, **2014**, 2243.

25. X.Q. Cao, R.Vassen, D. Stoever. *J. Eur. Ceram. Soc.*, 24, **2004,** 1.

26. A. Du, C. Wan, Z. Qu, W. Pan. *J. Am. Ceram. Soc.*, 92, **2009**, 2687.

27. *G*. Soyez, J. A. Eastman, L. J. Thompson, G.R. Bai, P. M. Baldo, A. W. McCormick, R. J. DiMelfi , A. A. Elmustafa, M. F. Tambwe, D. S. Stone, *Appl. Phys. Lett.*, 77(8), **2000**, 1155.

Chapter 3

Non-Wetting as well as Non-reactive properties of Lanthanum Phosphate and Composites

Lanthanum phosphate is investigated for its non-wetting characteristics with respect to water as well as molten metals in the form of coatings on glass surfaces and as sintered solid respectively. Coatings of lanthanum phosphate which do not need any further modification can function as hydrophobic surfaces even at higher temperatures and thus could be an effective, energy saving alternate for organo surface modified coatings and polymeric modifiers. Further, lanthanum phosphate is also non-reactive/non-wetting towards molten metals. The contact angle >105º has been measured for surfaces of sintered solid lanthanum phosphate, and 120° in the form of coatings with respect to water. There was no reactivity to molten metals like zinc, aluminium and silver and the contact angle measured with molten metals has an average value of 125°.

3.1 Hydrophobic property of Lanthanum Phosphate

3.1.1 Introduction

The contact angle provides the inverse measure of wettability of a surface with water. The contact angle (θ), which is the angle at which the liquid–vapour interface meets the solid–liquid interface, is determined by the resultant between adhesive and cohesive forces. As the tendency of a water drop to spread out over flat- solid surface increases, the contact angle decreases. A contact angle less than 90° (low contact angle) usually indicates that wetting of the surface is very favourable (**hydrophilic**), and the water will spread over a large area of the surface. Contact angle greater than 90° (high contact angle) generally means that

wetting of the surface is unfavourable (**hydrophobic**), were the water will minimize contact with the surface and form a liquid droplet *figure 1*.

Hydrophobicity can be explained as the physical property of a molecule or a material being water-repellent, i.e. tending to repel and not absorb water molecules. Over the hydrophobic material, water droplets tend not to touch large area of the surface and the shape of the droplet would be spherical.

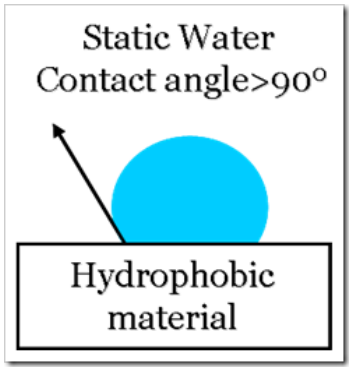

Figure 1) Schematic of droplet formation over a surface

Hydrophobic property of a material is of extreme prominence in inducing self-cleaning property to substrates and surfaces.[1-4] Hydrophobic coatings are of particular importance in wettability control. These types of coatings are expected to aid various industrial usages including anti-wetting, anti- ice, anti- rusting as well as reducing friction resistance due to the very low solid–liquid interaction.

Ceramic oxides like alumina and zirconia are hydrophilic in nature as hydrogen bonds with interfacial water molecules is established in order to fulfil octet configuration of electrons resulting in clathrate or hydrophilic hydration structure[5] leading to the wetting behaviour. An important property that administrates a material's affinity towards water molecules is the surface polarity. The increase in polarity generally leads to increased hydrophilicity.[6] *Azimi et al*[7] suggests that, rare earth oxides (REOs) which are expected to be polar and hydrophilic

have an intrinsic hydrophobic behaviour, primarily due to the electronic structure of the lanthanide series, where unfilled 4f orbitals of the rare earth atoms are shielded from interactions with the surrounding environment by the full octet of electrons in the $5s^2p6$ outer shell.[8,9] Consequently, such atoms would have a lower tendency to exchange electrons and form hydrogen bond with interfacial water molecules. Considering characteristic electronic structure of rare earth atoms, lanthanum phosphate is expected to be hydrophobic in nature and initial result (*chapter 2, page 56)* validates the argument. Also in the case of $LaPO_4$, the extra oxygen atoms present in its structure, compared to its oxide counterpart (La_2O_3), is expected to shield the La atom further from any bondage with the lone pair of electrons in the oxygen atom of water molecules.

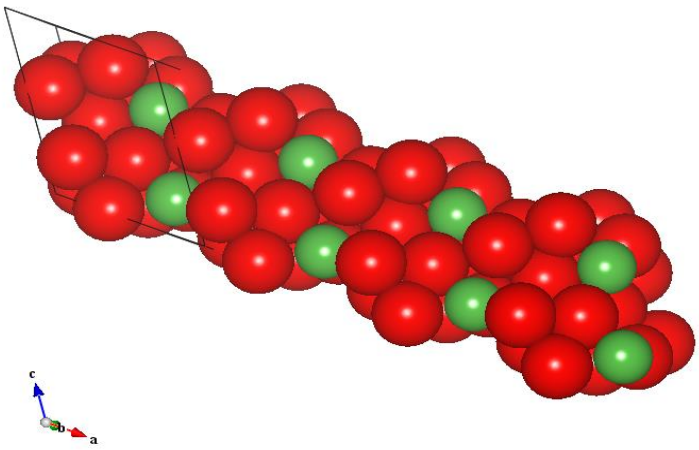

*The $LaPO_4$ structure (Green: **Lanthanum** and Red: **Oxygen**)*

Besides being one of the most stable and non-reactive La compounds and showing supreme phase stability even at very high temperatures, $LaPO_4$ is known for its applications in various fields including fluorescent and phosphor materials (both with and without dopants), sensors, proton conductors and as a highly heat resistant system (*chapter 2*). The hydrophobic nature of $LaPO_4$ could be of extreme importance in developing multifunctional applications. Here we try to analyse the intrinsic hydrophobicity in lanthanum phosphate ceramics prepared in the form of monoliths and also develop hydrophobic thin film coatings over glass substrate

surfaces. The elongated morphology of wet chemically derived lanthanum phosphate nanoparticles helps to further enhance the hydrophobic nature of the thin films through the formation of a unique surface morphology.

3.1.2 Experimental

Lanthanum Phosphate nano particles were synthesized through a sol gel approach (precipitation –peptization scheme) detailed in chapter 2 by hydrolysis from lanthanum chloride. The particles were uniaxially compacted at 100 MPa to circular discs of 50mm diameter and 5mm thickness. These discs were then sintered to maximum density at 1400 °C for 2h and polished to mirror finish to nullify errors during contact angle measurements. The densities of all the sintered discs were determined using Archimedes principle. The contact angle values of sintered $LaPO_4$ discs with water were analysed by sessile drop method using Hamilton 500 microlitre needle with a drop volume of 3 microlitre and flow rate of 1 microlitre/sec. The discs were checked for the hydrophobic behaviour by keeping in freezing condition as well as in hydrothermal condition and checking the shape of droplets over the surface.

The microstructural observation of the $LaPO_4$ specimen was done using a scanning electron microscope (JEOL JSM-6700F SEM, Japan). The phase identification was carried out using X-ray diffraction with Philips PW 1710 using Cu Kα radiation in 2θ range of 20-80°. Atomic force microscopy of the $LaPO_4$ coatings on glass was taken with NTEGRA (NT-MDT) operating in a tapping mode regime. Micro-fabricated TiN cantilever tips (NSG10) with a resonance frequency of 299 kHz and a spring constant of 20-80 Nm-1 were used. Adhesion studies on the coatings were carried out using micro-scratch method that involved generating a controlled scratch with a diamond tip on the coating surface under progressive load. The test was performed in a micro-scratch test system (Micro-Combi Tester, M/s CSM

Instruments, USA). The test parameters were fixed to those values that gave reproducible scratch maps. Testing was performed over a scratch length of 6 mm at a speed of 10 mm/min, with a final load value of 15 N.

3.1.3 Results and Discussion

The fabricated discs of lanthanum phosphate were heat treated at a temperature of 1400 °C to realise fully dense shapes of monoclinic $LaPO_4$ as shown in inset of *figure **1.*** X-ray diffraction pattern recorded for the disc is also provided in figure 1. The spectrum pattern matches with that of stable monoclinic phase of $LaPO_4$. The microstructure obtained on polished and thermally etched surface of $LaPO_4$ shown in *figure **4b*** is characteristic of a dense ceramic with sintered grains of ~1µm.

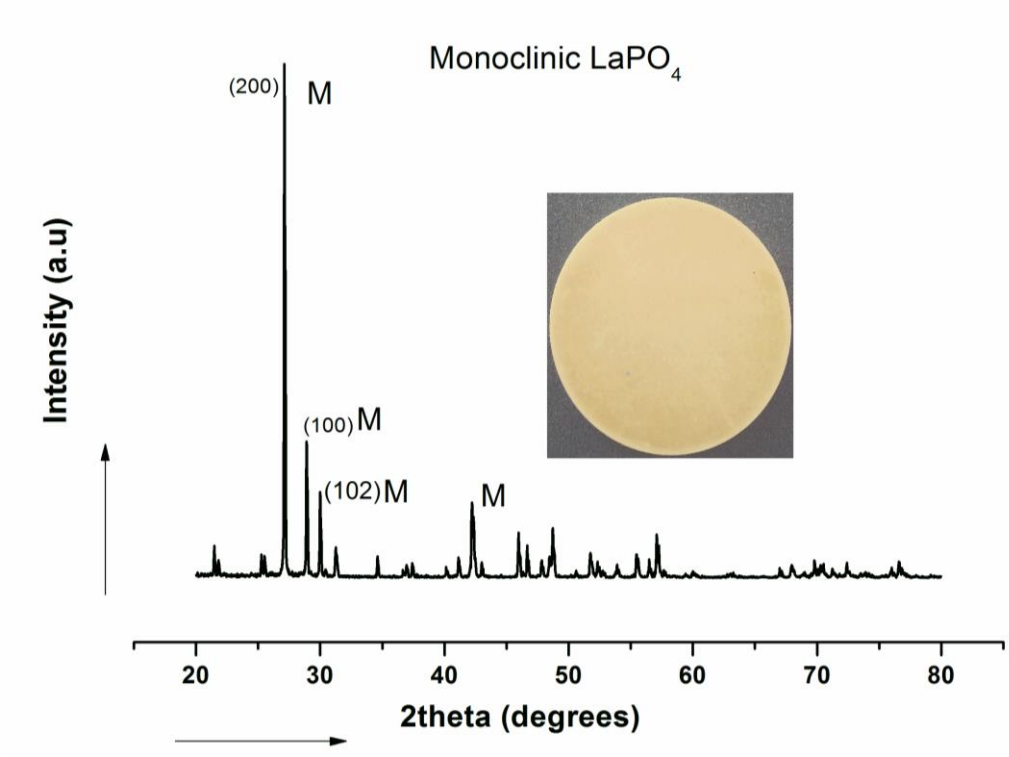

Figure 2) X-ray diffraction obtained for $LaPO_4$ pellet surface (inset) showing the monoclinic phase formed.

The wettability of a solid by a liquid is characterized in terms of the angle of contact that the liquid makes on the solid.[11] The contact angle, θ, is obtained from a balance of interfacial tensions and is defined from Young's equation, which applies to ideal surfaces that are perfectly smooth and devoid of all chemical and structural inhomogeneities according to which;

$$\sigma_{lv}.\cos\theta + \sigma_{ls} = \sigma_{sv}$$

Where σ_{lv}, σ_{ls}, and σ_{sv} are the interfacial tensions at the boundaries between liquid (l), solid (s), and vapour (v).

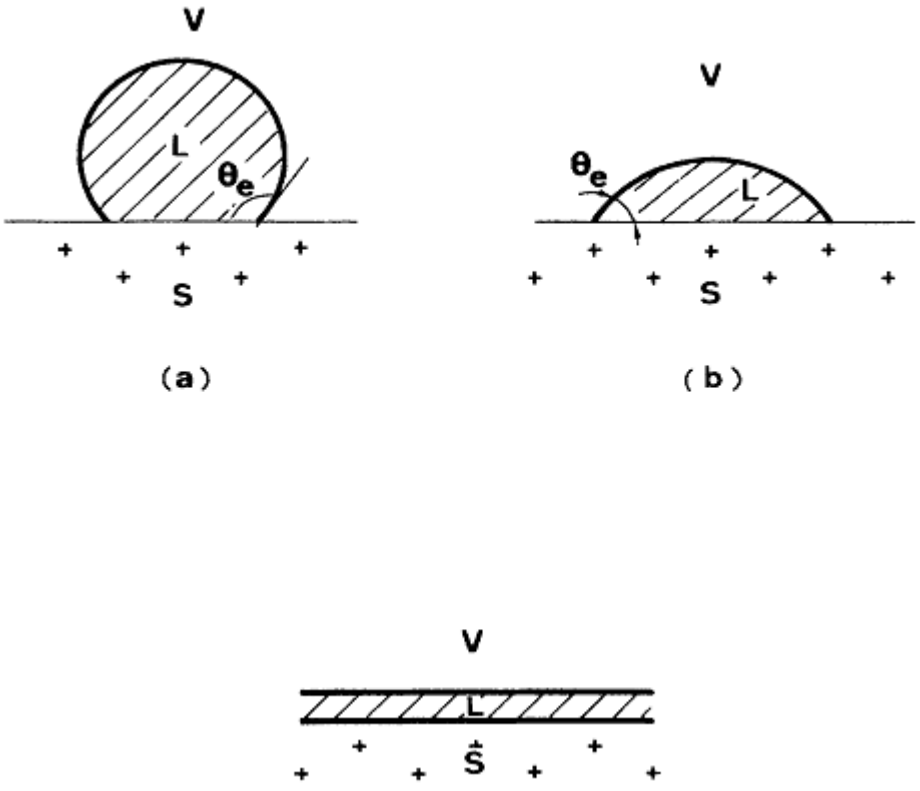

Figure 3) Various interfaces between solid(S), Liquid (L) and Vapour (V) phases

Hydrophobic nature of lanthanum phosphate surface was evaluated using water contact angle (WCA) measurements as shown in *figure **4a***. Employing sessile drop method and using a Hamilton 500 microlitre needle with a drop volume of 3 micro litre and flow rate of 1

microlitre /sec (inset of *figure 4a*), contact angle value of 105.5º on $LaPO_4$ monoliths was measured. The water droplets were seen to move over the disc without spreading. The inherent hydrophobic nature of $LaPO_4$ explained based on the electronic structure[7] is evident from the measurement values obtained. The scheme provided (*figure 4c*) shows the weak and unstable bond between the water molecules and the $LaPO_4$ surface inducing the hydrophobicity. As the 4f orbitals of rare-earth atoms are completely shielded by the octet electrons of the outer ($5s^2p^6$) orbitals, they have no tendency to interact with water molecules. Thus, water molecules adjacent to the surface cannot maintain their hydrogen-bonding network.

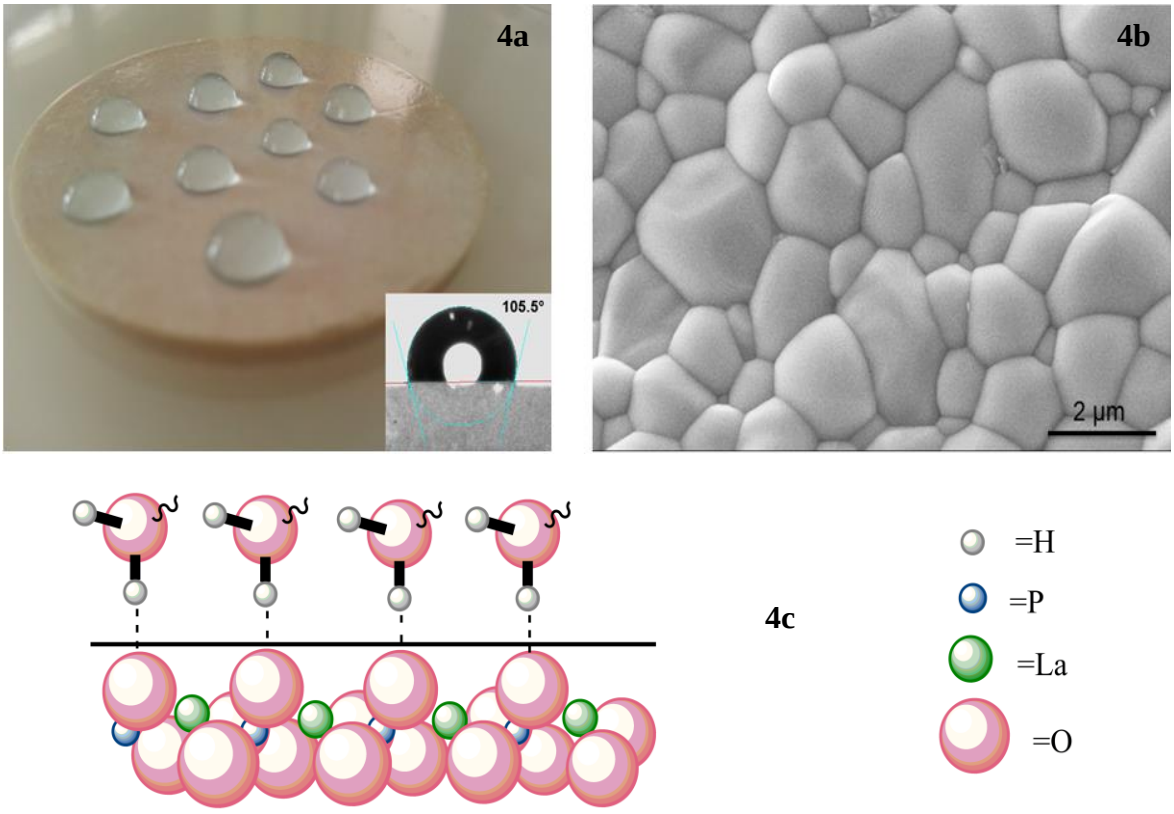

Figure 4a) Lanthanum phosphate sintered disc and corresponding contact angle value. **4b**) SEM micrograph of sintered, polished and etched $LaPO_4$ surface **4c**) scheme showing the electronic structure causing the weak bond with H_2O molecules in contact

Retaining hydrophobicity of a material under extreme conditions could open up a variety of advantages in applications. $LaPO_4$ disc with water droplets kept in freezing condition (*figure **5A***) retains the shape and the water droplets appear as ice balls over its surface confirming that $LaPO_4$ could also hold its hydrophobicity well under sub-zero temperatures. This characteristic feature offers opportunity for $LaPO_4$ to be employed as antifreeze coatings and thin films. Additionally, $LaPO_4$ discs kept in hydrothermal conditions of 200 °C for 24 hr indicated no weight changes and the hydrophobic character also remained unchanged (*figure **5B***). The non-vulnerability of the phosphate under fluctuating conditions stands testimony to their mechanical stability and reliability and hence is extremely promising

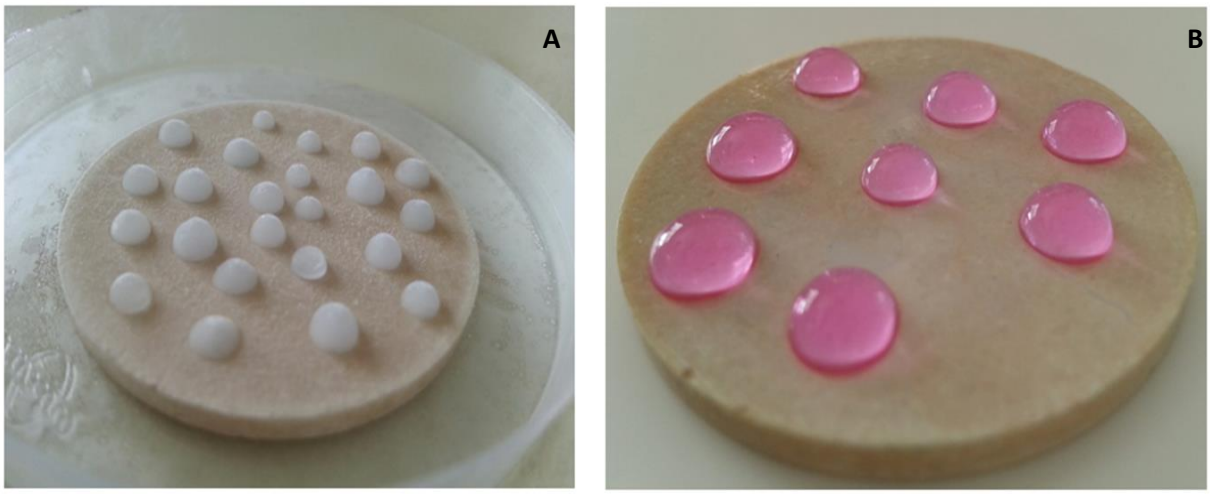

Figure 5) Hydrophobicity under extreme conditions **(A)** water droplets retaining the shape under freezing conditions **(B)** water droplets over $LaPO_4$ disc after hydrothermal exposure

3.1.4 Lanthanum Phosphate Coatings on Glass substrates

Thin films of Lanthanum phosphate were obtained by dip-coating (*section 2.4.1*) glass plates followed by heat treatment at 200- 400 °C. The films obtained after heat treatment in the temperature range had an average thickness of ~200 nm (*figure 6*) shows the nanocoating obtained by the sol coating.

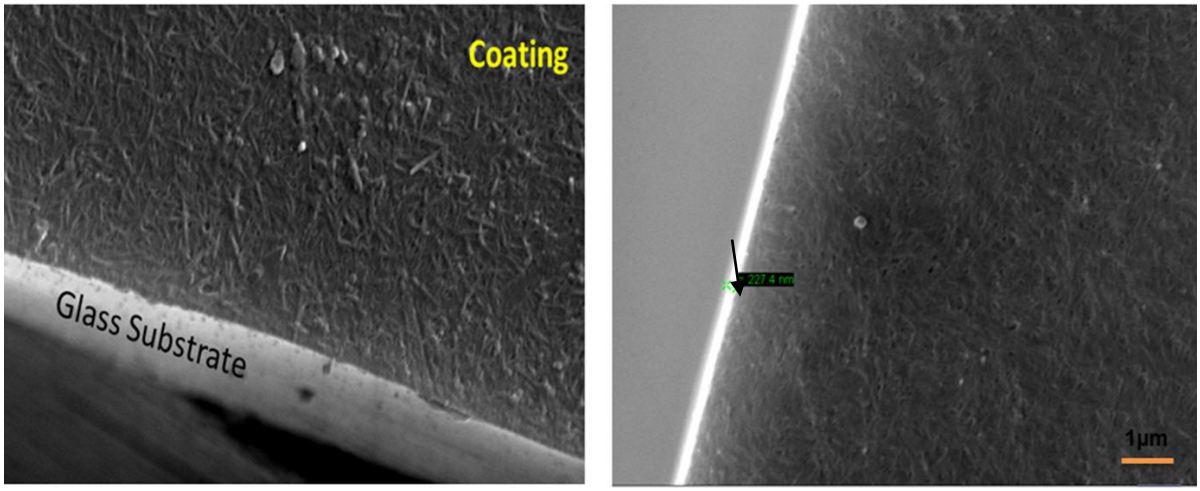

Figure 6) SEM images of the coated glass plate showing the thickness of the film formed

These films were checked for the hydrophobic behaviour using sessile drop method. The thin films showed water contact angle value as high as 120° (figure 7), which was significantly higher than the water contact angle values of ~20° measured for the uncoated glass substrate. The morphology of the coated surface (figure 9) (Cassie surface) and the roughness created as seen from AFM (figure 10) on the surface should have contributed to the increased contact angle because of the changes in solid-liquid interface. It is common practice to use flouro silane or other polymer as coatings on ceramic surfaces to obtain greater water contact angle values.[11]

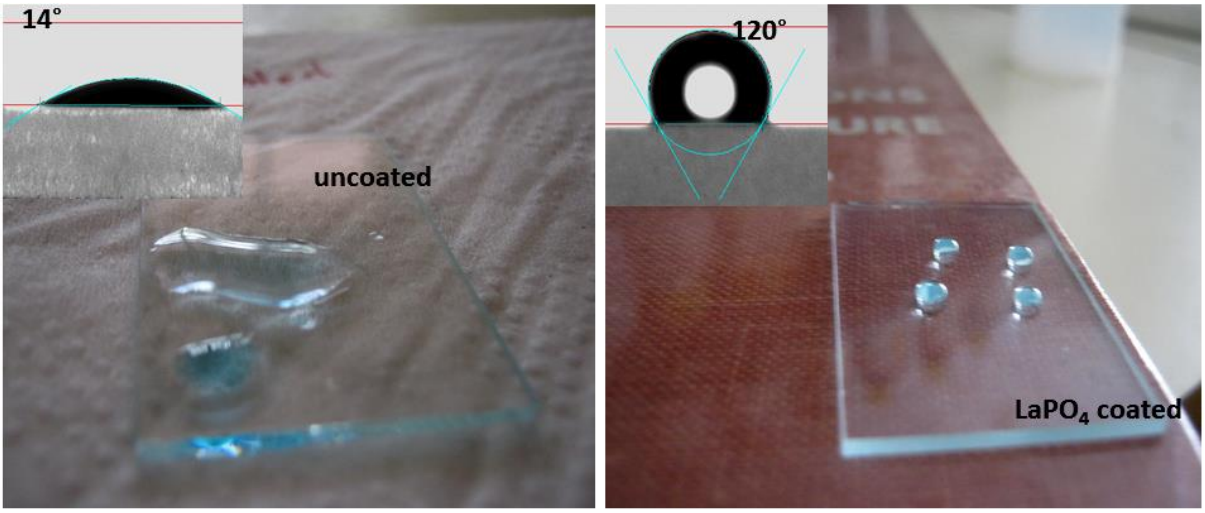

Figure 7) Hydrophobicity of Lanthanum Phosphate coating when compared to uncoated glass specimen.

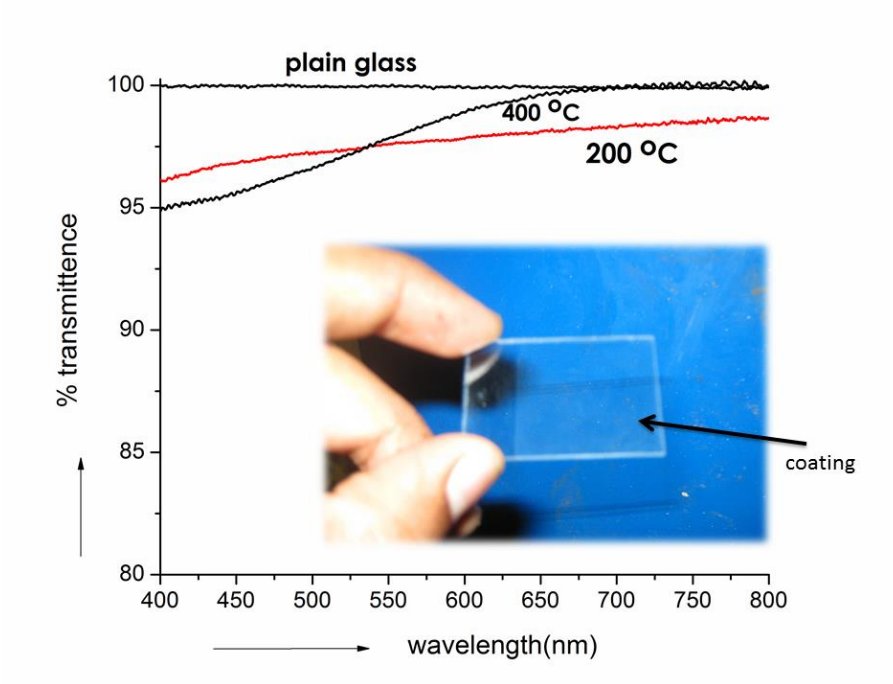

Figure 8) UV-Visible spectra obtained for the coatings along with the photograph of the transparent coated glass (transmittance of uncoated glass and glass coated and heat-treated at 200 °C and 400 °C are shown in figure)

In order to use hydrophobic coatings in applications in daily life, the demands of both high optical transparency and mechanical durability for the coatings are essential factors. The photograph of coated sample along with UV-Visible spectroscopy results of coated and

uncoated glass are shown in *Figure 8*. Transmittance value >95% could be measured for the coated samples across the spectrum of wavelength indicates very high optical transparency obtained for the coatings developed.

The SEM micrograph of the coatings provided in *figure 9* shows the typical rod like morphology of $LaPO_4$ present in the coatings. The rods appear to be organized to form a spike like arrangement over the surface forming a rougher surface which should be the cause for the increased water contact angle values measured on the thin films.

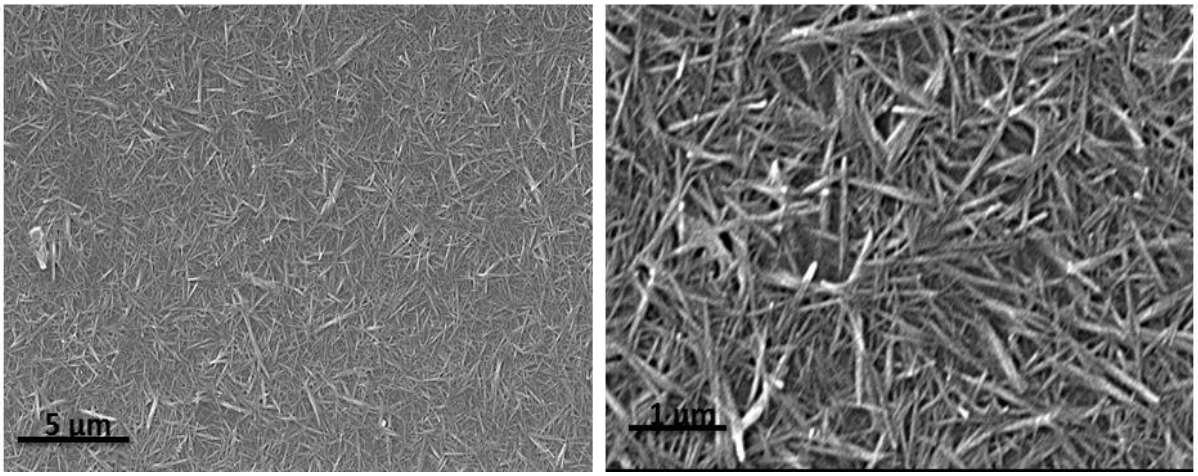

Figure 9) SEM images of the $LaPO_4$ coating made over the glass substrate

The surface roughness features of the coatings were analysed using atomic force microscopy and are provided in *figure 10*. The uncoated glass surface has a roughness of ~7nm while the coated surface showed roughness of ~ 34 nm which should have been imparted by the acicular morphology of the phosphate particles as well as their self-assembly. Increase in surface roughness is known to decrease the wetting ability of a surface due to the synergistic effects.[12]

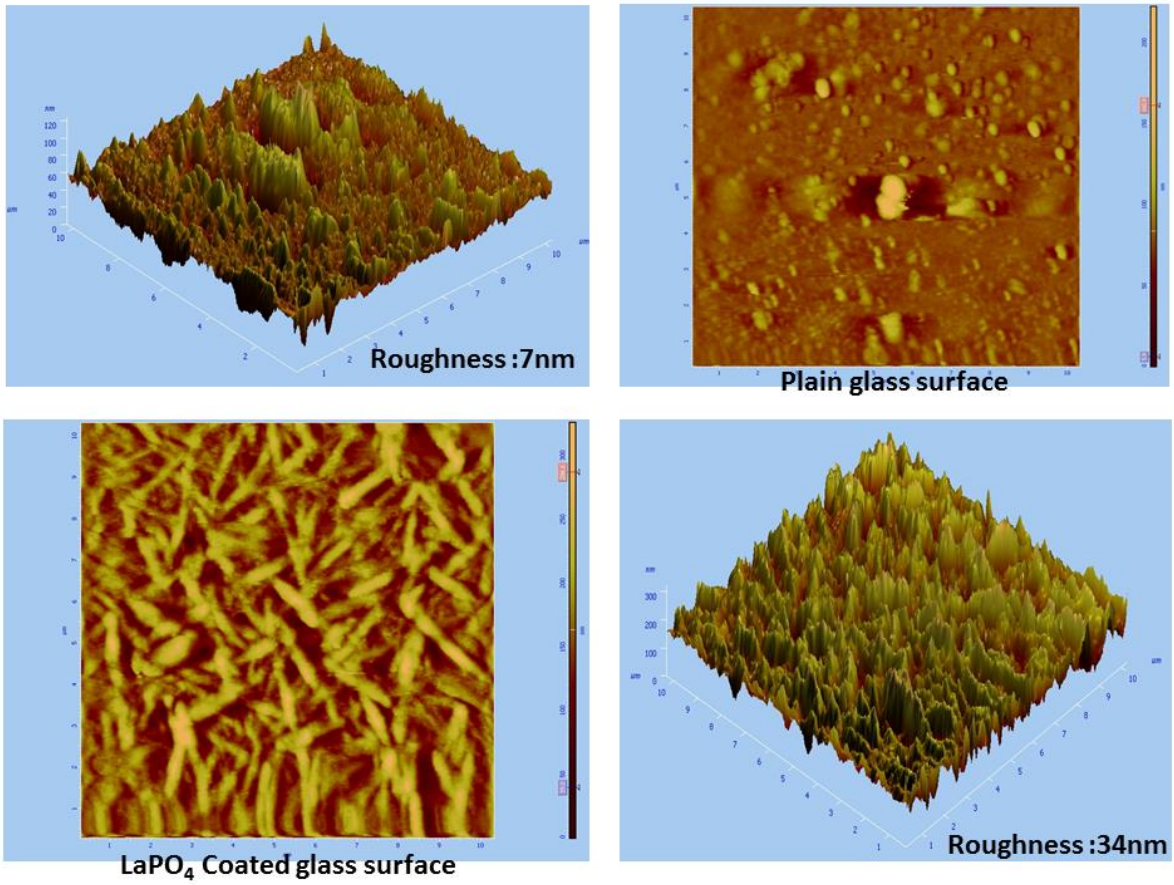

Figure 10) AFM images showing the features of the thin film made over the glass substrate

The adherence of the lanthanum phosphate coatings over the glass substrate was evaluated using micro scratch test. The critical loads for crack events (L1), (L2), (L3) (L4) and total delamination (L5) were determined from the data obtained during the test. The optical images (*figure 11*) collected from the instrument and the data generated evidenced good adherence behaviour for the coatings over the glass surface. From the optical images we can see that the peeling of the coating took place between L3 and L4 and the complete delamination occurred at L5. The scratch tip has intended the underlying glass, yet the primary coating still remained over the glass surface without getting fully detached or peeled off.

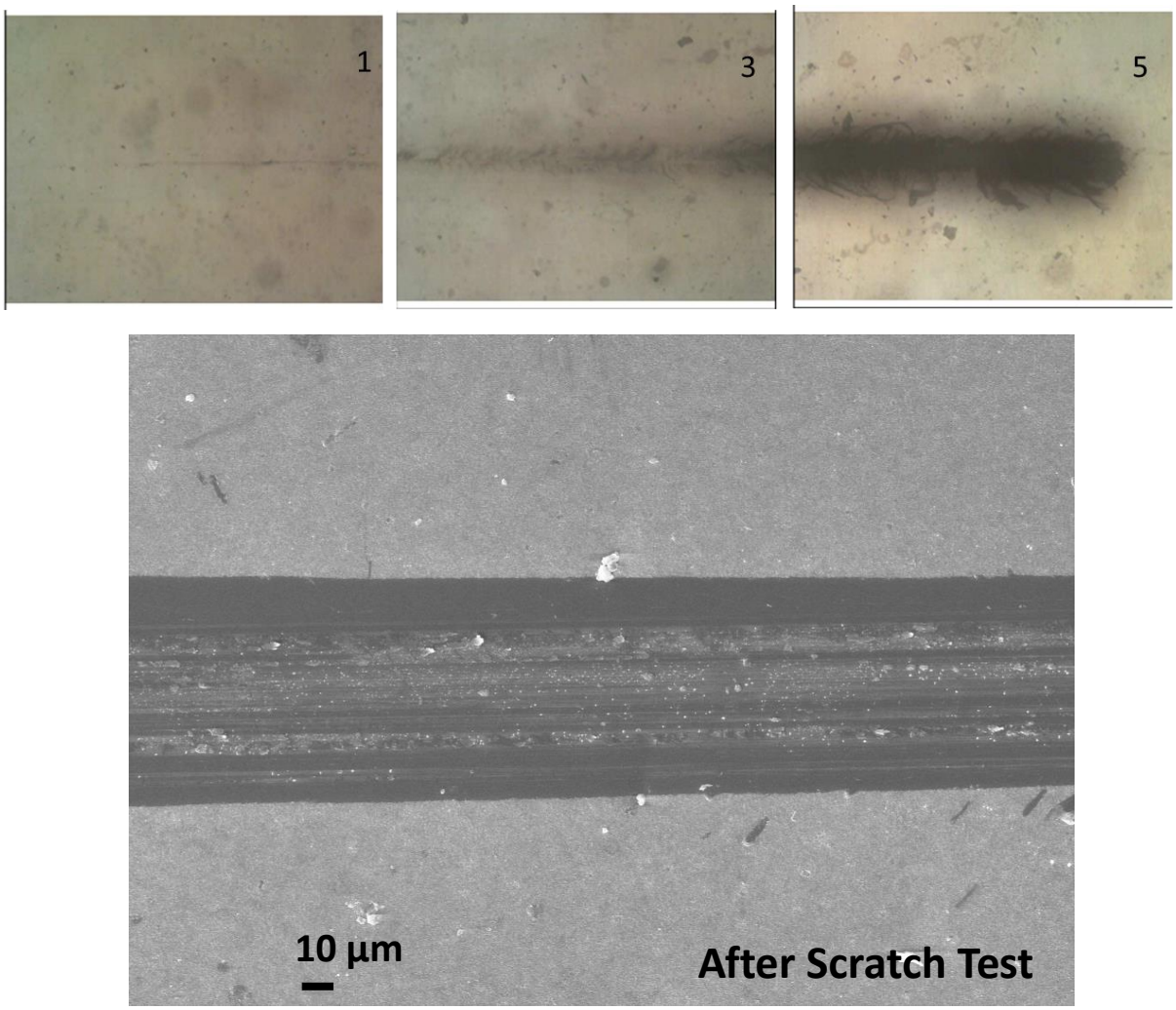

Figure 11) Adherence scratch test optical images 1) L1 3) L3 and 5) L5 and SEM image of the coating taken from a position after the scratch L4

3.1.5 Summary

Lanthanum phosphate, hence, offers an alternative hydrophobic surface for various engineering applications particularly where the temperature is high. Moreover, lanthanum phosphate is inorganic and is resistant to acids, alkalis and is biocompatible. This stability and durability will certainly give further advantages over the conventional surface modified coatings available thus far. To the best of our knowledge this is the first report on the excellent inherent hydrophobic characteristics of lanthanum phosphate and possibly rare earth phosphates in general and therefore, another pathway to realize hydrophobicity with an inorganic compound having additional properties like excellent thermal and mechanical

stability. Hydrophobic coatings of lanthanum phosphate could be an alternative for conventional surface modified coatings consisting of organic and polymeric modifiers.

3.2 Lanthanum Phosphate Non-Reactivity with molten metals

3.2.1 Introduction

In metallurgical processes, metals and alloys when heated to their melting points in ceramic crucibles tend to react or stick to the surface causing contamination from the crucibles and loss of the metals/alloys. In order to protect the surface of the crucibles from molten metal attack, many ceramic coatings are applied as slurries or suspensions of ceramic powders on them and sinter in place during heat-up.[13] Such coatings, being in an unsintered state, are fragile and prone to damage during loading of sharp heavy chunks of the metal charge.

Crucible materials for melting metals should not contaminate the melt. During metal casting operations the moulds/crucibles are usually coated with layers of release agents comprising mainly of inorganic materials like alumina, zirconia, hexagonal BN and graphite. The layers acting as an interfacial coating prevents chemical interaction with mould material and casting metal. Non-reactivity of lanthanum phosphate with the molten metals relates to the process of preparation of lanthanum phosphate based coatings and monoliths as non-reactive surfaces for molten metals for high temperature applications such as mould release coatings or crucibles for metal casting.

3.2.2 Lanthanum phosphate Monoliths/Crucibles

$LaPO_4$ precipitated from Lanthanum salt by adding ortho phosphoric acid is further flocculated by addition of 25% ammonia solution and the pH was maintained in the range 6.8 -7.8. The precipitate thus obtained was washed, dried and calcined at 1000 °C to obtain Lanthanum phosphate powders. The powders were then dispersed in water at pH 2 and ball milled for 6-12 h using alumina as milling medium. 1-2 drops of octanol was added to the suspension to prevent foaming. The slurry after deairing was slip cast to shapes of crucibles and containers using Plaster of Paris moulds. After the build-up of sufficient thickness the slip cast part was de-moulded and dried at 80 °C under controlled conditions of humidity and temperature (50 °C and 65-75% RH) and further under normal oven conditions for 15 h at 80 °C (***figure 12A***). The dried monolith is then sintered at 1400 °C and the crack free monoliths (***figure 12B***) are obtained.

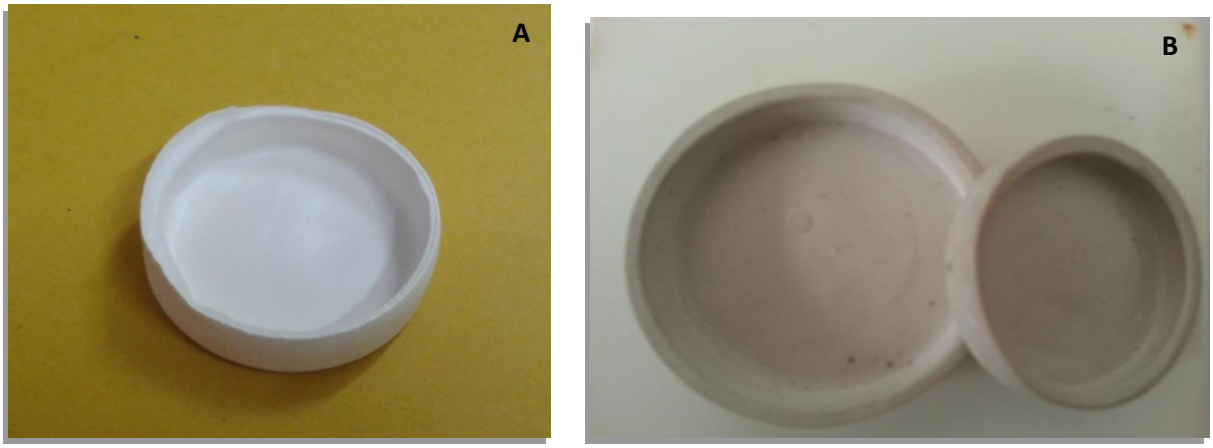

Figure 12) Photographs showing $LaPO_4$ crucibles casted **A**) green and **B**) sintered crucibles.

3.2.3 Lanthanum phosphate reactivity with metals

3.2.3.1 *Reactivity with Zinc metal*

The reactivity of $LaPO_4$ with Zinc metal was carried out using a procedure described as follows. Lanthanum phosphate nano powder synthesized was uniaxially pressed to form pellets. One of the pallets was covered with Zn metal foils (*Figure 13A*) in a ceramic crucible and was heated to the melting point of the metal with a holding time of ~ 30 mts. On cooling, it was found that the $LaPO_4$ is total non-reactive with the Zn metal which was confirmed by the EDX (*Figure 13C*) spectrum obtained from the pellet used which showed the absence of Zn over the surface. Figure 13B indicates the non-reactivity and the impregnation formed by the $LaPO_4$ pellet over the melted metal surface shows the anti-wetting behaviour.

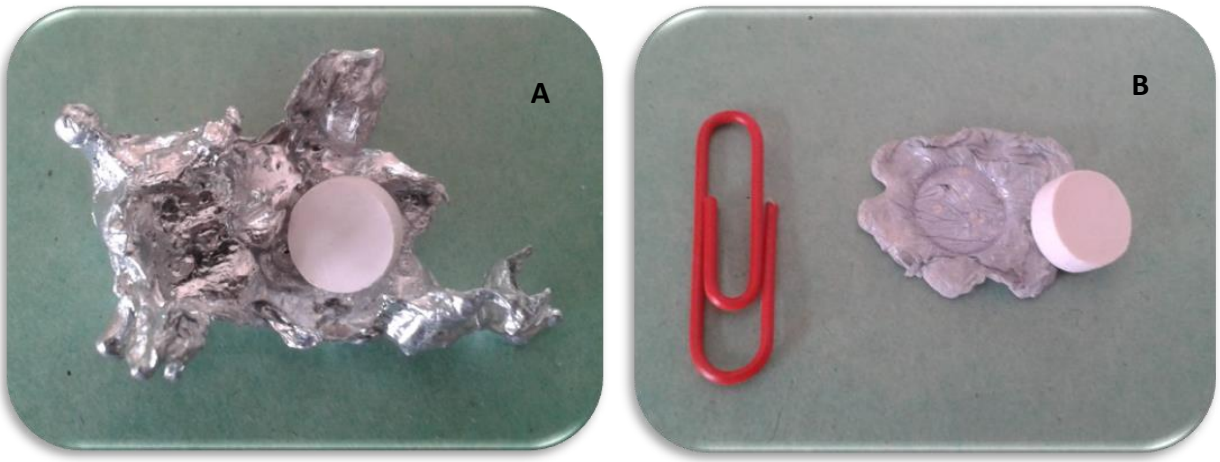

Figure 13A) $LaPO_4$ pellet placed inside Zn metal Chunk **B)** non-reactive $LaPO_4$ pellet easily separated from the metal surface

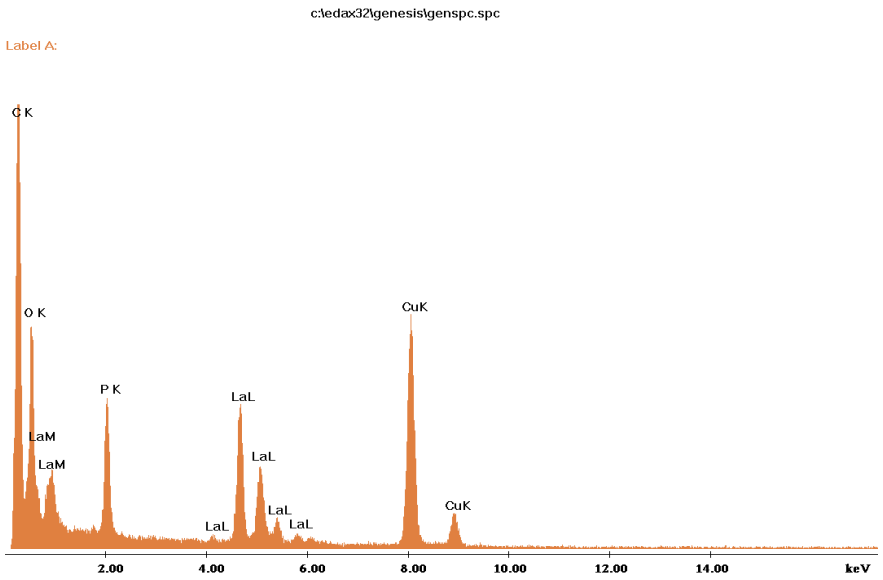

Figure 13C) EDAX spectrum of lanthanum phosphate pellet heated with Zn metal after heat treatment

The compatibility of $LaPO_4$ with Zn was examined by mixing the metal powder with $LaPO_4$ and analysing the thermal decomposition pattern (figure 14). From the TG-DTA analysis we can see that only the melting of Zn metal is seen, by the characteristic DTA peak around 430 °C and on cooling the metal gets back to its previous condition indicating the non- reactive nature of $LaPO_4$ with Zn.The weight loss is associated with the loss of physically adsorbed water and the nitrates present in the phosphate sample.

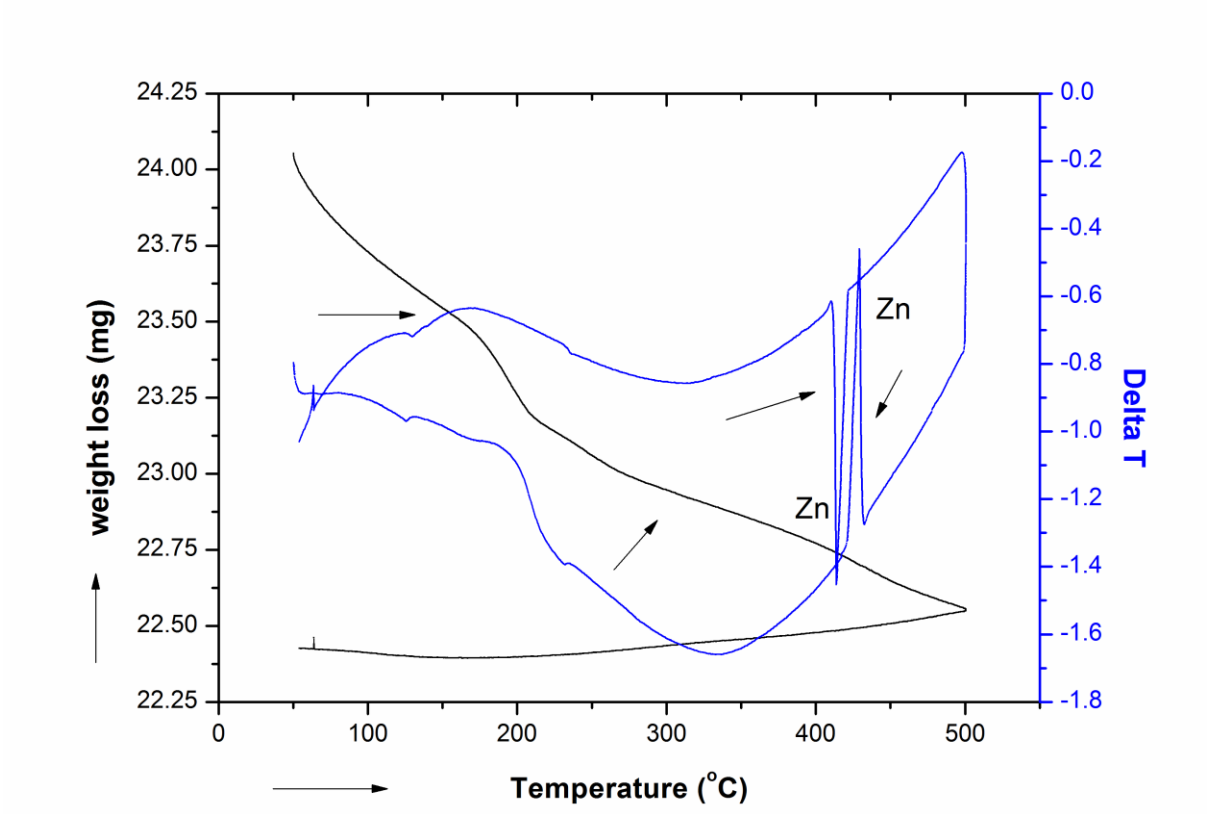

Figure 14) TG-DTA pattern of the powder mixture containing lanthanum phosphate and zinc metal

3.2.3.2. *Reactivity with Aluminium Metal*

Thermal analysis based study was carried out using pure aluminium metal - $LaPO_4$ mixture and the corresponding thermogram (*figure 15*) is given below**.** There are two steps of weight loss corresponding to physically adhered or chemically bound. The DTA peaks around ~ 700 °C shows the melting of Al and on cooling solidifies. There are no peaks identified for the formation of a new product by the metal- phosphate reaction which confirm that absolutely no reaction between $LaPO_4$ and aluminium metal. The melting of aluminium metal in a $LaPO_4$ crucible (figure 16A) with a hold time of ~ 1hour was done in a furnace. The molten Al metal floating over the surface of the crucible was visible on opening the furnace at the melting point. On cooling the solidified metal easily came out of the crucible without sticking (figure 16B), which confirms the no-reactivity of $LaPO_4$ with molten Al metal.

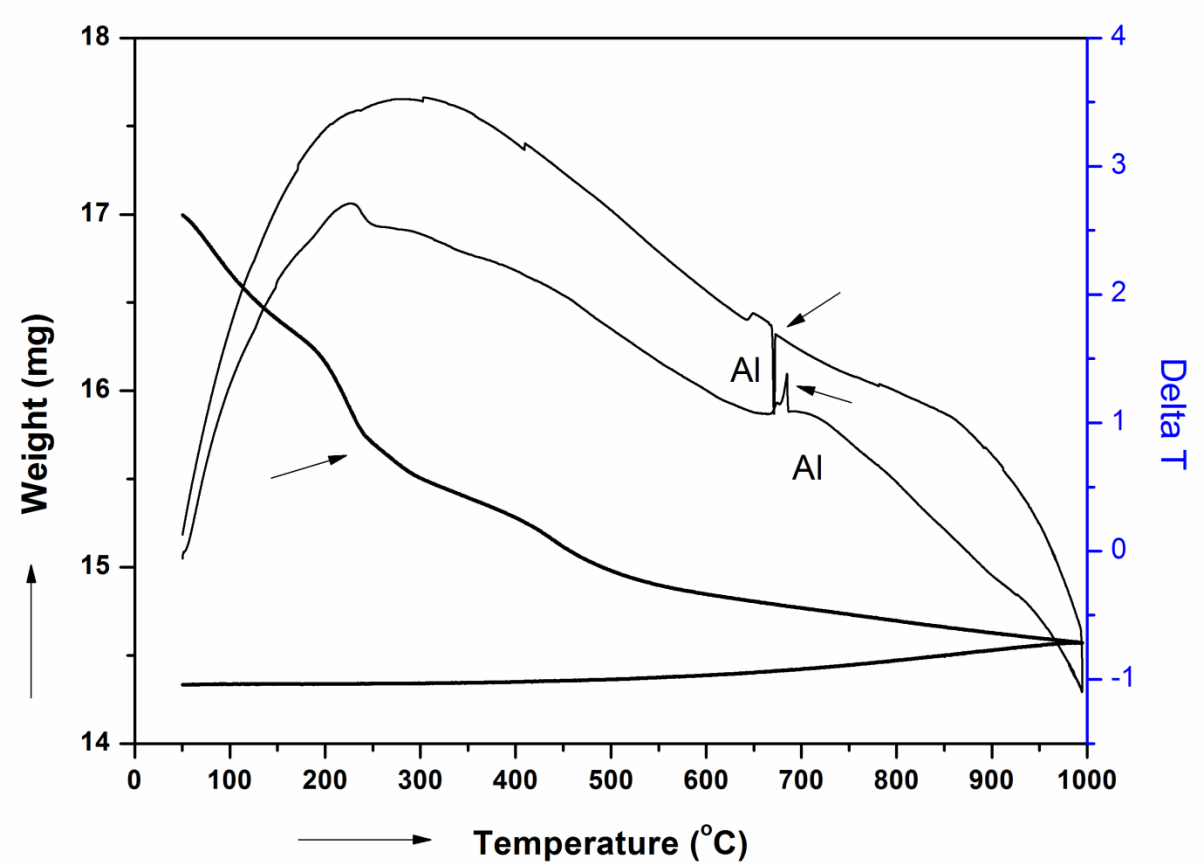

Figure 15) TG-DTA pattern of the powder mixture containing lanthanum phosphate and aluminium metal

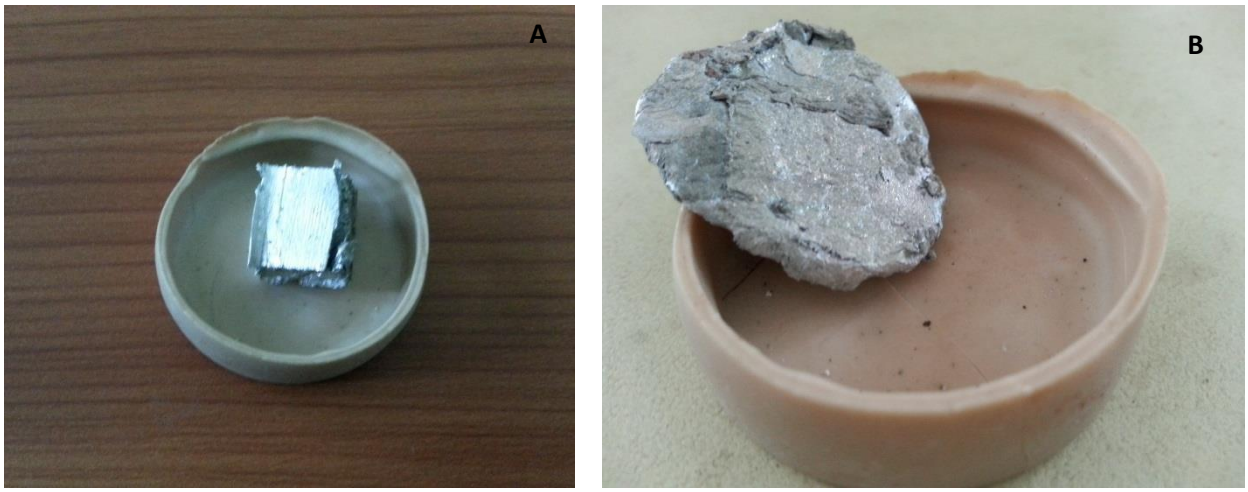

Figure 16) **A)** Pure aluminium metal placed over the lanthanum phosphate crucible **B)** melted and solidified Al metal easily coming out of the crucible

3.2.3.3 *Reactivity and contact angle measurement with Ag metal*

Metallic silver was placed in lanthanum phosphate crucible in a high temperature furnace and heated to its melting point. The different photographs (IR imaging) taken during different stages of the process are presented in figure 17. Silver attains globular shape after melting in the crucible indicating absence of reactive spreading of the metal over the surface. $LaPO_4$ is seen to have not affected by the molten metal over its surface. The molten metal globule made a contact angle of 125º with the surface indicating the antiweting characteristic. On increasing the temperature by further 50 ºC, the crucible seemed to be unaffected.

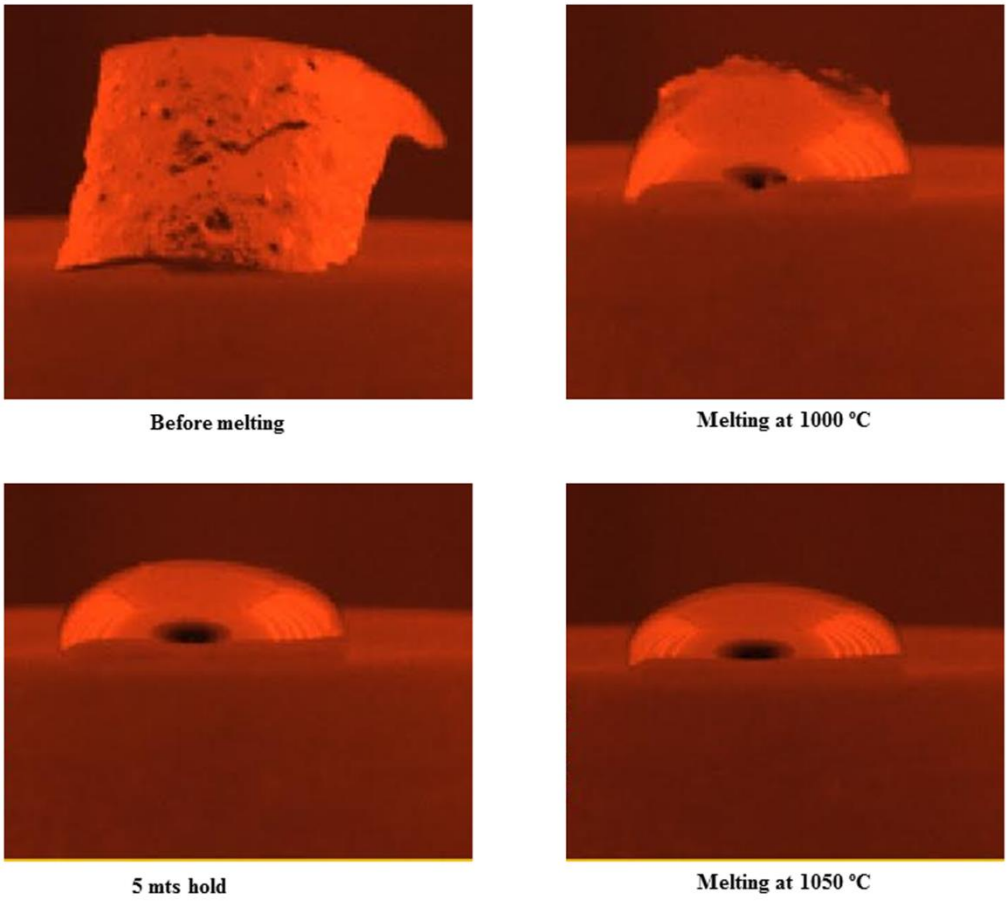

Figure 17) IR imaging on different stages of melting of pure silver (Ag) metal placed over lanthanum phosphate crucible

3.2.4 Wetting experiments of $LaPO_4$ for molten metal reactivity

The studies on the non-reactivity of Lanthanum phosphate with molten metals was extended in the form of finger tests where, sintered lanthanum phosphate bar samples of approx. 40mm length and 5 mm thickness having > 98% density were used for the analysis. The metals under study were Aluminium and Zinc. The bars were kept dipped in pure metal pieces in a ceramic crucible and then heated to the melting point of the metals. After holding for about 30 minutes the furnace was opened to see molten metal flowing over the LaP surfaces. The bars could be taken out without any sticking to the surface after the heat treatment schedule. The molten metal was evident as they easily peeled of the surface on cooling. This was further confirmed by the microscopic observations on morphology where no trace of metals sticking to surface of the sintered lanthanum phosphate was evident .the possible explanation based on surface energy for the characteristic could be explained as provided in 3.3.

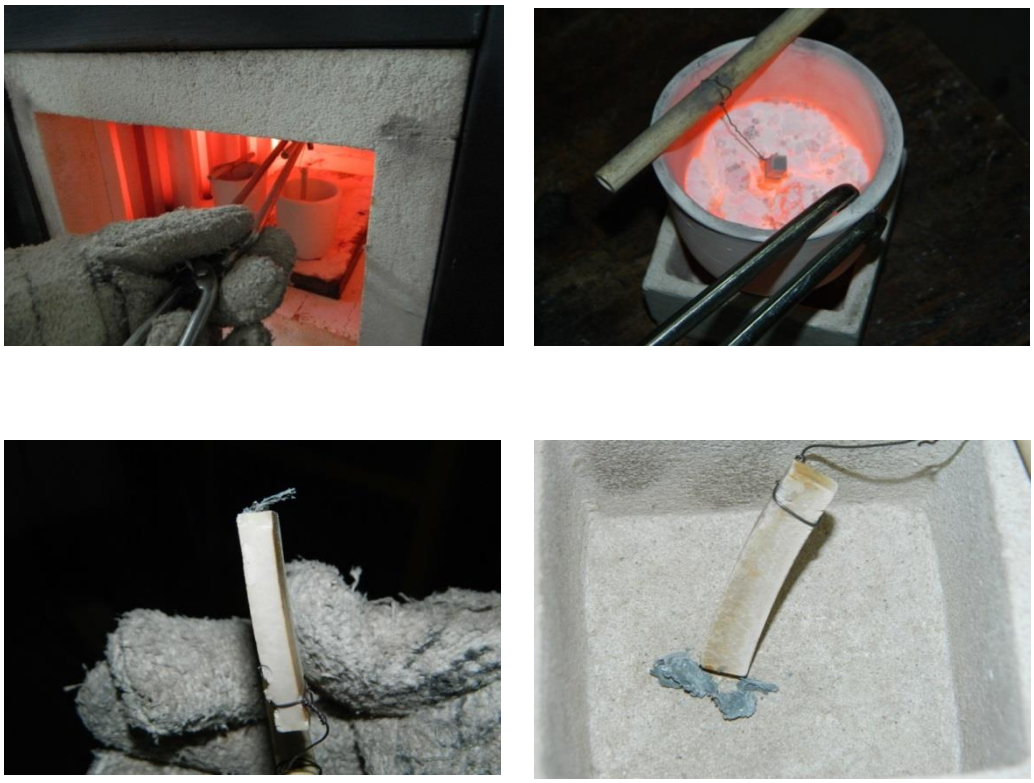

Figure 18) Photographs taken during the different steps of finger tests showing the metal chunks getting peeled easily of the surface

3.3 Surface Energy of $LaPO_4$

High energy substrates are reported to be easily wetting than low energy substrates and therefore more complete wetting will occur if the substrate has a higher surface energy than the liquid.[13,14] Schematic diagram (*figure 18*) shows the change in wetting behaviour of the substrate with respect to the difference in surface energies. The surface energy of $LaPO_4$ was measured with reference to a common ceramic material, alumina used in foundry/ metal melting application. The surface energy of $LaPO_4$ was measured to be 0.77 mJ/m^2 when compared to 1.5 mJ/m^2 obtained for the α-alumina. The value obtained clearly indicates the low surface energy prevailing for the $LaPO_4$ which keeps it anti-wetting and nonreactive to molten metals.

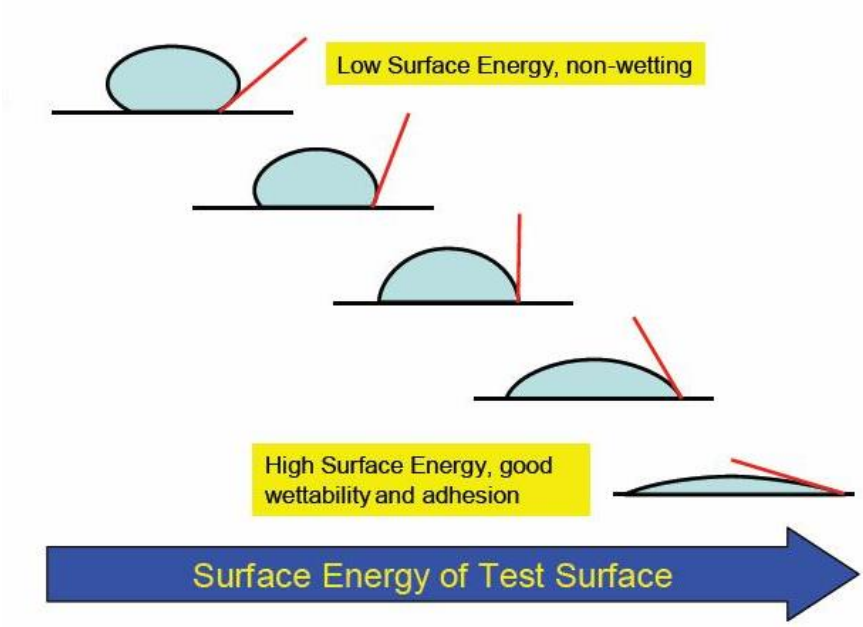

Figure 18) schematic diagram showing the substrate surface energy and wetting behaviour

Thus lanthanum phosphate is found to be no wetting to metals like aluminium, zinc and silver in their molten state and non-reactive even after holding at their melting temperatures which could be of immense importance in foundry applications. The low surface energy of $LaPO_4$ when compared to common oxide ceramics like alumina is believed to be the reason for low

wettability. The electronic structure of the phosphate where 'f' shells are prevented to form reactive sites could be also playing a part for the non-reactivity. By making use of the sol gel process $LaPO_4$ coatings could be developed over the commonly used crucible surfaces there by improving the efficiency and durability.

3.3.1 Surface Energy Calculations

We have calculated surface energy of lanthanum phosphate ($LaPO_4$) and Al_2O_3 using the following method;

Surface structure of $LaPO_4$ was modelled using slab approximation. Surface slab models were constructed based on corresponding optimized bulk crystal. A 2×2 cell was used for (010) $LaPO_4$ surface. The slabs were constituted of sixteen stoichiometric layers. The slabs were sandwiched by vacuum layers with a thickness of at least 10 Å (see figure 20).

Surface energy, γ_{lmn} was obtained using the difference in the Gibbs free energies of surface and that of corresponding bulk for unit surface area.

Gibbs free energy G is given by

$$G = U + pV - TS,$$

Where U is the internal energy of the system, p is the pressure and S is the entropy.

The difference in Gibbs free energies between the surface model and the bulk model of solid was calculated by the above method. We ignored zero-point energy and *pV* term as well as *TS* term because their differences in surface model and bulk model could be much smaller than the difference of internal energy. U is approximated by the total energy of the system. Therefore, Gibbs energy difference of the system becomes equal to the difference of the total energy, E^{total}.

Hence, surface energy could be obtained using the difference in the total energy of slab model and that of corresponding bulk model per surface area.

$$\gamma_{lmn} = \frac{E_{\text{slab}}^{\text{total}} - nE_{\text{bulk}}^{\text{total}}}{2A}$$

First principles calculations were performed by the PAW method as implemented in VASP code. The generalized gradient approximation with the exchange-correlation functional proposed by PBE was employed. The plane-wave cut-off energy was 400 eV.

As a first step, the cell parameters of bulk model were calculated. For this, the *k*-point sampling condition ensured a good accuracy of total energies for each crystalline species within 1 meV/atom. All atomic positions and cell parameters were allowed to relax until their forces converged to be less than 0.02 eV/A to obtain structure for bulk.

Then, structural relaxation of slab model constructed based on optimized bulk model was performed only on the position of atoms.

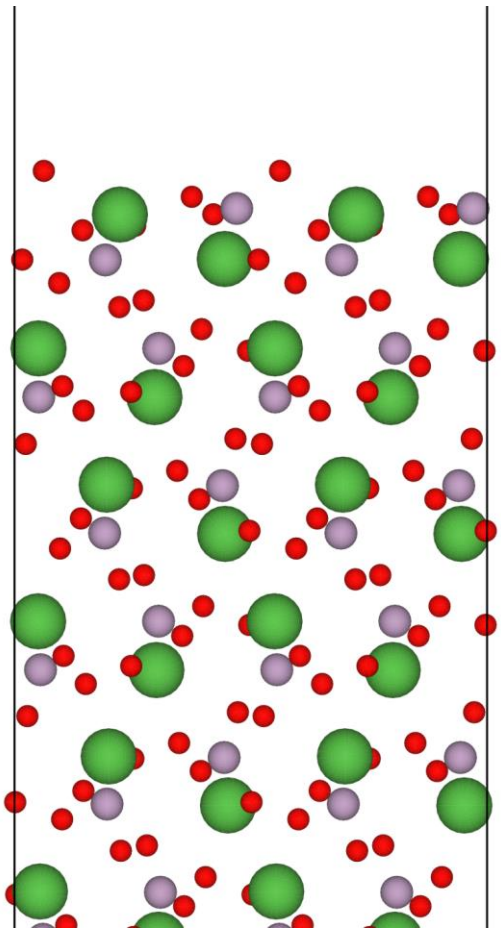

Figure 20) Surface model picture of $LaPO_4$ (La: Green, O: Red, P: Purple)

Calculated geometric parameters for bulk $LaPO_4$ crystals (monoclinic) compared with experimental data are shown in table below. As shown, calculated lattice parameters are in good agreement with corresponding experimental data. Similar calculations were performed for Gd_2O_3 (monoclinic), La_2O_3 (monoclinic) and Al_2O_3 (a) crystal structures as well. The surface energy values calculated for the four structures are reported here.

	Exp.[15]	(This work) calc.	Error [%]
a [Ang.]	6.482	6.51	0.4
b [Ang.]	7.057	7.09	0.4
c [Ang.]	8.2691	8.30	0.4
□ [deg.]	126.5	126.7	
La-O	2.5	2.5	
La-P	3.282	3.30	
P-O	1.524	1.54	
O-O	2.427	2.44	

Table 2) *Calculated geometric parameters of bulk $LaPO_4$ crystals*

3.4 Reactivity with Uranium Metal for $LaPO_4/Y_2O_3$ Composite

One of the most significant impacts that $LaPO_4$ can make with its non-reactivity with molten metals is in application related to melting of radioactive metals.[16] The compatibility between $LaPO_4/Y_2O_3$ was determined by sandwiching U between the composites. The experiment was performed under high purity Argon (Ar) with Uranium (U) trap. As the sandwich heated, U first decomposed to beta, followed by gamma. When U melted, it was held in the molten condition for 15 min. to find out any reaction to occur between composite and uranium. The molten metal was cooled and the all the phase changes were noted while cooling. This confirms that the composite does not undergo any reaction with uranium. The experiment was conducted in TG/DTA apparatus and plot is given in *figure 21*. After melting with U, the following observations were made:

1. No U /U compounds peaks are noticed in the DTA pattern (see Figure)
2. After melting, Uranium and $LaPO_4$-Y_2O_3 separated out without sticking.
3. Uranium was bright and shining after the reaction
4. $LaPO_4$/Y_2O_3 did not show the evidence of any reaction

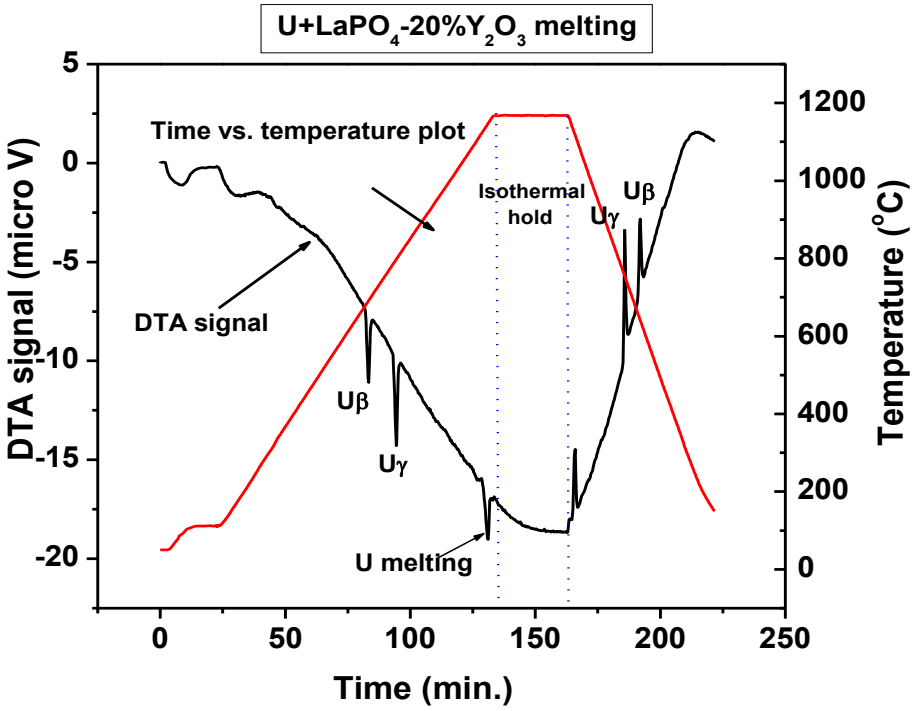

Figure 21) The DTA curve of $LaPO_4$-Y_2O_3 with uranium metal (Bhabha Atomic Research Centre)

Chapter 3

Conclusions

Lanthanum phosphate is thus identified as an all inorganic and versatile material for developing hydrophobic and nonreactive surfaces. Coatings and surfaces with multifunctional properties from transparency as well as hydrophobicity could be achieved by using $LaPO_4$. Non-reactive crucibles for metal melting applications and coatings that are anti-wetting to molten metals can be developed for foundry and laboratory applications using $LaPO_4$. $LaPO_4$-Y_2O_3 nanocomposite was found non-reacting with molten uranium metal which could be of great advantage for use in nuclear/strategic purposes and other high temperature applications. The inherent hydrophobic character as well as the non-reactivity with molten metals along with the excellent mechanical and thermal properties of $LaPO_4$ will be a tremendous boost in the respective areas of coatings and foundry applications.

Chapter 3

REFERENCES

1. L. Bocquet, E. A Lauga, *Nature Mater*., 10, **2011**, 334.
2. A. Nakajima, *NPG Asia Mater.*, 3, **2011**, 49.
3. D. Quéré, *Rep. Prog. Phys.*, 68, **2005**, 2495.
4. A. Lafuma, D. Quere, *Nature Mater.*, 2, **2003**, 457.
5. K.C. Hass, W.F. Schneider, A. Curioni, W. Andreoni, *Science*, 282, **1998**, 265.
6. G. Stirnemann, P.J. Rossky, J.T. Hynes, D. Laage, *Faraday Discuss*, 146, **2010**,263.
7. G. Azimi, R. Dhiman H-M. Kwon, A.T. Paxson, K. K. Varanasi, *Nature Mater*. 12, **2013**, 315.
8. N. Giovambattista, P.G. Debenedetti, P.J. Rossky, *J. Phys. Chem. B*,111, **2007**, 9581.
9. D. Argyris, P.D. Ashby, A. Striolo, *ACS Nano*, 5, **2011**, 2215.
10. A.W. Neumann, R.J. Good, *Surface and Colloid Science*, *New York: Plenum Press*, **1979**.
11. Y. Naoya, A. Yuu, S. Hiroaki, N. Akira, , O. Hisashi, , H. Kazuhito, W. Toshiya, *J. Am. Chem. Soc*., 128, **2006**,743.
12. V.S. Smitha, C.K. Jyothi, M.A Peer, S. Pillai, K.G. Warrier, *Dalton Trans.*, 42, **2013**, 4602
13. P. G. de Gennes, *Reviews of Modern Physics*, 57, **1985**, 827.
14. K. Kern, R. David, R.L. Palmer, G. Cosma, *Physical Review Letters*, 56, **1986**, 2823.
15. D.F. Mullica, W.O. Milligan, David A. Grossie, G.W. Beall, L.A. Boatner, *Inorg. Chim. Acta*, 95, **1984**,231
16. P.V. Ananthapadmanabhan, K.P. Sreekumar, T. K. Thiyagarajan, R.U.Satpute, K. Krishnan, N.K. Kulkarni, T.R.G. Kutty, *Mater. Chem. Phy.*, 113(1), **2009**,417.

Chapter 4

Colloidal Processing of Lanthanum Phosphate

Porous and dense monoliths of lanthanum phosphate were successfully fabricated using an environmentally benign colloidal forming process employing methyl cellulose. Concentration of 0.25 wt% methyl cellulose is found optimum to convert $LaPO_4$ slurry concentrations in the range of 50- 70 wt% solid loading to form shapes at a thermal consolidation temperature range (70- 80 °C). The casted shapes were sintered in the temperature range 1300 – 1500 °C in order to achieve porous (50%) and dense (>99%) ceramic bodies respectively. The porous lanthanum phosphate substrates obtained were found to be excellent adsorbents of perchlorate with >98% efficiency and with 100% reusability. Additionally, the effectiveness of such substrates as bio catalyst supports that facilitate biofilm formation of perchlorate reducing microbes (*Serratia marcescens* NIIST5*)* was investigated. Lanthanum phosphate has been found successful for the first time as a dual functional material that possesses an integrated adsorption/bioremediation property for the effective removal of ClO_4^- which is an increasingly important environmental contaminant. This dual functionality is due to the inherent hydrophobic character as well as the biocompatibility of $LaPO_4$.

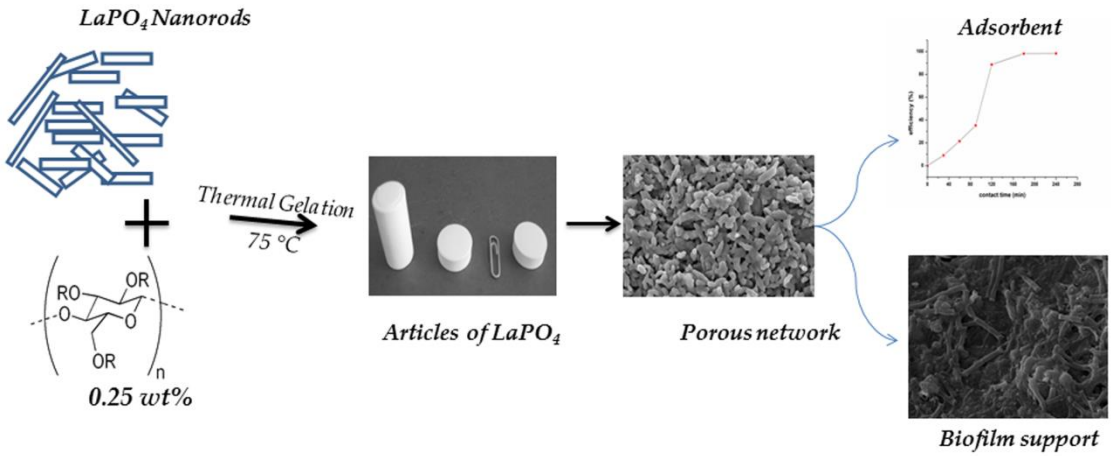

Chapter 4

4.1 Introduction

Lanthanum phosphate porous substrates may find certain applications due to its inherent properties of high temperature stability, hydrophobic nature and excellent bio compatibility. For both the applications it is necessary to find methods for consolidating the lanthanum phosphate particulates to specific shapes. The various methods for making porous shapes are slip casting, injection moulding, powder compaction and extrusion. All these methods need precursors designed for the process and should certain organic intermediates which should burn out during heat treatment for consolidation by sintering. Most of such precursors contain organic burnable component above 30% and the binder burn out times extends very long in addition to causing deformation in the process of heat treatment. Hence organic precursors preferably in non organic solvent medium and having possibility to contain high solid concentration are preferred.

Colloidal processing is a versatile technique for shape forming and is widely employed for the development of complex shaped dense and porous industrial ceramic products.[1-6] However, for shape forming nanoparticles and one-dimensional structures like nanorods, conventional processes like slip casting and injection moulding are often found to be unsuitable due to poor dispersibility of such powders in suspension. Moreover, gelation based on organic monomers like acrylamide suffers from the disadvantage of toxicity and hence has limited commercial viability.

Methyl cellulose, widely used for extrusion and injection moulding of ceramic articles undergo gelation and networking at 60-70 °C enabling it to be used for colloidal forming processes for ceramics.[7] Recently, thermal gelation of ceramic slurries containing very low concentrations of methyl cellulose is reported to be a feasible process for the colloidal casting

of highly dense (98% Theoretical Density) alumina ceramics.[8] Due to the extremely low binder content in casting slurries, the process enables faster heating schedules and is also environmentally benign. More recently, porous monolithic adsorbents prepared by ionotropic gelation are shown to possess high accessible surface area combined with high liquid flow permeability.[9] Such monoliths contained interconnected hierarchical pores in the range of 15 nm to 105 μm thereby enabling their use as effective biocatalysts.

The mechanism of thermal gelation involving methyl cellulose has been proposed by many.[10,11] *Hirren et al.*[12] showed that that hydrophobic interaction may have a role in the gelation of methylcellulose. At low concentration and low temperature, the methylcellulose well dissolved in water and solutions without aggregates were obtained. When the temperature and concentration increase, whatever the methylcellulose samples, hydrophobic interactions due to the presence of methyl groups appear. When the temperature is increased above the bimodal curve the concentration fluctuations generated by the phase separation lead to the formation of dense aggregates. The growth of these aggregates is limited by the concomitant gelation which decreases the mobility of the chains and hence forms rigid gels.

Perchlorate is known to interfere with the functioning of thyroid glands by reducing the level of thyroid gland hormones triiodothyronine ($\mathbf{T_3}$) and thyroxine ($\mathbf{T_4}$) responsible for regulation of metabolism in human beings. This interference can lead to many human physiological disorders including mental retardation in foetus and infants.[13] A host of techniques based on physico-chemical and biological processes are now available for removing perchlorate (ClO_4^-) from water.[14,16] The techniques include adsorption based processes employing tailored activated carbon,[17,18] hydrotalcite[19] as well as modified ion-exchange media.[20] More recently, the use of two stage hydrogen based membrane biofilm reactor was employed for

the complete reduction of perchlorate in the presence of nitrate and sulphate ions.[21] Phytoremediation of perchlorate by free floating macrophytes is also reported recently.[22] However most of these processes need regeneration of the adsorbent material as a secondary step and therefore integrated technologies based on novel matrices having improved properties of adsorption and simultaneous degradation of the compound are highly attractive. The present work is an attempt to explore the suitability of lanthanum phosphate porous substrates for the adsorption of perchlorate from water. The intrinsic hydrophobic nature of lanthanum phosphate (*chapter 3*) can, in addition, facilitate biofilm growth of perchlorate reducing microbes owing to the better adherence of the bacteria on the hydrophobic substrates .[23,24]

Aqueous based precursors preferably using thermal gelation are being investigated recently with considerable success for alumina ceramics. However, such colloidal processing techniques are not reported in the case of rare earth phosphates. Further the porous sintered lanthanum phosphate was tested for biofilm formation as phosphate was tested for perchlorate ions which cause serious environmental hazard. The primary objective of the present study is therefore to develop crack free porous monoliths and dense bodies of lanthanum phosphate through a modified cellulose based gel casting process. The porous monoliths developed are then evaluated for the removal of perchlorate (ClO_4^-) ions, a toxic oxyanion and ground water contaminant of increasingly serious concern. The motivation for employing lanthanum phosphate for such an application is primarily ascribed to its biocompatibility coupled with very low solubility in water.

4.2 Experimental

4.2.1 $LaPO_4$ Monolith Synthesis

Lanthanum phosphate ($LaPO_4$) powder was synthesised following a modified sol- gel process as reported in chapter 2. The $LaPO_4$ thus obtained was calcined at 600 °C and dispersed in distilled water to prepare suspensions of 50-70 wt % solid loading. Dilute nitric acid was used as the dispersant and suspension pH was maintained at ~2. The prepared suspension was then transferred to poly propylene bottles and ball milled for 6 hours using alumina balls. 2 wt% methyl cellulose stock solution was prepared by dissolving methyl cellulose in distilled water. Methyl cellulose (Methocel F7M, Dow Deutschland GmbH & Co. OHG, Stade, Germany), equivalent to a concentration of 0.25 wt% of $LaPO_4$ powder weight) was then added to the suspension and milling was continued for two more hours. The gelation characteristics of $LaPO_4$ slurry containing methyl cellulose was measured in a rheometer (MCR 50, Anton-Paar, Austria) using a parallel plate configuration at a gap size of 0.25 mm in oscillation mode. The gelation studies were performed in the temperature range of 25-75 °C, after heating to the measurement temperature at a ramp rate of 1 °C/min.

Slurry after de-airing was cast in Teflon moulds and the cast shapes were heated to 80°C in an oven. The lanthanum phosphate powder and the powders derived from green samples of cast lanthanum phosphate (dried at 100 °C) were characterized by Transmission Electron Microscopy (Tecnai G^2, FEI, The Netherlands operated at 300 kV) at an accelerating voltage of 300 KeV. The samples, released from mould after 1 hr, were dried under controlled humidity conditions of 45 °C and 75% RH for 24 hr and further sintered in the temperature range of 1300-1500 °C for 2 hr. Heat treated samples were characterised for their density (Archimedes Principle) and microstructure (scanning electron microscopy, JEOL JSM-6700F SEM, Japan).

4.2.2 Perchlorate adsorption studies

In a typical experiment, lanthanum phosphate porous monoliths weighing 2.5gm were immersed in ClO_4^- (ammonium salt) solution of various concentrations ranging from10 – 100 µg/L, in a 100 mL conical flask. The pH of the solution was maintained neutral (~7) so as to check the viability of monoliths in removing ClO_4^- in drinking water samples. The flasks were kept in a rotary shaker maintained at 30 °C. Samples were taken every 30 minutes up to 5 hours and residual ClO_4^- concentration in the water was measured.

4.2.3 Biofilm Growth on $LaPO_4$ substrate

The study is conducted by placing $LaPO_4$ material in an effluent containing less than 1 mg/L of ClO_4^-. A perchlorate reducing microbial biofilm was grown on the $LaPO_4$ surface within a week's time and was visible as a greenish slimy layer. The substrate was mechanically cleaned and used again for biofilm growth to confirm biofilm formation on repeated use of the substrate. The PRB collected from the biofilm was gently washed before staining with SYBR Green I SYBR Green I Stain is an asymmetrical cyanine dye used as a nucleic acid stain in molecular biology. SYBR Green I binds to DNA. The resulting DNA-dye-complex absorbs blue light (λ_{max} = 497 nm) and emits green light (λ_{max} = 520 nm).. After incubation for 30min, they were observed with an epifluorescent microscope

4.3 Results and Discussion

The morphological features of as precipitated and calcined (600 °C) lanthanum phosphate ($LaPO_4$) powders are presented in *Figure 1*. As shown, the precipitation conditions lead to well dispersed nanorods of length 400-700 nm and diameter of 15 nm. The rod shaped morphology is a characteristic feature of lanthanum phosphate that crystallises in rabhdophane structure and is ascribed to the preferential growth along the c direction.[25] A change in aspect ratio was observed on the rods during calcination at 600 °C, though the morphology was retained to a good extent.

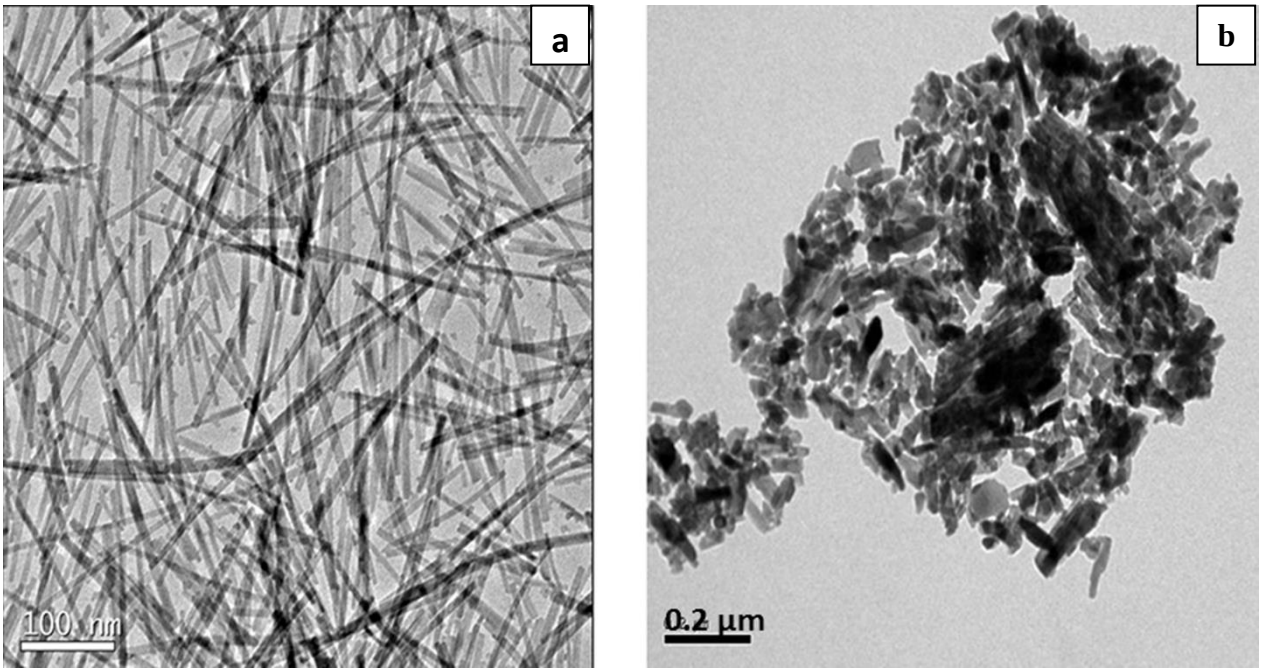

Figure 1) *TEM of a) as precipitated nanorods & b) powder after calcination at 600 °C*

Aqueous dispersions of these rods can be readily obtained through controlling the pH of the slurry to ~2. Slurries of solid loading varying from 50 to 70 wt% were subjected to viscosity measurements with varying shear rates to characterise their flow behaviours. The plots

presented in *figure 2a* clearly indicate a shear thinning behaviour as viscosity at low shear rates depended on the solid loading. The viscosity values of all the suspensions decreased considerably faster in the shear rate region of 1-100 s^{-1} and thereafter remained constant up to 900 s^{-1}.The shear thinning behaviour facilitated the viscosity values to remain high during the casting process and avoided sedimentation of $LaPO_4$ nanorods.

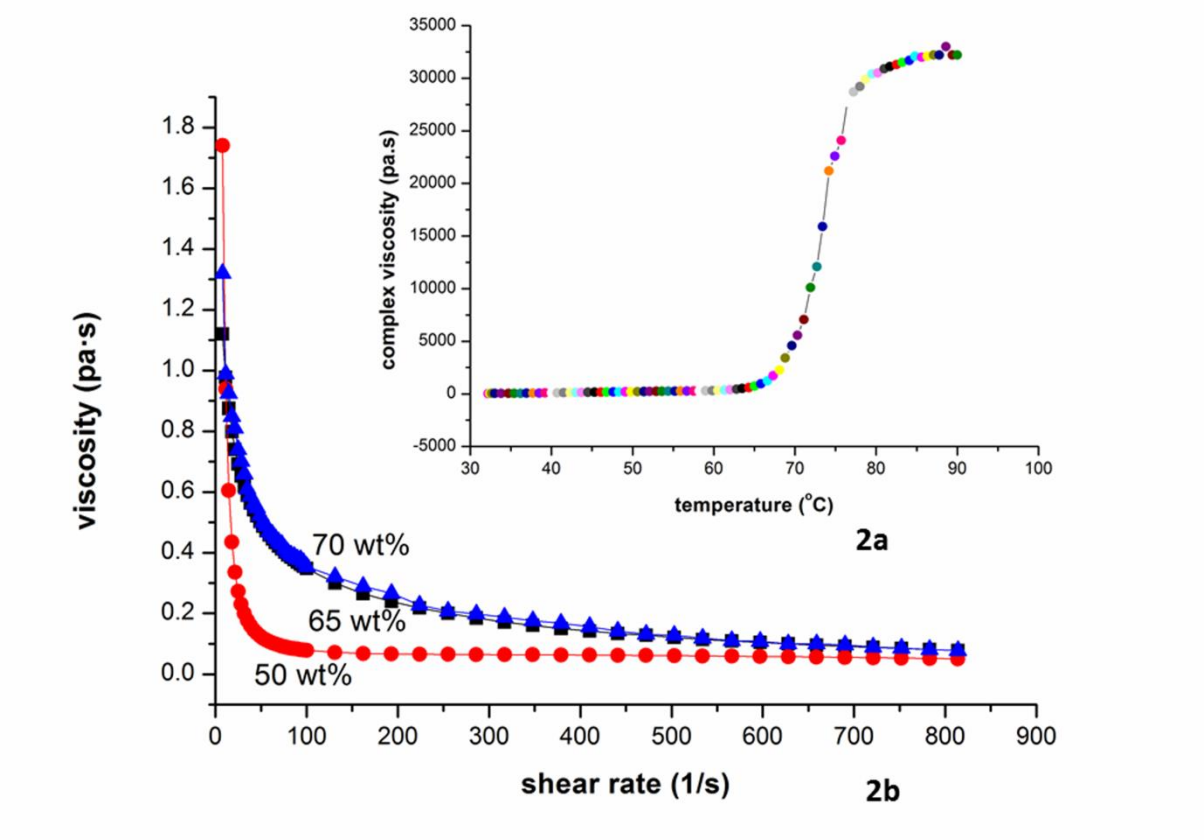

Figure.2a.*Viscosity with shear rate plots of* $LaPO_4$ *slurries with varying solid loading*
Figure.2b*. Change in viscosity with temperature for* $LaPO_4$ *slurry containing 0.25wt% methyl cellulose*

The thermal gelation behaviour of $LaPO_4$ slurry containing 0.25 wt% methyl cellulose was studied by following the viscosity changes with temperature (*Figure 2b*). A constant viscosity value was recorded till the temperature reached 65 °C. The rapid increase in viscosity value observed in the temperature range of 65-80 °C confirmed the thermal gelation process.

Dehydration of methyl cellulose particles leads to hydrophobic interactions between the polymer molecules and the network structure that resulted transformed the slurry to a solid (*Figure 3*).

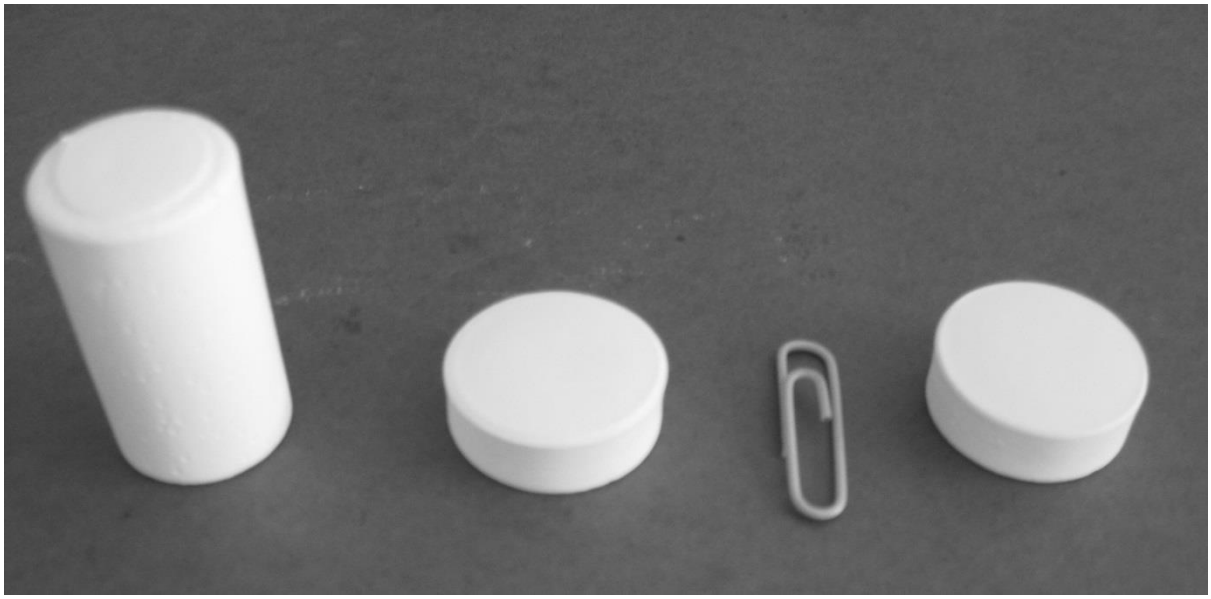

Figure 3) Photographs of $LaPO_4$ monoliths obtained via colloidal processing

The $LaPO_4$ nanorod-cellulose binder interaction was obtained from the TEM analysis of the cast green samples (powdered and re-dispersed in acetone). The formation of a thin amorphous layer of methyl cellulose particles uniformly cascading the nanorods is clearly evident in the TEM micrographs. The surface coverage of nanorods by methyl cellulose particles and subsequent networking helps the shape forming process. A well-defined peak of carbon found in the EDAX spectrum (*Figure 4*) of the samples indicated that the amorphous layer formed was of methylcellulose origin.

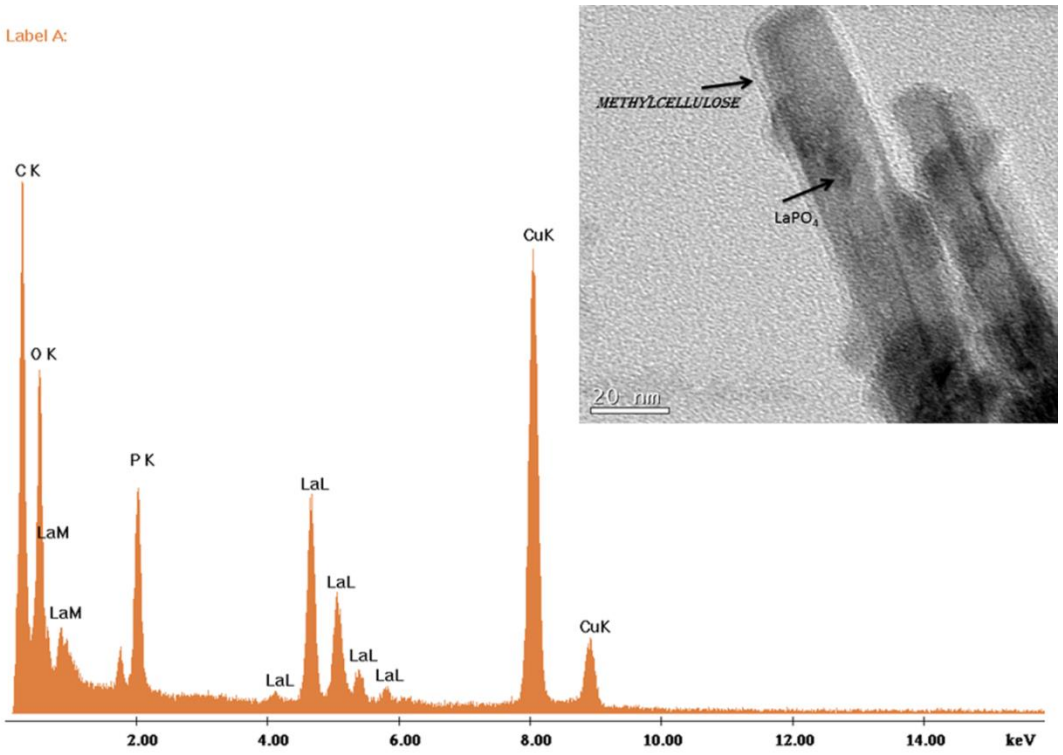

Figure 4) TEM image of green samples (powdered and re-dispersed in acetone) of $LaPO_4$ containing 0.25 wt% methyl cellulose and the corresponding EDX spectrum confirming the presence of carbonaceous layer

The green density of samples derived from suspensions of varying solid loading (50, 65 and 70 wt %) is presented in *figure 5a*. Solid loading of 50 wt% in suspension lead to very low green density values < 20% of theoretical density. The green density values of monoliths increased with increasing solid loading and a value of 30 wt% was obtained for samples with 70 wt% $LaPO_4$These values were lower for a colloidal casting process involving suspension forming. This is primarily attributed to the rod morphology of $LaPO_4$ leading to poor particle packing. The network forming attributes of methyl cellulose is therefore responsible for the shape formation and integrity. The densification behaviour of samples during heat treatment in the temperature range of 1300-1500 °C is also presented in *figure 5a*.

Samples derived from suspension of 50 wt% solid loading achieved highest densification of 80% at 1500 °C. Sintered density values as low as 50% were realised from such samples by limiting the firing temperature to 1300 °C. Microstructure of samples fired at 1300 °C indicated highly porous structure with interconnected porosity and 1.5- 2µm sized pores (*figure 5b*).The microstructure was further characterised by elongated grain morphology with average lengths of 2-3 microns. As sintering temperature is increased further densification and grain growth takes place. The elongated particle morphology undergoes changes.

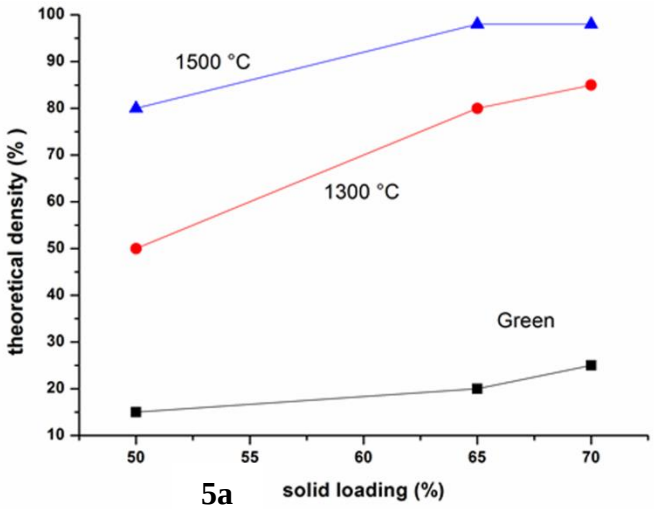

5a

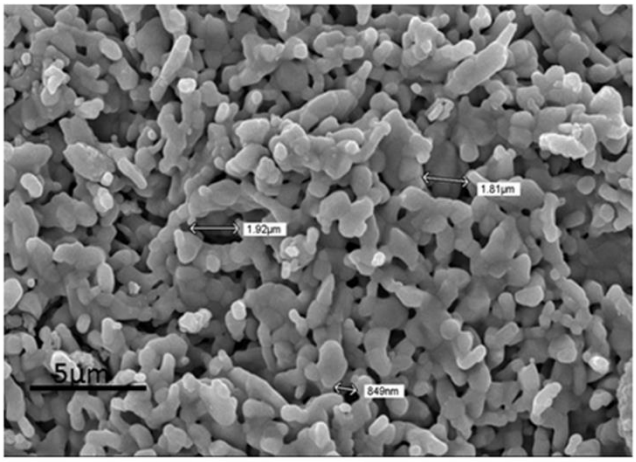

5b

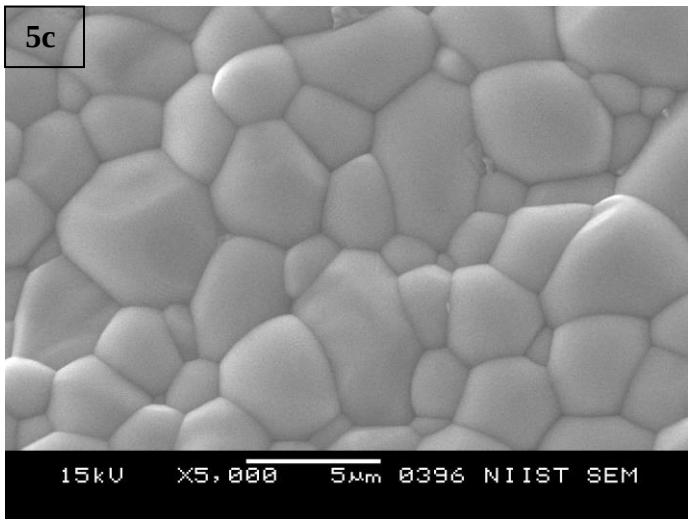

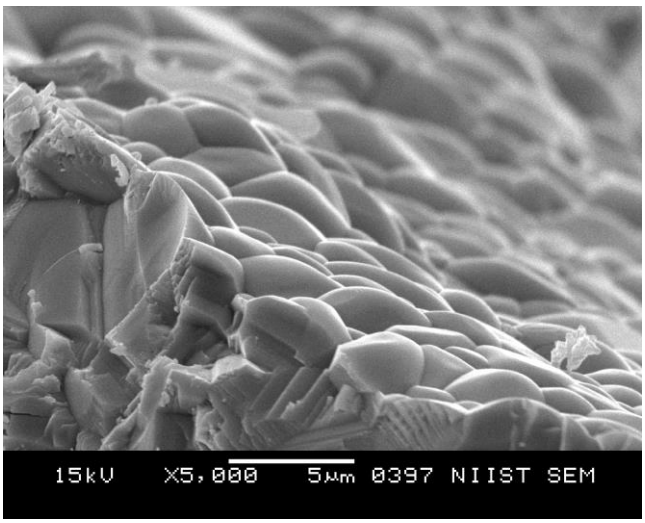

Figure 5 ***a)*** *Densification behaviour of* $LaPO_4$ *samples with temperature and solid loading* ***5****b) Porous* $LaPO_4$ *obtained from 50 wt% suspension and fired at 1300* °C 5c) Dense $LaPO_4$ obtained on firing at 1500 °C

4.3.1 Adsorption of perchlorate ions using porous $LaPO_4$ monoliths

For the present study, we had chosen four different ClO_4^- concentrations in the range of 10 to 100 µg/L in order to ascertain the efficiency of $LaPO_4$ in the lower concentration range. The changes in ClO_4^- concentration with time for the four initial concentrations of 12, 20, 55 and 100 µg/L are presented in Figure 6a and Figure 6b. Solutions having high concentrations of ClO_4^-showed a drastic reduction (>80%) in ClO_4^- within 30 minutes of contact time. After 300 minutes of contact time >98% removal of ClO_4^- was obtained in all solutions used in the study. The reusability study was carried out after desorbing ClO_4^- from the sample by changing the pH to a lower level. The regenerated monolith showed continued adsorption of the ClO_4^- ion in repeat experiments thereby ensuring reusability of the material, which is a very desirable characteristic for any potential adsorbent.[26] Investigations on the adsorption ability with varying pH values revealed that the maximum adsorption capability was at pH 7. The adsorption capacity decreased considerably at pH values above and below 7.

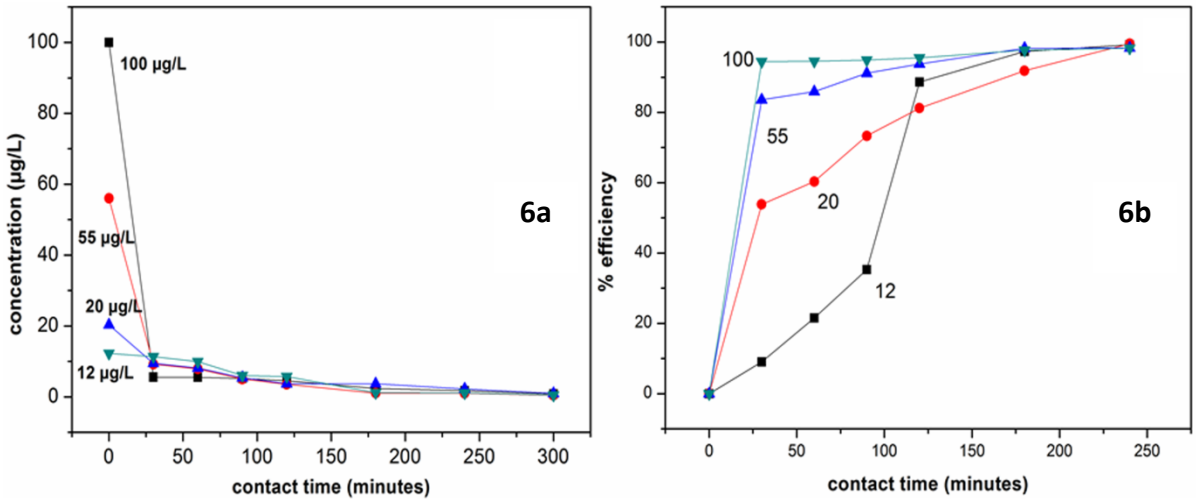

Figure 6) Graphs showing ClO_4^- adsorption efficiency and capacity by the samples at pH 7. **6a**) Effect of concentration, **6b**) Effect of contact time

The FTIR spectrum (*figure 7*) of the ClO_4^- adsorbed $LaPO_4$ (sample ground and dried at 100 °C) showed the presence of peaks corresponding to ClO_4^- ions at1080 cm^{-1} and 940 cm^{-1} and clearly confirmed ClO_4^- ion adsorption as expected.[27]

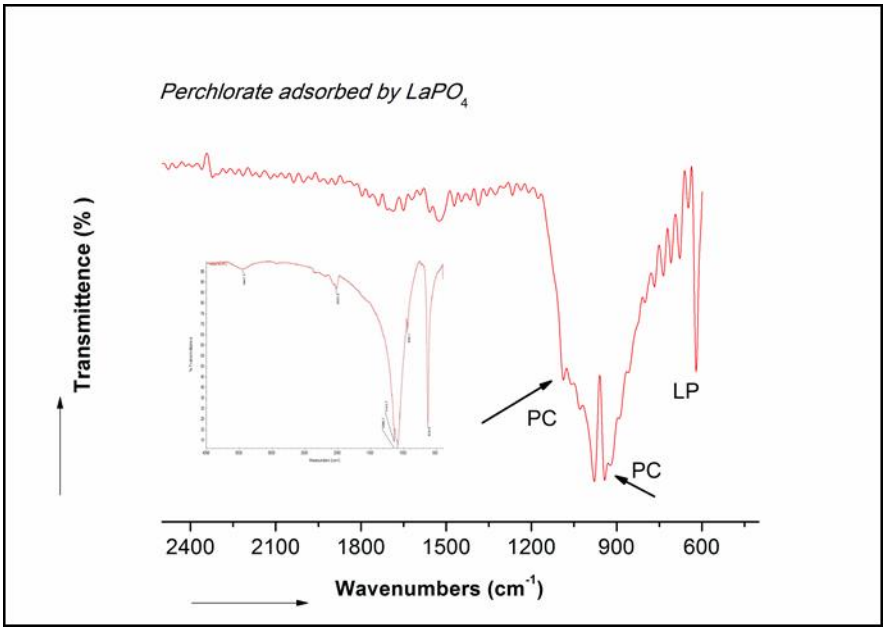

Figure 7) FT- IR spectrum of perchlorate adsorbed porous $LaPO_4$ (**PC**: Perchlorate and **LP**: $LaPO_4$)

From the adsorption data, the amount of ClO_4^- ions adsorbed on lanthanum phosphate monoliths was calculated by using the equation (1),

$$qe = (\frac{Co-Ce}{m})v \quad \text{..... (1)}$$

where $\mathbf{C_o}$ is the initial concentration at zero contact time, $\mathbf{C_e}$ is the concentration at the equilibrium time, **V** is the initial volume of ClO_4^- used for measurement and **m** is the mass of the adsorbent used. The lanthanum phosphate monoliths gave an adsorption capacity value of 0.0039 mg/g while adsorbing from a solution with an initial ClO_4^- concentration of 100 µg/L. More than 80% of the adsorption was completed within 30 minutes of contact time; which is better than the 80% ClO_4^- removal in 6 h reported for calcined layered double hydroxide

(LDH).[28] The adsorption capacity of $LaPO_4$ monoliths increased with increasing concentration of the ClO_4^- ions. The saturation capacity of the material was not examined in our studies as our priority was to examine the efficiency of $LaPO_4$ as a ClO_4^- ion scavenger at low concentrations. New generation adsorbents like graphene reportedly showed an adsorption capacity of 0.024 mg/g at an initial concentration of 2 mg/L,[29] whereas ferric granular hydroxide showed a much higher adsorption capacity of 20 mg/g at room temperature for the concentration range of 0.05 mg/L- 500 mg/L.[30] It should be noted that, the adsorption system in the present study was designed to repeatedly remove low concentrations of ClO_4^- ions from water. The available surface area of the monoliths is much smaller compared to the surface area of adsorbent powders and hence the lower adsorption capacity in terms of weight of adsorbent is justifiable. $LaPO_4$ powders or porous substrates coated with $LaPO_4$ could be also considered for adsorption applications for higher ClO_4^- ion loading per unit weight of $LaPO_4$.

The adsorption data plotted using the Langmuir, Freundlich, and a Dubinin- Kaganer-Radushkevich (DKR) isotherm are presented in *Figure 8*. The linear form representations of these isotherms are as follows;

$$\frac{C_e}{q_e} = \frac{1}{K_l q_o} + \frac{C_e}{q_o} \quad \text{(2)}$$

$$Lnq_e = \left(\frac{1}{n}\right) LnC_e + LnK_f \quad \text{(3)}$$

$$Lnq_e = lnq_m - \beta\varepsilon^2 \quad \text{(4)}$$

in which, K_l (l/mg) and K_f (mg/g) are the Langmuir and Freundlich constants and $\mathbf{q_m}$, $\mathbf{C_e}$ (mg/ L) the concentration of ClO_4^- ions remaining in the solution at equipoise, **n** (g/L) is the

Freundlich constant which is related to the adsorption intensity, $\boldsymbol{\beta}$ (mol^2/ J^2) is a constant related to the adsorption energy and $\boldsymbol{\varepsilon}$ is the Polanyi potential obtained using,

$$\boldsymbol{\varepsilon = RT\ Ln\left(\frac{1}{Ce} + 1\right)} \quad \ldots\ldots (5)$$

where, **R** (J/ mol/ K) is a gas constant and T (K) the absolute temperature.

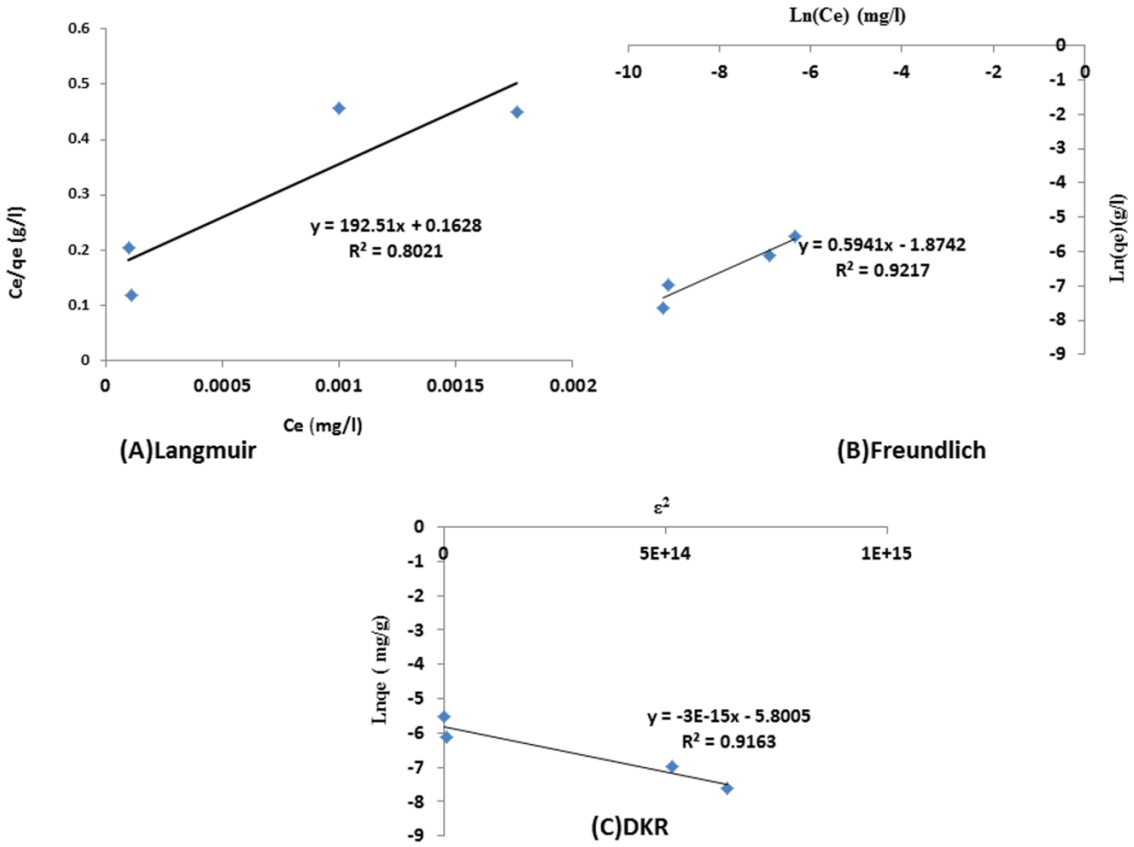

Figure 8 A) Langmuir **B)** Freundlich **C)** DKR isotherm schemes for ClO_4^- adsorption by the $LaPO_4$ samples at different concentrations

The adsorption isotherms plotted corresponding to different concentrations of ClO_4^- ions were analysed for identification of the mechanisms involved. Among the three isotherm plots, R^2 values were found largest for Freundlich isotherm (0.921) followed by DKR (0.916) whereas fitting to Langmuir isotherm gave the worst R^2 value of 0.802. Perchlorate bonds

through electrostatic interactions on the lanthanum phosphate surfaces and as the surface coverage increases the ClO_4^- adsorption slows down as validated by the good fit with Freundlich isotherm.[28]

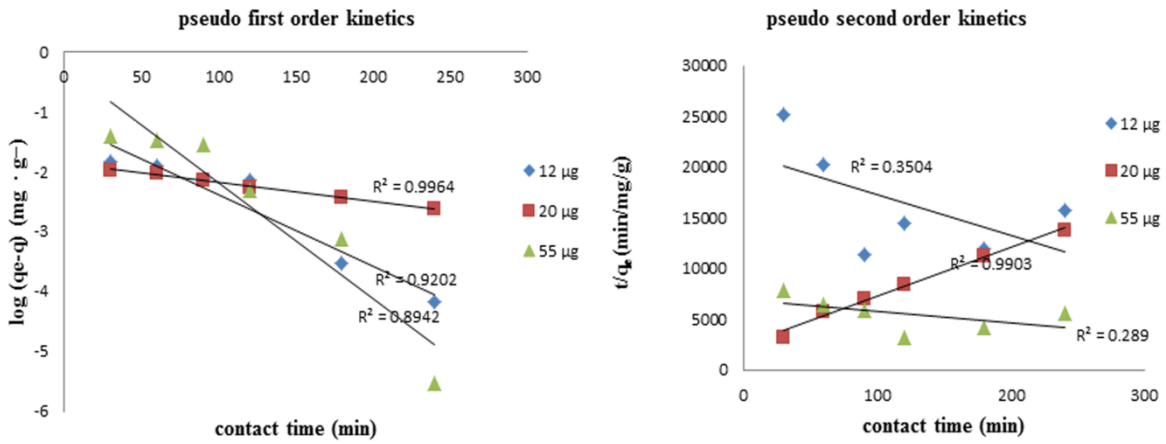

Figure 9) Typical Pseudo first order and second order kinetics respectively for adsorption of ClO_4^- ions by lanthanum phosphate articles for the concentrations under study. (1 concentration omitted for clarity)

The rate of adsorption of ClO_4^- ions by the lanthanum phosphate articles was analysed using Lagergren pseudo-first order, pseudo-second order kinetics and is presented in Figure .9. It was observed that the pseudo first order kinetics is > pseudo second order kinetics with R^2 values close to 1 for the adsorption patterns. Hence it is clear from the analysis that first order kinetics prevail during the adsorption of ClO_4^- ions by lanthanum phosphate articles.

4.3.2 Porous Lanthanum Phosphate as Substrates for Biofilm growth

The porous lanthanum phosphate monoliths obtained by thermal gelation process were also investigated as supporting substrates for ClO_4^- reducing microbial biofilm formation. This property of $LaPO_4$ can be used potentially for the development of fixed film type of bioreactors where microbes are immobilized for enhancing bioremediation activity. Earlier reports suggested that the factors controlling the growth of biofilm are hydrophobicity of substrate and porosity of monolith.[26] The hydrophobic interaction between the microbial surface and the substrate enables the microbes to overcome the repulsive forces operating within short distances of the substrate and to get attached irreversibly. Colloidal forming of porous lanthanum phosphate and its inherent hydrophobic behaviour[25] thus favour biofilm adhesion. Figure 8 presents the scanning electron microscope image of a section of the substrate with the biofilm. The photograph of original porous pellet (1) and pellet after 1 week biofilm growth (2) are shown in *figure* below. The green slimy layer in (2) is a visual indication of the growth of PRBs.

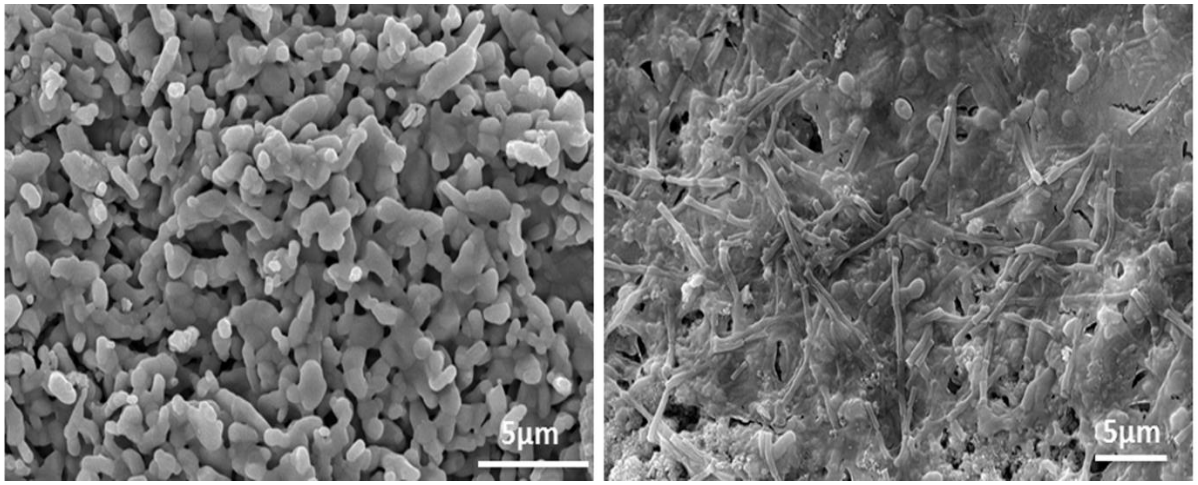

Figure 10) SEM micrographs of **a**) bare porous $LaPO_4$surface and **b**) $LaPO_4$ surface with biofilm of perchlorate reducing bacterium culture

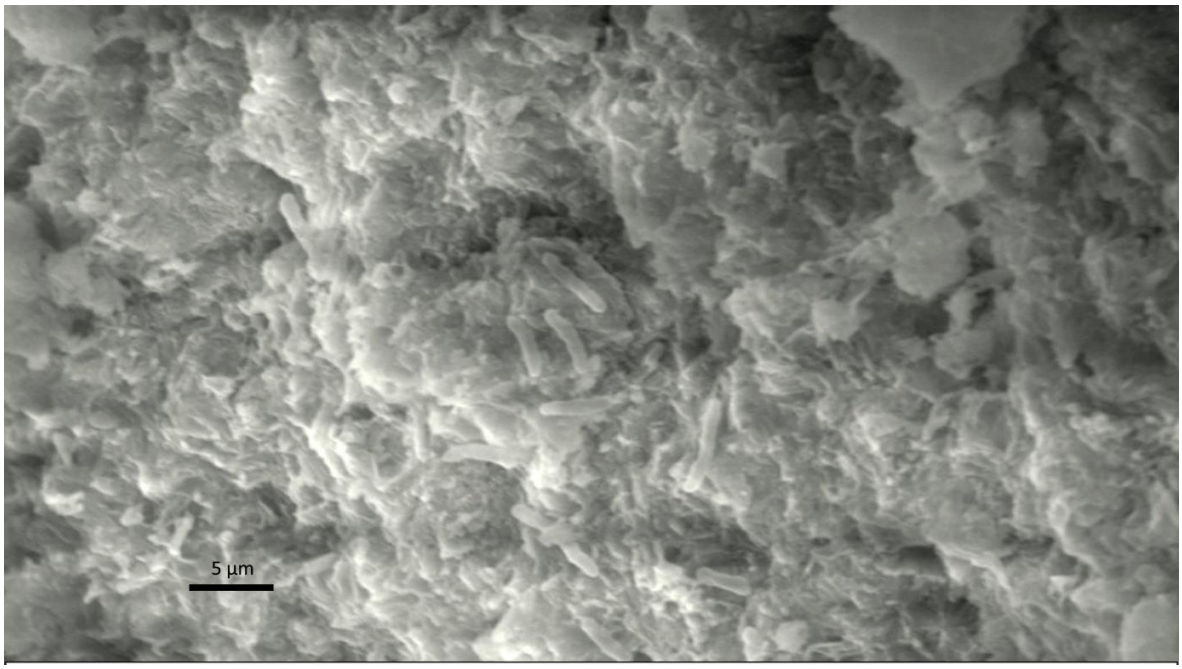

Figure 11) SEM micrograph of a $LaPO_4$ surface with specific perchlorate strains of *Serratia marcescens* NIIST5

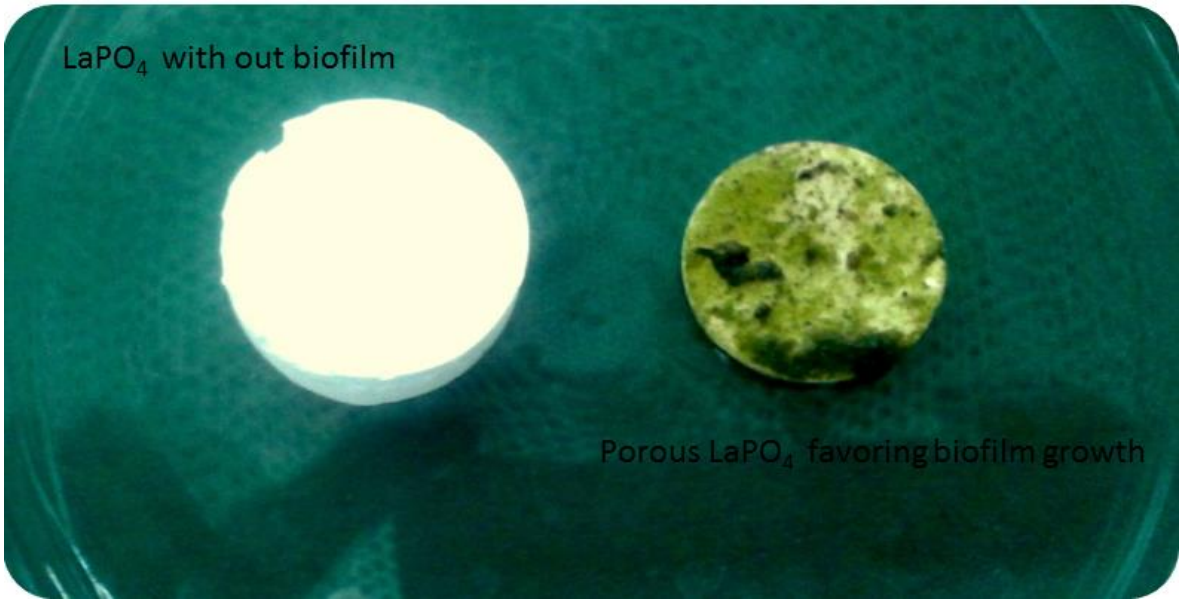

Serratia marcescens NIIST5 that formed biofilm over the $LaPO_4$ surface is a known perchlorate reducing bacteria.[31] *Figure 11* shows the successful congregation of ClO_4^- reducing bacterial strains of *Serratia marcescens* NIIST5 over the $LaPO_4$ substrate without the necessity of any intermediate coating. The formation of biofilm over $LaPO_4$ surface

makes it an ideal substrate for the growth of specific perchlorate reducing bacteria and thus will effectively reduce the adsorbed ClO_4^- completely to chloride.

The sample containing attached biofilm was crushed and stained with DNA intercalating fluorescent dye SYBR Green I. SYBR Green I Stain is an asymmetrical cyanine dye used as a nucleic acid stain in molecular biology. SYBR Green I binds to DNA. The resulting DNA-dye-complex absorbs blue light (λ_{max} = 497 nm) and emits green light (λ_{max} = 520 nm). The PRB collected from the biofilm was gently washed before staining with SYBR Green I. It was subsequently examined under an epifluorescent microscope (Leica DM 2500) equipped with a digital camera DFC300FX. *Figure 12* shows the microscopic images and the green fluorescence patches confirm incipient ClO_4^- reducing microbial cells.

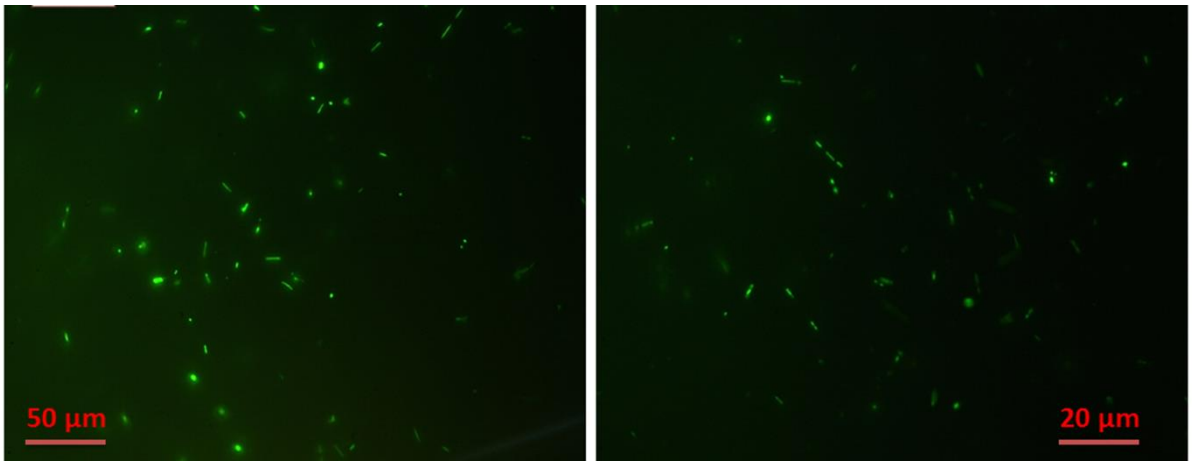

Figure 12) Fluorescence staining of an enriched ClO_4^- reducing bacteria culture attached on $LaPO_4$ thermal gel with the DNA-intercalating dye SYBR Green I.

The present study therefore demonstrated the possibility of using porous monoliths of $LaPO_4$ for the multiple functions of ClO_4^- adsorption and biofilm formation of ClO_4^- reducing bacteria. As the microbes are capable of reducing the adsorbed ClO_4^-, the $LaPO_4$ surfaces can be in situ regenerated offering an integrated adsorption and bioremediation property. However further studies are required to revalidate this bi-functional property of $LaPO_4$ monoliths.

Chapter 4

Conclusions

A novel, simple and cost effective colloidal processing approach involving thermal gelation of methyl cellulose is reported first time for the development of porous and dense shapes of lanthanum phosphate. Thermal gelation of methyl cellulose at 70-80 °C was used to convert suspensions of lanthanum phosphate nanorods to highly porous green bodies which on subsequent heat treatment changed to porous monoliths having up to 50% porosity. The $LaPO_4$ porous monoliths function as bifunctional substrates performing adsorption and bioremediation of perchlorate. The porous monoliths of $LaPO_4$were found excellent as adsorbents for ClO_4^- ions at concentrations as low as 10 µg/L and with greater than 98% removal efficiency. The porous monoliths, due to the functional features of $LaPO_4$, were also shown to be novel supports for the growth of perchlorate reducing *Serratia marcescens* NIIST5 bacteria.

REFERENCES

1. R. Janssen, S. Scheppokat, N. Claussen, *J. Eur. Ceram. Soc.*, 28, **2008**, 1369.

2. R. S. Kumar, K. Rajeswari, B. Praveen, U. S. Hareesh, R. Johnson, *J. Am. Ceram. Soc.*, 93, **2010**, 429.

3. M. Lombardi, V. Naglieri, J. M Tulliani, L. Montanaro, *J. Porous Mater.*,16, **2009**, 393.

4. X. J. Mao, S. Z. Shimai, M. J. Dong, S.W. Wang, J. Am. Ceram. Soc., 91, **2008**, 1354.

5. X. Xu, Z. Wen, J. Lin, N. Li, X. Wu, Ceram. Int., 36, **2010**, 187.

6. U.S. Hareesh, R. Anantharaju, P. Biswas, K. Rajeswari, R. Johnson, *J. Am. Ceram. Soc.*, 94, **2011**, 749.

7. D. Dong, Y. Huang, X. Zhang, L. He, C-Z. Li, H. Wang, *J. Mater. Chem.*, 19, **2009**, 7070

8. T. Y. Klein, L. Treccani, J Thoeming, K. Rezwan, *RSC Adv.*, 3, **2013**, 13381

9. B.P. Chaplin , M. Reinhard , W.F. Schneider, C. Schüth , J.R. Shapley, T.J. Strathmann , C.J. Werth, *Environ. Sci. Technol.*, 46, **2012**, 3655**.**

10. D. A Rees, *Chem. Ind. London*, **1972**, 630.

11. N. J. Sarkar, *Appl. Polym. Sci*., 24, **1979**, 1073

12. M. Hirrien, C. Chevillard, J. Desbrieres, M. A. V. Axelos, M. Rinaudo, *Polymer* 39, (25), **1998**, 6251

13. P. Yin-Xian, Z. Lu, C. Cui-Yun, Z. Ming-Long, Z. Yang, W. Chun-Du, *J. Chem. Soc. Pak.*,34,**2012,**819.

14. http://oehha.ca.gov/water/phg/pdf/finalperchlorate31204.pdf,Public health goal for perchlorate in drinking water, **2004**

15. R. Srinivasan, G. A. Sorial, *Sep. Puri. Technol.*, 69, **2009,** 7.

16. L. Ye, H. You, J. Yao, H. Su, *Desalination***,** 298, **2012**, 1

17. J. K. Choe, M.H. Mehnert, J. S. Guest, T J. Strathmann, C. J. Werth, *Environ. Sci. Technol***.,** 47, **2013,** 4644.

18. R. Parette, F.S. Cannon, *Water Research.* , 39, **2005**, 4020.

19. W. Chen, F.S. Cannon, J.R. Rangel-Mendez, *Carbon*, 43, **2005**, 581.

20. Y. Yang, N. Gao, W. Chu,Y. Zhang, Y. Ma, *J. Hazard. Mater.*, 209–210 ,**2012**, 318.

21. K. Hristovski, P. Westerhoff, T. Möller, P. Sylvester, W. Condit, H. Mash , *J. Hazard. Mater.*, 152 ,**2008**, 397.

22. H.P. Zhao, A.O. Valencia, Y. Tang, B. O. Kim, Z. E. Ilhan, R. K. Brown, B. Rittmann, *Environ. Sci. Technol*., 47, **2013**, 1565.

23. B. Krishnakumar, V. N. Anupama, T. Soumya, B. S.Liji, G. P. V. Prajeesh, *J. Hazard. Mater.*, 260, **2013**. 901.

24. M.R. Fernández, M.G. Casabona, V.N. Anupama, B. Krishnakumar, G.A. Curutchet, D.L. Bernik, *Colloid Surface B.*, 81, **2010**, 289.

25. S. Sankar, K.G. Warrier. *J. Sol-Gel Sci. Technol.*, 58, **2011**, 195.

26. T. Y. Klein, L. Treccani, J Thoeming, K. Rezwan, *RSC Adv.*, 3, **2013**, 13381.

27. R. M. Donlan, *Emerging Infectious Diseases*, 8, **2002**, 9

28. Y. Yang, N. Gao, Y. Deng, S. Zhou, *Appl. Clay Sci.*, 65–66, 2012, 80.

29. J. Lakshmi, S. Vasudevan, *Environ. Sci. Pollut. Res.*, 20(8), **2013**, 5114.

30. E. Kumar, A. Bhatnagar, J.A. Choi, U. Kumar, B. Min, Y. Kim, H. Song, K.J. Paeng, Y. M. Jun, R.A.I. Abou- Shanab, B.H. Jeon, *Chem. Eng. J.*, 159, **2010**, 84.

31. V.N. Anupama, G. P. V. Prajeesh, B. Krishnakumar, *FEMS Microbiol. Lett.*, 339 , 2013,117.

Chapter 5

Summary of Investigations

Lanthanum phosphate is one among the lanthanide family of "rare earths" in the periodic table of elements. It is characterized by certain excellent properties compared to the other phosphates like aluminium phosphate and calcium phosphate. Known under the generic name, Monazite, the rare earth phosphates have melting points above 1900 °C, high thermal phase stability, low thermal conductivity, and thermal expansion coefficient similar to some of the high temperature oxides like alumina and zirconia. Studies related to machinability of sintered lanthanum phosphate ceramics due to its low hardness, and as host for luminescent compositions are also reported. In this respect, although less investigated, the lanthanum phosphate is learnt to have excellent possibilities for use in various applications. A few of the properties which need further investigation are the lanthanum phosphate based composites, hydrophobic properties, non-reactivity with molten metals and certain bio functionality.

The synthesis of stoichiometric $LaPO_4$ and composites is very important since any non-stoichiometry may reduce the high temperature properties. A simple technique of preparing stoichiometric $LaPO_4$ by precipitating from lanthanum chloride and converting to precursor gels and further processing to nano size powder was developed as the first step. The use of ammonia intermediate ensures easy removal of remaining anions and leaves the gel separated. The lanthanum phosphate has 100-120 nm size in the as precipitated condition and 60-80 nm as sol particles, rod like morphology (average aspect ratio 4) and good thermal stability. The powder compact can be sintered to > 99% density at 1300 °C. Nano composites of $LaPO_4$ with Y_2O_3 and ZrO_2 were also prepared with varying compositions in the range 5-20 wt% oxides.

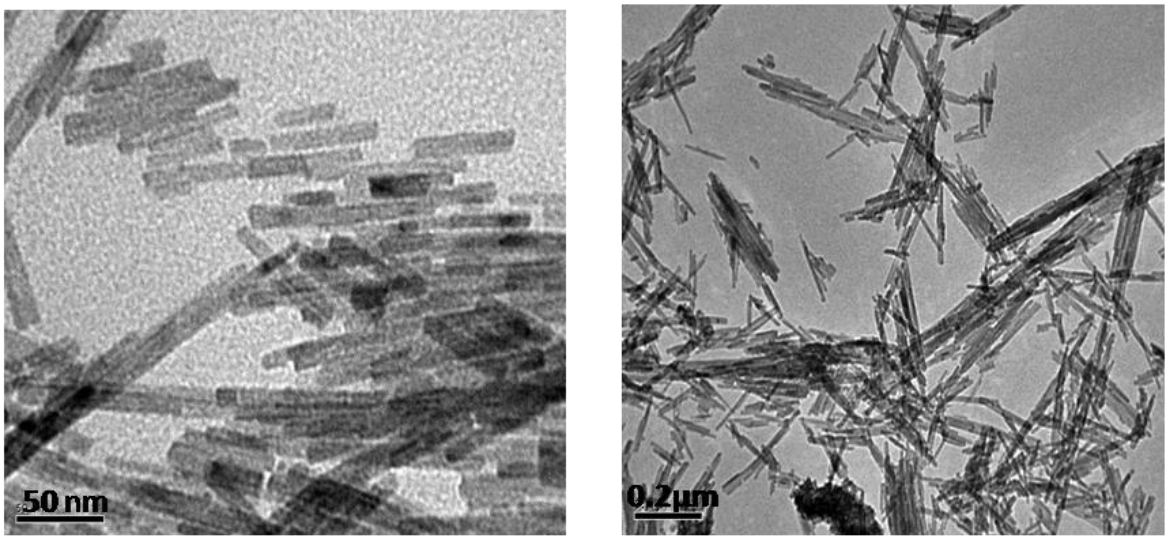

Lanthanum phosphate nanorods

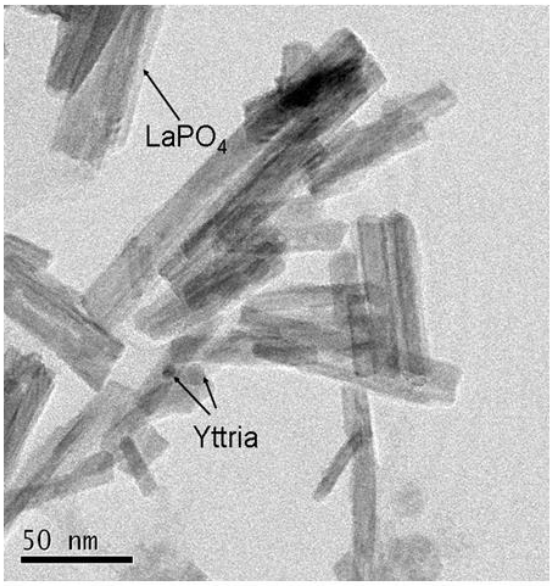

$LaPO_4$- 20 wt%Y_2O_3 nano composite

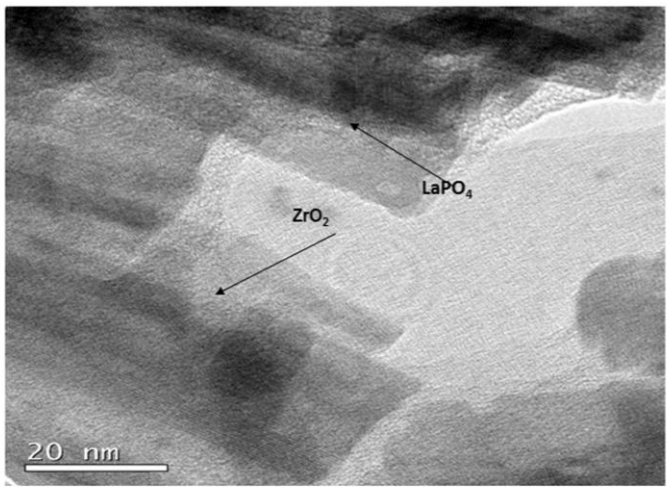

$LaPO_4$- 5-wt%ZrO_2 nano composite

Chapter 5

Two major properties which are less investigated earlier were studied in detail in the thesis. The inherent property of water non-wettability (hydrophobicity) and non-reactivity with molten metal are investigated further. The other is the extension of the hydrophobic features of porous lanthanum phosphate in growing biofilms containing perchlorate reducing microbes and removing the contaminant from water while facilitating increased absorption of perchlorates, especially applicable to industrial waste streams.

Lanthanum phosphate has low wetting features with water, possessing contact angles $>95^{o}$ and this is explained based on the electronic structure of the rare earths in general. The unfilled 'f' orbitals of rare earth atoms are shielded from the interaction with surrounding environment by the full octet of electrons in the $5s^2p^6$ outer shell, thus preventing formation of hydrogen bonds with interfacial water molecules (Azimi et al, Hydrophobicity of rare-earth oxide ceramics, *Nature Mater*. 12, **2013**, 315). Lanthanum phosphate coatings were made on glass and these coatings exhibited contact angles 120^{o} and this is attributed to the synergistic effect of inherent hydrophobicity of rare earth phosphates as well as the surface roughness created by the rod shaped particles which was confirmed by Scanning Electron Microscopy (SEM) and Atomic force Microscopy (AFM) through mapping of the surface profile.

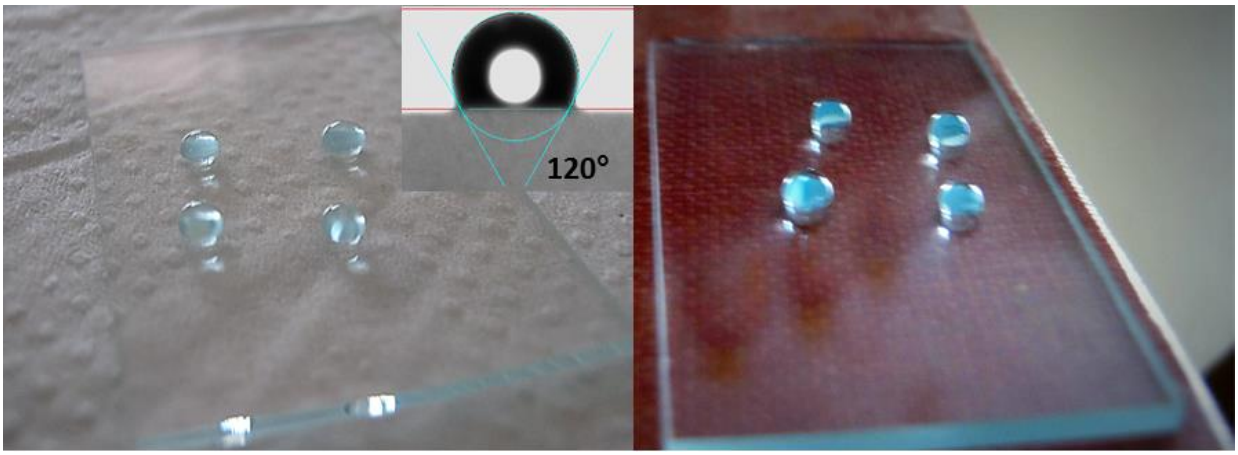

Hydrophobic $LaPO_4$ coating with water drops

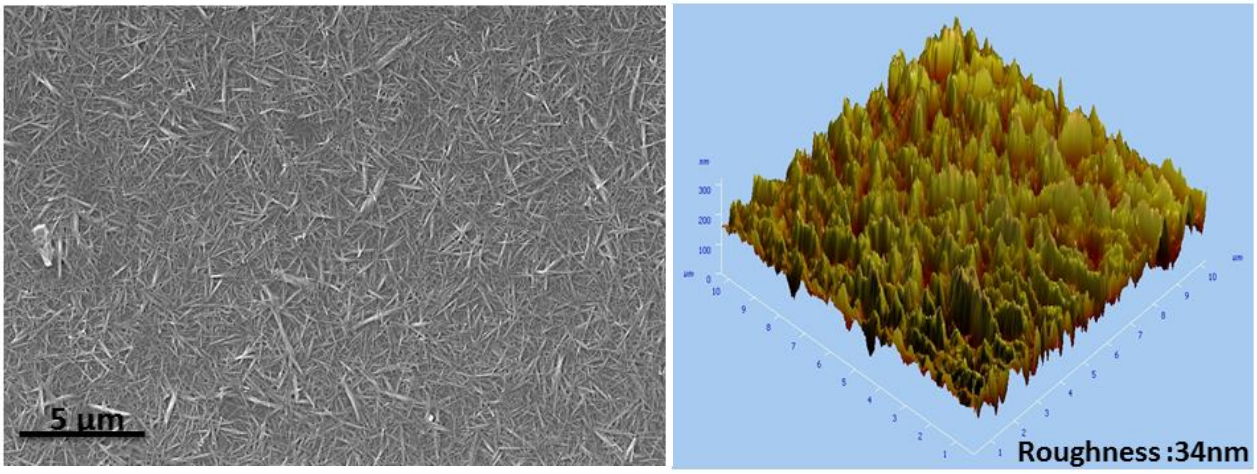

SEM showing the morphology and AFM showing the roughness of coating

Non-wetting property and non-reactivity with molten metal are features which are very attractive to the metal processing industry. During melting of metals or handling of molten metal, considerable melt sticks to the walls of the crucible or container and gets lost. This is especially grave in the case of expensive and rare metals and in particular, radioactive metals like Uranium which is widely used in atomic power plants. The disposal of contaminated crucibles or containers should be done carefully as per the practicing protocols. In this thesis, detailed high temperature melting and reactivity experiments were done on lanthanum phosphate and common

metals such as Zinc, Aluminium and Silver and the resultant samples were analyzed. Surprisingly in all the cases, no contamination had occurred. A small piece of the respective metal (2 cm x 2 cm x 1 mm thick) was kept on a sintered lanthanum phosphate ceramic disc on the polished side and the system was heated in a muffle furnace and kept for 2 hr at about 50 °C higher than the melting point of metal. The silver melted as a globule and remained on the surface with minimum contact area. Contact angle of 125^{o} was measured.

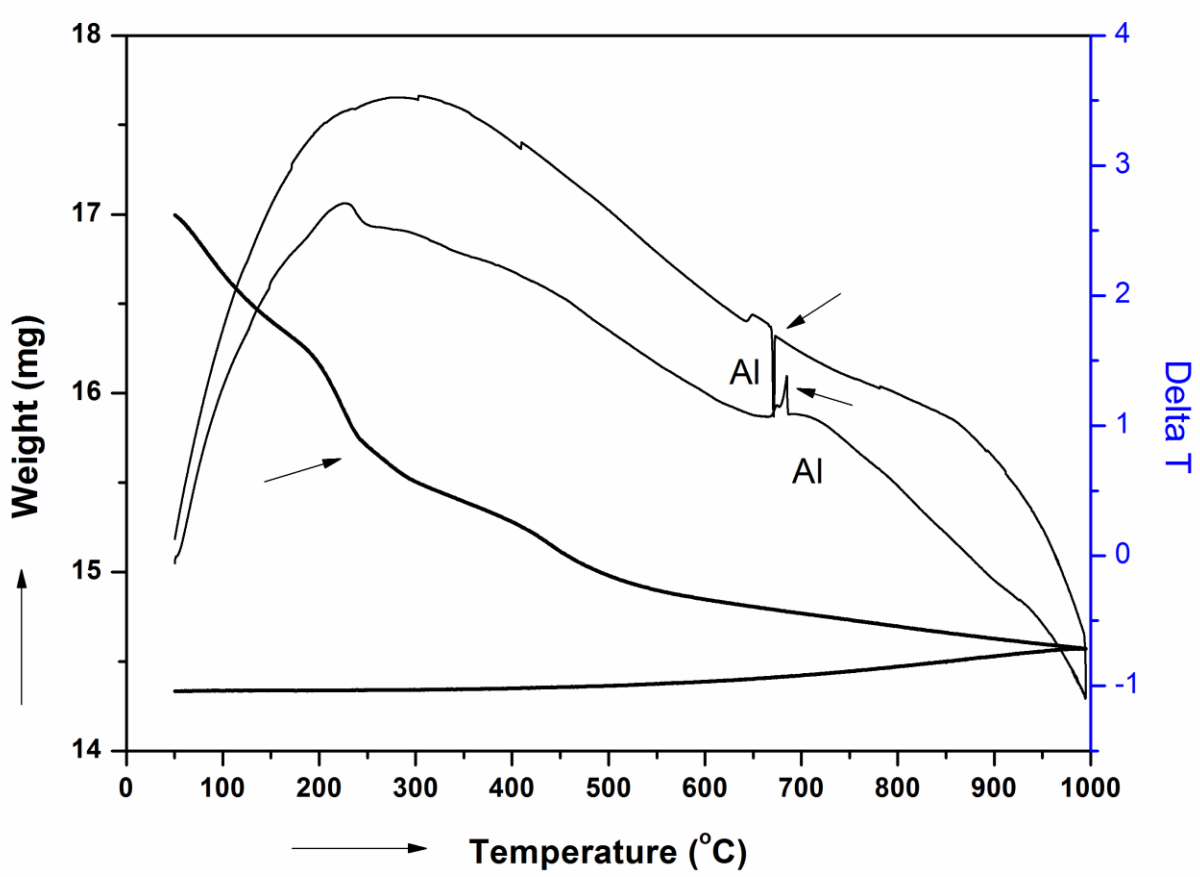

TG- DTA of $LaPO_4$ with Al metal

(The arrows above DTA curves shows the corresponding endothermic and exothermic peaks associated with melting and solidification of Al metal)

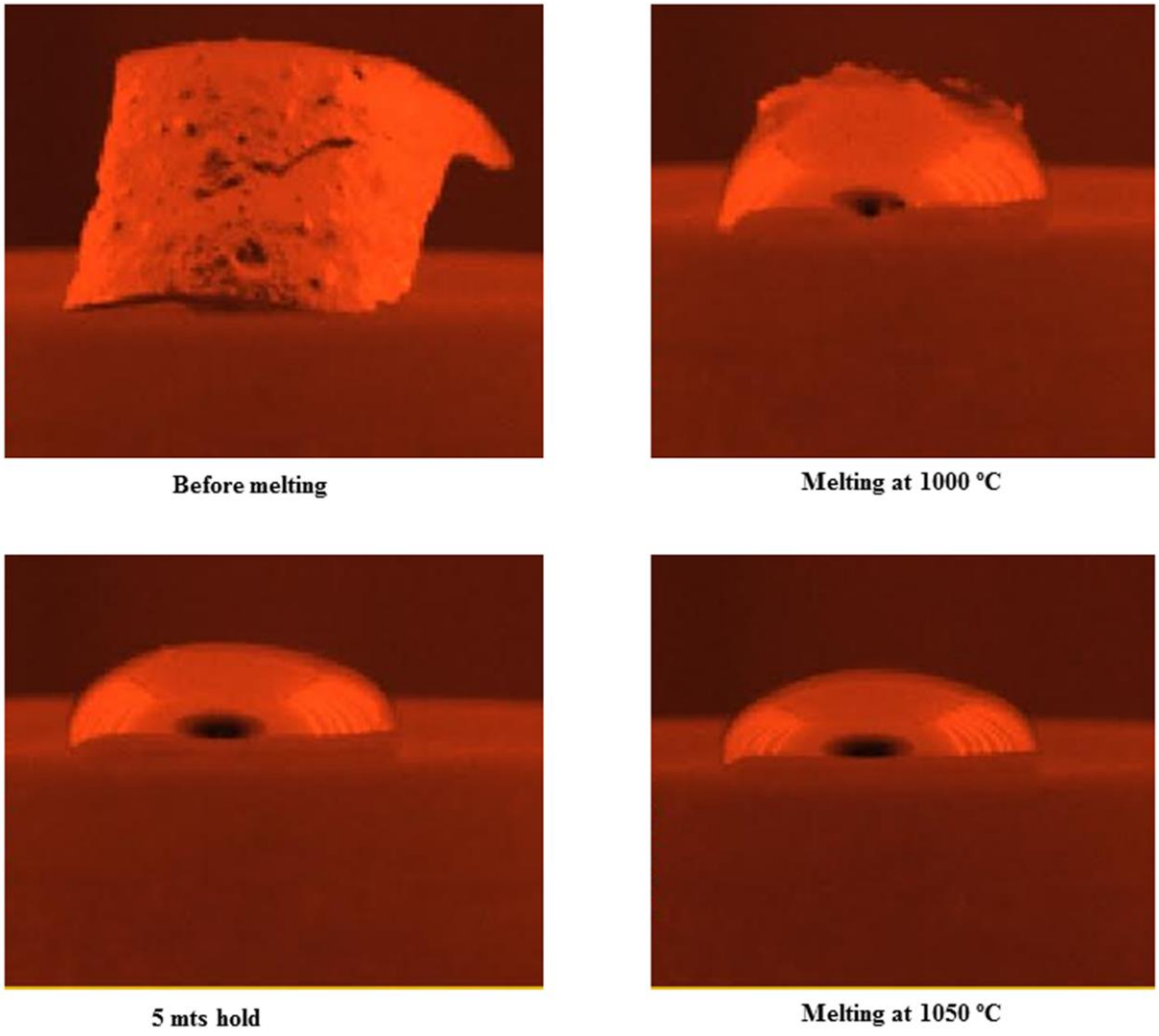

IR imaging of Ag metal heated over $LaPO_4$ surface (different stages)

The second property which was investigated in detail is the processing of $LaPO_4$ to porous substrates by thermal gelation process involving methyl cellulose as the organic intermediate (0.25 wt%) where 50% porous $LaPO_4$ was obtained on gel cast sample sintered at 1300 ^oC. These porous substrates were investigated for simultaneous multifunctional property of high

volume absorption of perchlorate ions from aqueous medium and also for the growth of biofilms of perchlorate reducing microbes. This is important because the current methods involve first adsorption of perchlorate on porous substrate and further reduction is achieved through secondary processing, and multifunctional substrates can achieve both the functions in single step.

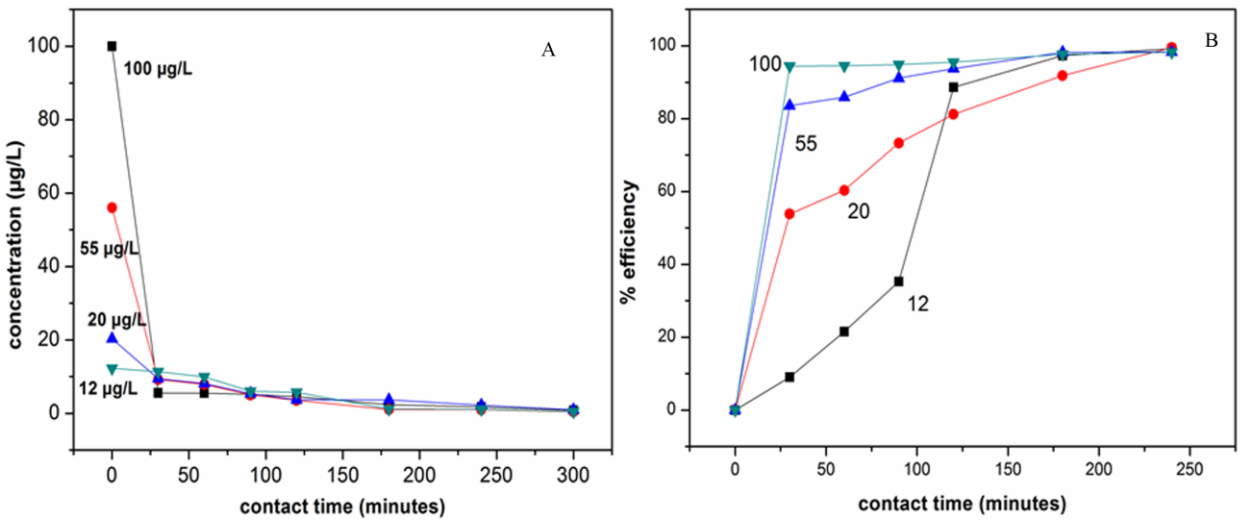

Adsoprtion of perchlorate ions by the $LaPO_4$ monoliths

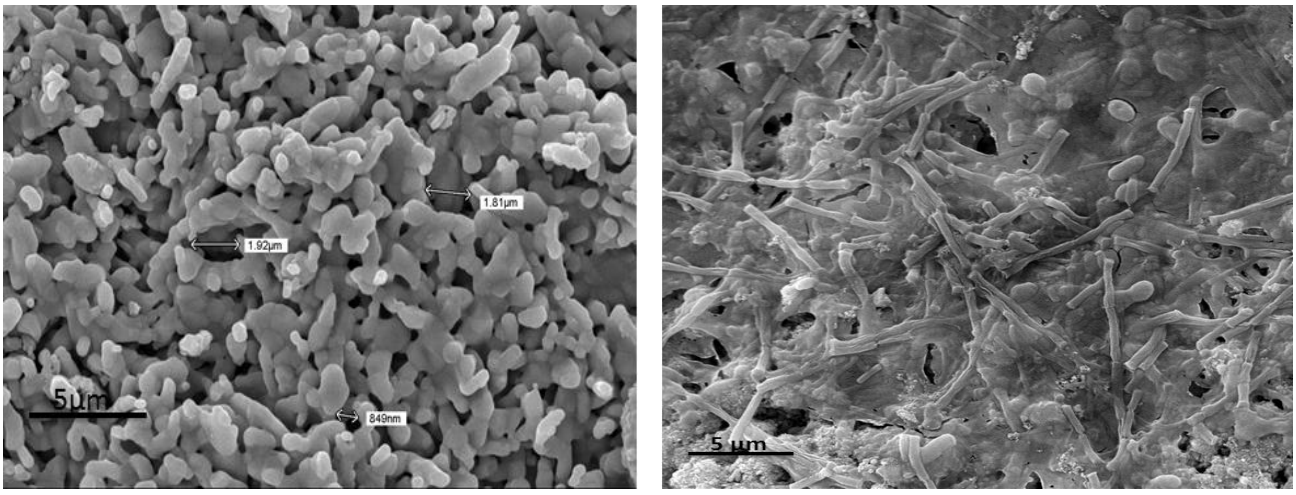

Porous $LaPO_4$ microstructure and the biofilm over the $LaPO_4$ surface

The above exceptional property has been explained on the basis of the hydrophobic nature of the surface which promotes the biofilm growth of perchlorate reducing microbes. The thermal gelation process employed in this work for achieving designed pore structure is instrumental in enhanced absorption of the perchlorate ions.

The thesis therefore, explores the synthesis of nano size lanthanum phosphate and composites containing yttrium and zirconium oxides as second phase by aqueous sol-gel technique followed by characterization of the products. Further, features such as hydrophobicity (non-wettability) are investigated in much detail and these properties are demonstrated through model experiments. The reason for the enhanced hydrophobicity is related to structure of rare earths in general where the interaction with OH sites is prevented due to the shielding of ‘f ‘ shell by full octet filled outer shell, unlike in many oxides like aluminium oxide and zirconium oxide. Similarly $LaPO_4$ coatings had rough surface due to elongated particle morphology and hence hydrophobic. The thesis also demonstrates the possibility of $LaPO_4$ as non-reactive to molten metal.

Structure-property correlation has been drawn between the structural and morphological characteristics of lanthanum phosphate and the observed properties of non-wettability, non-reactivity and biofilm formation. Lanthanum phosphate and possibly other phosphates of the rare earths family could be a group of materials quite useful in specific areas of thermal environment, surface non-wettability and non-reactivity with molten metals.

LIST OF PUBLICATIONS

1) **Sankar S,** Prajeesh GPV, Anupama VN, Krishnakumar B, Hareesh P, Nair BN, **K.G.K. Warrier** and US, Hareesh, Bifunctional lanthanum phosphate substrates as novel adsorbents and biocatalysts supports for perchlorate removal, *Journal of Hazardous Materials*, 275,**2014**,222

2) **Sasidharan Sankar**, Athira N. Raj, C.K. Jyothi, **K.G.K. Warrier**, P.V.A. Padmanabhan, Room temperature synthesis of high temperature stable lanthanum phosphate–yttria nano composite, *Materials Research Bulletin* 47 ,**2012,** 1835

3) **Sasidharan Sankar, Krishna Gopakumar Warrier,** Rajesh Komban**, "**High surface area neodymium phosphate nano particles by modified aqueous sol–gel method", *Materials Research Bulletin,* 46, **2011,** 2373

4) **Sasidharan Sankar** and **K.G.K. Warrier**, "Aqueous sol-gel synthesis of lanthanum phosphate nano rods starting from lanthanum chloride precursor", *Journal of Sol-Gel Science and Technology*, 58 (1) **2011,** 195

5) **S. Sankar et al.** Investigation on the hydrophobicity of lanthanum phosphate as an alternate to its unstable oxide and wide spectrum of possible applications(***communicated)***

6) **S. Sankar et al.** Fine grain sintered and low thermally conducting lanthanum Phosphate – ZrO_2 thermal ceramics (***communicated***)

7) Kanakkanmavudi B. Jaimy**,** Swapankumar Ghosh**, Sasidharan Sankar** and **K.G.K. Warrier,** An aqueous sol-gel synthesis of Chromium(III) doped mesoporous titanium dioxide for visible light photo catalysis, *Materials Research Bulletin,* 46 (6), **2011**, 914

8) Chembolli K. Jyothi, Kanakkanmavudi B. Jaimy, Swapankumar Ghosh, **Sasidharan Sankar**, V.S. Smitha, **K.G.K. Warrier**, Titania–lanthanum phosphate photoactive and hydrophobic new generation catalyst, *Journal of Solid State Chemistry* 184 (7), **2011**, 1867

Patent Filed

Sankar Sasidharan, Rajesh Komban, Abdul Azeez Peer Mohamed, Solaippan Ananthakumar, Unnikrishnan Nair Saraswathy Hareesh and Krishna Gopakumar Warrier, ***Lanthanum Phosphate based coatings and monoliths as non- reactive surfaces for molten metals*** (**Ref No. 0163NF2014 dtd 23.09.2014***)*

Conference Proceedings

1. S. Sankar, G.P.V Prajeesh, V.N Anupama, B. Krishnakumar, M. Midhun , Balagopal N. Nair, K.G.K Warrier, U.S Hareesh, Lanthanum phosphate Monoliths for Perchlorate Removal, **ICONSAT -2014,** March 03 - 05, 2014, Panjab University, Chandigarh
2. Sankar Sasidharan, Lanthanum phosphate: Synthesis, Shaping and Functional Applications, **Processing and Utilization of Beach sand Minerals**, March-2013, IMA House, Kochi. (**Best Poster**)
3. **Sankar Sasidharan,** Athira N Raj, K.G.K Warrier and PVA Padmanabhan, Lanthanum Phosphate Nano Composites for High Temperature Applications, **STAR-2011**: National Conference on Science, Technology and Applications of Rare Earths 2011,Munnar 19-20 August 2011
4. **Sankar Sasidharan**, Divish K and K.G.K Warrier, Aqueous sol gel synthesis of lanthanum phosphate nanorods from lanthanum chloride precursor, **ICMST-2010** Oct. 29-31, IIST-Trivandrum
5. Anas S, **Sankar S**, Mangalaraja R V and Ananthakumar S, Studies on structural and functional properties of morphologically tuned ZnO, SGPAC-2009 Oct. 11-14 ,IGCAR-Kalpakkam
6. Anas S, Shajesh P, **Sankar S**, Mangalaraja R V and Ananthakumar S, Synthesis of ZnO morphologies and their functional properties, ICAFM-2009 Dec 9-10,NIIST-Trivandrum.
7. Sanoop P.K, Anas S, **Sankar Sasidharan**, Smitha S, Ananthakumar S, sonochemical synthesis of nanocrystalline bio-polymer composites and there functional characteristics,SGPAC-2009 Oct. 11-14 ,IGCAR-Kalpakkam